A Thesis for the Degree of Doctor of Philosophy

Investigation of Integral Stereoselectivity Based on Kinetic Modeling for Lipase-catalyzed Triacylglycerol Hydrolysis

트리아실글리세롤 가수분해의 동역학 모델 기반 라이페이스 통합적 입체선택성 구명

Feburary, 2023

Yoonseok Choi

Department of Agricultural Biotechnology

College of Agriculture and Life Sciences

Seoul National University

Investigation of Integral Stereoselectivity Based on Kinetic Modeling for Lipase-catalyzed Triacylglycerol Hydrolysis

트리아실글리세롤 가수분해의 동역학 모델 기반 라이페이스 통합적 입체선택성 구명

지도교수 장 판 식

이 논문을 농학박사학위논문으로 제출함

2023년 2월

서울대학교 대학원

농생명공학부

최 윤 석

최윤석의 박사학위논문을 인준함

2023년 2월

위 원 장 최 영 진 (인)

부위원장 장 판 식 (인)

위 원 이 도 엽 (인)

위 원 최 승 준 (인)

위 원 박 경 민 (인)

Abstract

Choi, Yoonseok

Department of Agricultural Biotechnology

The Graduate School

Seoul National University

Lipase is an enzyme that holds a great significance in various fields of industry including dairy, pharmaceutical, and food processing, mainly for fat and oil modification. Stereoselectivity, which refers to the ability to differentiate between enantiomeric positions (*sn*-1 and *sn*-3) in triacylglycerol (TAG), is a distinctive characteristic of lipase which plays a major impact on its application for the synthesis of structured lipids including enantiomeric diacylglycerol (DAG) and monoacylglycerol (MAG). The stereoselectivity has been determined by enantiomeric excess of diacylglycerol (DAG). However, this is insufficient to represent the true stereoselective nature of lipase because various isomers of DAG and MAG involved in the consecutive steps of TAG hydrolysis, along with non-enzymatic acyl migration, can all affect the overall outcome of the reaction. To overcome this limitation, this study suggested the concept ‘integral stereoselectivity’, which represents the selectivity of lipase toward all the acylglycerols produced in different steps of

TAG hydrolysis. For this purpose, the present study established analytical methods for determination of integral stereoselectivity and investigated the integral stereoselectivity of model lipases.

First, an HPLC-ELSD method was established for the direct and simultaneous resolution of trioleoylglycerol (TOG) and its seven hydrolysates (*i.e.*, oleic acid, monooleoylglycerol (MOG) and dioleoylglycerol (DOG) isomers). Using a single chiral stationary phase (CSP) column composed of amylose tris-(3,5-dimethylphenylcarbamate), the enantiomeric MOGs (1-*sn*-MOG and 3-*sn*-MOG) and DOGs (1,2-*sn*-DOG and 2,3-*sn*-DOG) were baseline-resolved at resolution factors of over 1.5 in the run-time of 20 minutes. The time course of TOG hydrolysis in reverse micelle by lipases from the following sources was then analyzed to validate the established method; porcine pancreas (PPL), *Chromobacterium viscosum* (CVL), *Pseudomonas fluorescens* (PFL), and lipase A from *Candida antarctica* (CALA). As a result, all model lipases yielded DOG profiles that match those of the previous reports, which strongly demonstrated the improved efficiency, accuracy, and suitability of the established method for the analysis of lipase-catalyzed TOG hydrolysis compared to the previous tandem-column method.

Next, a kinetic model of stereoselective lipase-catalyzed TAG hydrolysis was established and validated to quantitatively demonstrate the integral stereoselectivity. The kinetic model was constructed based on Ping-

Pong Bi-Bi mechanism of lipase catalysis, competitive inhibition by fatty acid (FA), and non-enzymatic acyl migration. Nonlinear regression was used to fit the time courses of TOG hydrolysis with changes in the initial substrate concentration. The twelve kinetic parameters (K_1-K_{12}) representing the conversion rate in all positions of TAG, DAG, and MAG isomers were estimated for the four model lipases. Comparison of the kinetic parameters showed that the main reaction pathways for TOG hydrolysis by PPL, CVL, and PFL were from TOG to 1,2-*sn*-DOG or 2,3-*sn*-DOG and then 2-*sn*-MOG, while that for CALA was from TOG to 1,3-*sn*-DOG and then 1-*sn*-MOG. Therefore, the integral stereoselectivity determined with the kinetic model was able to describe the whole process of the lipase-catalyzed TAG hydrolysis.

Based on these analytical processes established with TOG as model substrate, the integral stereoselectivity under the influence of varying FA chains was analyzed to investigate the effects of the substrate type on the lipase-catalyzed TAG hydrolysis. An HPLC-ELSD method was established for simultaneous separation and quantification of all isomers of TAG, DAG, and MAG composed of the following FA chains with varying lengths and saturation degrees; C14:0, C16:0, C18:0, or C18:2. The acylglycerols with C16:0 FA were resolved using the same single CSP column used for the analysis of TOG under a slightly modified mobile phase condition. The acylglycerols with C14:0, C18:0, and C18:2 FAs were separated using a CSP

column composed of cellulose tris-(3-chloro-4-methylphenylcarbamate). The resolution factors for all enantiomers of DAG and MAG were over 1.60 in the run-time of 35 minutes, except that for 1,2-*sn*-DAG and 1,3-*sn*-DAG with C18:0 FA 1.31. To the best of my knowledge, this is the first study to demonstrate a methodology for simultaneous and direct resolution of acylglycerols and FAs of varying acyl chains.

Finally, kinetic modeling of lipase-catalyzed TAG hydrolysis was carried out to determine the integral stereoselectivity of the four model lipases on TAG, DAGs, and MAGs composed of the aforementioned FAs. The kinetic parameters demonstrated that PPL and CVL do not display significant differences in selectivity when FA types are varied in TAG, indicating that their main reaction pathways remain unaltered. PFL, which was capable of cleaving the *sn*-2 position of TOG, showed exceptionally low *sn*-2 selectivity for TAG with C16:0 FA. In addition, CALA displayed contrasting selectivity depending on the saturation degree of FA. The highest selectivity on the *sn*-2 position for TAG and 1,3-*sn*-DAG among DAGs was observed for unsaturated FAs, while the *sn*-3 position for TAG and 1,2(2,3)-*sn*-DAG among DAGs were the most dominant for saturated FAs. Such dramatic differences in stereoselectivity suggested that the integral stereoselectivity affecting the production of DAG and MAG should be evaluated in a substrate-dependent manner.

In conclusion, integral stereoselectivity determined by the enzymatic kinetic model based on the simultaneous resolution of TAG and its hydrolysates is a novel and accurate index for lipase stereochemistry. The concept of integral stereoselectivity and its analytical method ultimately contribute to the processes of selection, screening, and development of stereo-specific lipids for various industrial applications.

Keywords: lipase, integral stereoselectivity, enantiomeric separation, kinetic modeling

Student number: 2018-29815

Contents

List of figures

List of tables

Chapter I

General introduction

I-1. Lipase as stereoselective biocatalyst

Lipase (triacylglycerol acylhydrolase, EC 3.1.1.3) is an enzyme that hydrolyzes the ester bond in triacylglycerols (TAGs) to produce diacylglycerols (DAGs), monoacylglycerols (MAGs), glycerols, and free fatty acids (FFAs). Lipase has been utilized in the food, cosmetic, detergent, and pharmaceutical industries for its unique catalytic activity on various substrates in hydrolysis, acidolysis, alcoholysis, and transesterification (Bajaj, Lohan, Jha, & Mehrotra, 2010; Bornscheuer & Kazlauskas, 2006; Chnadhapuram & Sunkireddy, 2012; Goswami, Basu, & De, 2013; Schmid & Verger, 1998; Soumanou & Bornscheuer, 2003). In particular, research on lipase with high selectivity has been intensively conducted for the synthesis of structured lipids with distinct fatty acid compositions and stereospecific distributions, for use as a human milk fat substitute, low-calorie cocoa butter equivalent, and DAGs suppressing body fat accumulation (Han, Xu, Huang, Meng, Liu, & Wang, 2011; Lo et al., 2007; Willis, Lencki, & Marangoni, 1998; Zou et al., 2012). Moreover, the use of lipase for the production of MAG and DAG has attracted interest because it results in much stereospecific MAG or DAG products under milder reaction conditions compared with chemical synthesis (Bornscheuer et

al., 2006). Both enantiomeric 1,2(2,3)-*sn*-DAG and 1(3)-*sn*-MAGs are potential precursors for the synthesis of phospholipids, glycolipids, and enzyme agonist/antagonists with pharmaceutical function, including 1,2-*sn*-DAG itself as a potent dietary supplement for systemic inflammatory diseases (Berger & Schnelder, 1992; Garzon-Aburbeh, Poupaert, Claesen, & Dumont, 1986; Jacob, Hesse, & Shashoua, 1990; Wang, Lee, Huang, & Kuo, 2016).

The selectivity mechanisms for lipase can be divided into typoselectivity (i.e., the ability to hydrolyze a particular type of fatty acid ester), regioselectivity (i.e., the ability to hydrolyze carboxylic ester groups at the *sn*-1(3) position as compared with the *sn*-2 position), and stereoselectivity (i.e., the ability to differentiate enantiomeric positions in TAGs) (Muralidhar, Chirumamilla, Marchant, Ramachandran, Ward, & Nigam, 2002). Stereoselectivity is the most important property distinguishing lipase from other hydrolases, such as protease, glycosidase, and nuclease, which react with only one optical isomer of their substrates. In contrast, lipase can react not only with both enantiomers of their substrates (with a preference for one enantiomer over the other) but also with prochiral molecules such as trioleoylglycerol (TOG) (Rodriguez et al., 2008). This unique stereoselectivity of lipase needs to be understood in-depth because, together with regioselectivity, it is a key factor in the lipase-catalyzed synthesis of specific-structured lipids (Iwasaki & Yamane, 2000).

I-2. Analysis of lipase stereoselectivity

To determine the stereoselectivity of lipase, most studies measured the enantiomeric excess of 1,2-*sn*-DAG over 2,3-*sn*-DAG at a specific point, i.e. when there was a low hydrolysis level, using prochiral TAG as the substrate and not considering the subsequent reactions (i.e., the transition of DAGs to MAGs, and of MAGs to glycerol) (Ewa Rogalska, Cudrey, Ferrato, & Verger, 1993; E Rogalska, Ransac, & Verger, 1990). Unfortunately, this does not provide a complete description of stereoselectivity, because lipase-catalyzed hydrolysis of TAG involves sequential reactions of regioisomers and enantiomers of DAG (i.e., 1,2-*sn*-, 1,3-*sn*-, and 2,3-*sn*-DAG) and MAG (i.e., 1-*sn*-, 2-*sn*-, and 3-*sn*-MAG). Furthermore, due to the conversion of DAGs to MAGs by lipase during the early phase of hydrolysis, the enantiomeric excess of DAG may not be equivalent to the stereoselectivity of lipase against TAG (Aloulou et al., 2007; Mitchell, Rodriguez, Carrière, & Krieger, 2008).

Considering these facts, to describe the sequential steps of hydrolysis in the determination of stereoselectivity, Rodriguez et al. measured variations in acylglycerol species (i.e., TAG, DAG, MAG) and the enantiomeric excess of 1,2-*sn*-DAG over 2,3-*sn*-DAG as a function of the degree of hydrolysis using

TOG as a substrate (Rodriguez et al., 2008). However, their approach was only applied to lipases hydrolyzing only *sn*-1 and *sn*-3 positions of TAG to produce 1,2-*sn*-DAG and 2,3-*sn*-DAG under the assumption that acyl migration does not occur. Therefore, to describe the stereochemistry of lipase during every possible step in the TAG hydrolysis reaction such as the hydrolysis of the *sn*-2 position of TAG, it is necessary to analyze the time-course of acylglycerol species based on the resolution of both regioisomers and stereoisomers.

An analytical method was previously developed, based on normal-phase high-performance liquid chromatography (HPLC) with a tandem connection of silica column and CSP column, for the separation and quantitation of TAG and all DAG and MAG isomers (Deng, Nakano, & Iwasaki, 2007). However, this method was limited by low resolution and long retention time which requires advances for the determination of integral stereoselectivity from the time-course of each compound. Although other HPLC-based methods have been developed for the direct separation of enantiomeric MAGs or DAGs (Deng, Nakano, & Iwasaki, 2008; García, Franco, Álvarez, & de Lera, 2011; Yutaka Itabashi, 2011; Yuki Itabashi & Kuksis, 2009; Piyatheerawong, Iwasaki, & Yamane, 2005), they were not applicable for simultaneous resolution of TAG, all DAG and MAG isomers, and FFA. Therefore, a novel analytical method for direct and simultaneous resolution TAG, all DAG and MAG isomers, and FFA is required.

I-3. Kinetic modeling of lipase-catalyzed hydrolysis

Because lipase-catalyzed hydrolysis of TAG consists of sequential reactions (TAG to DAGs, DAGs to MAGs, and MAGs to glycerol), several studies have been conducted to model the reaction progress in order to quantitatively assess the efficiency and selectivity of the lipases for industrial applications (Al-Zuhair, Hasan, & Ramachandran, 2003; Morales-Medina, Munio, Guadix, Guadix, & Camacho, 2018; Voll et al., 2012). In the case of kinetic modeling which considers the stereoselective feature of lipase, Mitchell et al. proposed a simplified kinetic model for quantitative analysis of stereoselectivity in lipase-catalyzed hydrolysis of TOG using plots of TOG, dioleoylglycerol (DOG) enantiomers, monooleoylglycerol (MOG), and enantiomeric excess (Mitchell, Carrière, & Krieger, 2008; Mitchell, Rodriguez, Carrière, Baratti, & Krieger, 2008; Mitchell, Rodriguez, Carrière, & Krieger, 2008). However, the application of this model was limited to lipases hydrolyzing only the *sn*-1 and *sn*-3 positions of TAG in an oil-in-water emulsion reaction system. Moreover, acyl migration, which refers to the non-enzymatic spontaneous migration of a fatty acid moiety between the *sn*-2 and *sn*-1/3 position of DAGs and MAGs (Compton, Vermillion, & Laszlo, 2007;

Kodali, Tercyak, Fahey, & Small, 1990), was not considered in the model.

The other kinetic modeling approaches for lipase-catalyzed TAG hydrolysis based on the mechanism of lipase activity were conducted in an oil-water two-phase system (Hermansyah, Kubo, Shibasaki-Kitakawa, & Yonemoto, 2006), and the model fit to experimental data was improved by applying lipase regioselectivity (Hermansyah, Wijanarko, Kubo, Shibasaki-Kitakawa, & Yonemoto, 2010). However, there was no measurement of DAG or MAG isomers, limiting the application of such models in stereoselectivity analyzes. Therefore, to overcome these limitations and comprehensively describe the stereoselective nature of lipase during the whole steps of the TAG hydrolysis reaction, this study suggests the concept 'integral stereoselectivity', the selectivity of lipase for all positions of acylglycerols. Based on a time-course of TAG, FFA, regioisomers, and enantiomers of DAG (i.e., 1,2-*sn*-, 1,3-*sn*-, and 2,3-*sn*-DAG) and MAG (i.e., 1-*sn*-, 2-*sn*-, and 3-*sn*-MAG) obtained with the developed analytical method, the integral stereoselectivity of lipase was quantified as a kinetic constant for each step of the reaction.

I-4. References

Al-Zuhair, S., Hasan, M., & Ramachandran, K. B. (2003). Kinetics of the enzymatic hydrolysis of palm oil by lipase. *Process Biochemistry, 38*(8), 1155-1163.

Aloulou, A., Rodriguez, J. A., Puccinelli, D., Mouz, N., Leclaire, J., Leblond, Y., & Carrière, F. (2007). Purification and biochemical characterization of the LIP2 lipase from *Yarrowia lipolytica*. *Biochimica et Biophysica Acta, 1771*(2), 228-237.

Bajaj, A., Lohan, P., Jha, P. N., & Mehrotra, R. (2010). Biodiesel production through lipase catalyzed transesterification: an overview. *Journal of Molecular Catalysis B: Enzymatic, 62*(1), 9-14.

Berger, M., & Schnelder, M. P. (1992). Enzymatic esterification of glycerol II. Lipase-catalyzed synthesis of regioisomerically pure 1(3)-*rac*-monoacylglycerols. *Journal of the American Oil Chemists' Society, 69*(10), 961-965.

Bornscheuer, U. T., & Kazlauskas, R. J. (2006). *Hydrolases in organic synthesis: regio-and stereoselective biotransformations*. (second edition). Weinheim: Wiley-VCH.

Chnadhapuram, M., & Sunkireddy, Y. R. (2012). Preparation of palm olein enriched with medium chain fatty acids by lipase acidolysis. *Food Chemistry, 132*(1), 216-221.

Compton, D. L., Vermillion, K. E., & Laszlo, J. A. (2007). Acyl migration kinetics of 2-monoacylglycerols from soybean oil via 1H NMR. *Journal of the American Oil Chemists' Society, 84*(4), 343-348.

Deng, L., Nakano, H., & Iwasaki, Y. (2007). Direct separation of regioisomers and enantiomers of monoacylglycerols by tandem column high-performance liquid chromatography. *Journal of Chromatography A, 1165*(1), 93-99.

Deng, L., Nakano, H., & Iwasaki, Y. (2008). Direct separation of monoacylglycerol isomers by enantioselective high-performance liquid chromatography. *Journal of Chromatography A, 1198-1199*, 67-72.

García, P., Franco, P., Álvarez, R., & de Lera, Á. R. (2011). Separation of regioisomers and enantiomers of underivatized saturated and unsaturated fatty acid monoacylglycerols using enantioselective HPLC. *Journal of Separation Science, 34*(9), 999-1003.

Garzon-Aburbeh, A., Poupaert, J. H., Claesen, M., & Dumont, P. (1986). A lymphotropic prodrug of L-DOPA: synthesis, pharmacological properties and pharmacokinetic behavior of 1,3-dihexadecanoyl-2-

[(*S*)-2-amino-3-(3,4-dihydroxyphenyl)propanoyl]propane-1,2,3-triol. *Journal of Medicinal Chemistry, 29*(5), 687-691.

Goswami, D., Basu, J. K., & De, S. (2013). Lipase applications in oil hydrolysis with a case study on castor oil: a review. *Critical Reviews in Biotechnology, 33*(1), 81-96.

Han, L., Xu, Z., Huang, J., Meng, Z., Liu, Y., & Wang, X. (2011). Enzymatically catalyzed synthesis of low-calorie structured lipid in a solvent-free system: optimization by response surface methodology. *Journal of Agricultural and Food Chemistry, 59*(23), 12635-12642.

Hermansyah, H., Kubo, M., Shibasaki-Kitakawa, N., & Yonemoto, T. (2006). Mathematical model for stepwise hydrolysis of triolein using *Candida rugosa* lipase in biphasic oil–water system. *Biochemical Engineering Journal, 31*(2), 125-132.

Hermansyah, H., Wijanarko, A., Kubo, M., Shibasaki-Kitakawa, N., & Yonemoto, T. (2010). Rigorous kinetic model considering positional specificity of lipase for enzymatic stepwise hydrolysis of triolein in biphasic oil–water system. *Bioprocess and Biosystems Engineering, 33*(7), 787-796.

Itabashi, Y. (2011). Development and application of chromatographic methods for glycerolipid analysis. *Chromatography, 32*(2), 59-72.

Itabashi, Y., & Kuksis, A. (2009, May 3-6). Direct enantiomer separation of

mono- and diacylglycerols by reversed-phase HPLC on polysaccharide-type chiral stationary phases. 100 th AOCS Annual Meeting & Expo, Orlando.

Iwasaki, Y., & Yamane, T. (2000). Enzymatic synthesis of structured lipids. *10*(1-3), 129-140.

Jacob, J. N., Hesse, G. W., & Shashoua, V. E. (1990). Synthesis, brain uptake, and pharmacological properties of a glyceryl lipid containing GABA and the GABA-T inhibitor gamma-vinyl-GABA. *Journal of Medicinal Chemistry, 33*(2), 733-736.

Kodali, D. R., Tercyak, A., Fahey, D. A., & Small, D. M. (1990). Acyl migration in 1,2-dipalmitoyl-*sn*-glycerol. *Chemistry and Physics of Lipids, 52*(3), 163-170.

Lo, S.-K., Cheong, L.-Z., Arifin, N., Tan, C.-P., Long, K., Yusoff, M. S. A., & Lai, O.-M. (2007). Diacylglycerol and triacylglycerol as responses in a dual response surface-optimized process for diacylglycerol production by lipase-catalyzed esterification in a pilot packed-bed enzyme reactor. *Journal of Agricultural and Food Chemistry, 55*(14), 5595-5603.

Mitchell, D. A., Carrière, F., & Krieger, N. (2008). An analytical method for determining relative specificities for sequential reactions catalyzed by the same enzyme: General formulation. *Biochimica et Biophysica Acta*

(BBA) - Proteins and Proteomics, 1784(4), 705-715.

Mitchell, D. A., Rodriguez, J. A., Carrière, F., Baratti, J., & Krieger, N. (2008). An analytical method for determining relative specificities for sequential reactions catalyzed by the same enzyme: Application to the hydrolysis of triacylglycerols by lipases. *Journal of Biotechnology, 133*(3), 343-350.

Mitchell, D. A., Rodriguez, J. A., Carrière, F., & Krieger, N. (2008). Determination of the quantitative stereoselectivity fingerprint of lipases during hydrolysis of a prochiral triacylglycerol. *Journal of Biotechnology, 135*(2), 168-173.

Morales-Medina, R., Munio, M., Guadix, A., Guadix, E. M., & Camacho, F. (2018). A lumped model of the lipase catalyzed hydrolysis of sardine oil to maximize polyunsaturated fatty acids content in acylglycerols. *Food Chemistry, 240*, 286-294.

Muralidhar, R. V., Chirumamilla, R. R., Marchant, R., Ramachandran, V. N., Ward, O. P., & Nigam, P. (2002). Understanding lipase stereoselectivity. *World Journal of Microbiology and Biotechnology, 18*(2), 81-97.

Piyatheerawong, W., Iwasaki, Y., & Yamane, T. (2005). Direct separation of regio- and enantiomeric isomers of diacylglycerols by a tandem column high-performance liquid chromatography. *Journal of*

Chromatography A, 1068(2), 243-248.

Rodriguez, J. A., Mendoza, L. D., Pezzotti, F., Vanthuyne, N., Leclaire, J., Verger, R., . . . Fotiadu, F. (2008). Novel chromatographic resolution of chiral diacylglycerols and analysis of the stereoselective hydrolysis of triacylglycerols by lipases. *Analytical Biochemistry, 375*(2), 196-208.

Rogalska, E., Cudrey, C., Ferrato, F., & Verger, R. (1993). Stereoselective hydrolysis of triglycerides by animal and microbial lipases. *Chirality, 5*(1), 24-30.

Rogalska, E., Ransac, S., & Verger, R. (1990). Stereoselectivity of lipases. II. Stereoselective hydrolysis of triglycerides by gastric and pancreatic lipases. *Journal of Biological Chemistry, 265*(33), 20271-20276.

Schmid, R. D., & Verger, R. (1998). Lipases: interfacial enzymes with attractive applications. *Angewandte Chemie International Edition, 37*(12), 1608-1633.

Soumanou, M. M., & Bornscheuer, U. T. (2003). Lipase-catalyzed alcoholysis of vegetable oils. *European Journal of Lipid Science and Technology, 105*(11), 656-660.

Voll, F. A. P., Zanette, A. F., Cabral, V. F., Dariva, C., De Souza, R. O. M. A., Filho, L. C., & Corazza, M. L. (2012). Kinetic modeling of solvent-free lipase-catalyzed partial hydrolysis of palm oil. *Applied*

Biochemistry and Biotechnology, 168(5), 1121-1142.

Wang, Y.-F., Lee, G.-L., Huang, Y.-H., & Kuo, C.-C. (2016). *sn*-1,2-diacylglycerols protect against lethal endotoxemia by controlling systemic inflammation. *Immunobiology, 221*(11), 1309-1318.

Willis, W. M., Lencki, R. W., & Marangoni, A. G. (1998). Lipid modification strategies in the production of nutritionally functional fats and oils. *Critical Reviews in Food Science and Nutrition, 38*(8), 639-674.

Zou, X.-Q., Huang, J.-H., Jin, Q.-Z., Liu, Y.-F., Tao, G.-J., Cheong, L.-Z., & Wang, X.-G. (2012). Preparation of human milk fat substitutes from palm stearin with arachidonic and docosahexaenoic acid: combination of enzymatic and physical methods. *Journal of Agricultural and Food Chemistry, 60*(37), 9415-9423.

Chapter II

Establishment of analytical method for characterization of integral stereoselectivity on trioleoylglycerol

II-1. Introduction

Trioleoylglycerol (TOG) is a triacylglycerol (TAG) composed of the same oleate moiety on *sn*-1, *sn*-2, and *sn*-3 position of glycerol backbone which have been used as a standard substrate for analysis of stereoselectivity. This is because hydrolysis of TAGs composed of fatty acids other than a single type results in the generation of diacylglycerols (DAGs) and monoacylglycerols (MAGs) affected by typoselectivity (Muralidhar, Chirumamilla, Marchant, Ramachandran, Ward, & Nigam, 2002). Therefore, TOG was adopted for the determination of integral stereoselectivity. For the measurement of reaction mixtures of lipid class, the high-performance liquid chromatography (HPLC) equipped with evaporative light-scattering detector (ELSD) has been used, since ultraviolet detection limits the mobile phase composition and shows low sensitivity (Donot et al., 2013; Stolyhwo, Martin, & Guiochon, 1987). In the kinetic modeling of lipase-catalyzed TAG hydrolysis, each consecutive step of hydrolysis should reflect the enzymatic mechanism of the catalysis. The Ping-Pong Bi-Bi mechanism is the most general, accurate, and accepted description of the catalytic action of lipase with many applications for kinetic modeling demonstrated (Paiva, Balcão, &

Malcata, 2000a).

Collectively, this chapter aimed to establish the analytical method for the determination of integral stereoselectivity of lipase on TOG, a standard substrate. The direct and simultaneous resolution and quantification of TOG and its hydrolysates, namely dioleoylgylcerol (DOG) and monooleoylglycerol (MOG) isomers, and oleic acid (OA), were achieved by HPLC-ELSD equipped with a single chiral stationary phase (CSP) column. Subsequently, a kinetic model explaining integral stereoselectivity was constructed and verified by applying it to the TOG hydrolysis of four model lipases.

II-2. Materials and methods

II-2-1. Materials

Glyceryl trioleate (TOG, > 99%), 1,2-dioleoyl-*rac*-glycerol (1,2-*rac*-DOG, > 99%), 1,2-dioleoyl-*sn*-glycerol (1,2-*sn*-DOG, > 99%), 1,3-dioleoyl-*sn*-glycerol (1,3-*sn*-DOG, > 99%), 1-oleoyl-*rac*-glycerol (1-*rac*-MOG, > 99%), OA (> 99%), olive oil (highly refined, low acidity), bis(2-ethylhexyl) sulfosuccinate sodium salt (Aerosol-OT, AOT, > 99%), and Trizma base (Tris, > 99%) were purchased from Sigma-Aldrich (St. Louis, MO, USA). 1-Oleoyl-*sn*-glycerol (1-*sn*-MOG, 92%) and 2-oleoyl-*sn*-glycerol (2-*sn*-MOG, > 99%) were purchased from Santa Cruz Biotechnology (Dallas, TX, USA) and Avanti Polar Lipids (Alabaster, AL, USA), respectively. Trifluoroacetic acid (guaranteed reagent grade) and hydrochloric acid (HCl) were purchased from Samchun Pure Chemicals (Gyeonggi-do, Republic of Korea). Acetonitrile, acetone, and isooctane (J.T. Baker, Phillipsburg, NJ, USA) were of HPLC grade. Purified lipase from *Pseudomonas fluorescence* (PFL) was purchased from Sigma-Aldrich. All other chemicals were of extra pure grade and used without further purification.

II-2-2. Chromatographic resolution of oleic acid and oleoylglycerols

A CSP column, CHIRALPAK IA (amylose tris-(3,5-dimethylphenylcarbamate) immobilized on 5 μm silica gel, 250 × 4.6 mm; Daicel Chemical Ind., Osaka, Japan), was used to separate OA, enantiomers, and regioisomers of MOG and DOG, and TOG simultaneously. The HPLC system consisted of a Waters Alliance e2695 separation module (Waters Co., Milford, MA, USA) and an Alltech ELSD 2000 instrument (Alltech Co., Deerfield, MA, USA). The column was eluted with acetonitrile-acetone-trifluoroacetic acid (90:10:0.1, v/v/v) at a flow rate of 0.5 mL/min and the column temperature was maintained at 30ºC. The drift pipe temperature and nitrogen flow rate were 70°C and 1.8 L/min, respectively. An aliquot (10 μL) of a sample containing authentic standards dissolved in acetonitrile-acetone (90:10, v/v) was injected into the HPLC system and the peaks were detected with the ELSD. With the analytical condition above, the separation of analytes was characterized by separation factor (α) and resolution factor (Rs), which were calculated from the chromatograms as follows:

$$\alpha = \frac{t_{R2} - t_D}{t_{R1} - t_D}$$

$$R_s = \frac{(t_{R2} - t_{R1})}{w_1 + w_2}$$

where t_R is retention time, t_D is delay time, and w is peak width. An indexed 1

and 2 refers to the former and the later of two adjacent peaks.

II-2-3. Hydrolysis of trioleoylglycerol in the reverse micelle

To prepare the reverse micelle containing model lipases, each freeze-dried lipase powder was solubilized in 50 mM Tris-HCl buffer (pH 7.0, CALA; pH 7.7, PPL; pH 8.0, CVL and PFL). The lipase solution and AOT/isooctane were then mixed vigorously for 1 min to obtain a transparent mixture, indicating the formation of reverse micelle. The reverse micelle containing lipase (3.6 mL) was pre-incubated in a water bath at 37°C with magnetic stirring at 500 rpm. Lipase-catalyzed hydrolysis was initiated by adding 400 μL of TOG/isooctane, a substrate solution. The final concentrations of AOT and the *R*-value ($[H_2O]/[AOT]$) of the reverse micelle were 100 mM and 10, respectively. The final concentrations of TOG were 10, 20, and 30 mM. At various time points up to 24 h, aliquots (50 and 100 μL) of the reactant were collected and diluted with 1.15 and 1.10 mL of acetonitrile-acetone (90:10, v/v), respectively. Then, the mixtures were vortexed for 30 s to obtain a transparent phase and filtered through a 0.45 μm PTFE syringe filter. After filtration, 10 μL of each filtrate was injected into the HPLC system for analysis of OA and seven oleoylglycerols. The degree of hydrolysis was defined as the percentage of the acyl chain released from TOG, as follows:

$$Hydrolysis\ (\%) = \frac{100 \times FFA}{3 \times TAG_0}$$

where TAG_0 is the initial number of mols of TOG and FFA is the number of

mols of OA.

II-2-4. Kinetic modeling of lipase-catalyzed triacylglycerol hydrolysis

II-2-4-1. Construction of the kinetic model

The kinetic model describing the stepwise stereoselective hydrolysis of TAG hydrolysis including acyl migration was formulated based on the following assumptions: Each hydrolysis reaction is catalyzed by lipase via the Ping-Pong Bi-Bi mechanism (Hermansyah, Wijanarko, Kubo, Shibasaki-Kitakawa, & Yonemoto, 2010; Paiva, Balcão, & Malcata, 2000b); the inhibition by free fatty acid is based on the competitive inhibition mechanism (Goto, Goto, Nakashio, Yoshizuka, & Inoue, 1992; Prazeres, Lemos, Garcia, & Cabral, 1993); the rates for cleaving ester bonds at *sn*-1, *sn*-2, and *sn*-3 positions of the respective substrates and acyl migration between DAG and MAG isomers were assumed to be different from one another.

As depicted in the schematic diagram of the hydrolysis reaction shown in Figure II-1, TAG hydrolysis proceeds via the following stepwise reactions:

$$\mathrm{T} + \mathrm{W} \rightarrow \mathrm{D}_{13} + \mathrm{F} \quad (1)$$

$$\mathrm{T} + \mathrm{W} \rightarrow \mathrm{D}_{13} + \mathrm{F} \quad (2)$$

$$\mathrm{T} + \mathrm{W} \rightarrow \mathrm{D}_{23} + \mathrm{F} \quad (3)$$

$$\mathrm{D}_{12} + \mathrm{W} \rightarrow \mathrm{M}_{1} + \mathrm{F} \quad (4)$$

$$\mathrm{D}_{12} + \mathrm{W} \rightarrow \mathrm{M}_{2} + \mathrm{F} \quad (5)$$

$$\mathrm{D}_{13} + \mathrm{W} \rightarrow \mathrm{M}_{1} + \mathrm{F} \quad (6)$$

$$D_{13} + W \rightarrow M_3 + F \quad (7)$$

$$D_{23} + W \rightarrow M_2 + F \quad (8)$$

$$D_{23} + W \rightarrow M_3 + F \quad (9)$$

$$M_1 + W \rightarrow G + F \quad (10)$$

$$M_2 + W \rightarrow G + F \quad (11)$$

$$M_3 + W \rightarrow G + F \quad (12)$$

where T, D_{12}, D_{13}, D_{23}, M_1, M_2, M_3, G, W, and F denote TAG, 1,2-*sn*-DAG, 1,3-*sn*-DAG, 2,3-*sn*-DAG, 1-*sn*-MAG, 2-*sn*-MAG, 3-*sn*-MAG, glycerol, water, and FA, respectively. As each hydrolysis reaction follows the Ping-Pong Bi-Bi mechanism as shown in Figure II-2, two partial reactions, i.e. acylation and deacylation, proceed sequentially. The acylation starts with the free enzyme, E, reacting with TAG, T, to form the first complex, ET. Subsequent cleavage of the ester bond at the *sn*-1, *sn*-2, or *sn*-3 positions of ET produces 2,3-*sn*-DAG, 1,3-*sn*-DAG, and 1,2-*sn*-DAG, respectively, and the acyl-enzyme intermediate, E*. Then in the deacylation step, E* reacts with water to release FA, although this process is not accounted for due to the large contribution of water to overall composition compared to substrate concentration. The mechanisms of the hydrolysis of the DAG and MAG isomers are similar to that described above. In the case of competitive inhibition by FA, the reaction is as follows:

$$E + F \leftrightharpoons EF \quad (13)$$

where E and EF denote lipase and the enzyme-inhibitor complex, respectively. In addition, non-enzymatic acyl migrations are expressed as follows:

$$D_{12} \leftrightarrows D_{13} \leftrightarrows D_{23} \quad (14)$$

$$M_1 \leftrightarrows M_2 \leftrightarrows M_3 \quad (15)$$

The conceptual scheme of the overall reaction mechanism is shown in Figure II-3, where k_1 to k_{29} denote the rate constants of the respective elementary reactions. The reaction rates of the substrate and products, except G which is not measured but calculable from the rest, are given as follows:

$$d[T]/dt = -k_1[E][T] + k_{-1}[ET] \quad (16)$$

$$d[D_{12}]/dt = k_2[ET] - k_5[E][D_{12}] + k_{-5}[ED_{12}] + k_{22}[D_{13}] - k_{23}[D_{12}] \quad (17)$$

$$d[D_{13}]/dt = k_3[ET] - k_6[E][D_{13}] + k_{-6}[ED_{13}] - k_{22}[D_{13}] + k_{23}[D_{12}] + k_{24}[D_{23}] - k_{25}[D_{13}] \quad (18)$$

$$d[D_{23}]/dt = k_4[ET] - k_7[E][D_{23}] + k_{-7}[ED_{23}] - k_{24}[D_{23}] + k_{25}[D_{13}] \quad (19)$$

$$d[M_1]/dt = k_8[ED_{12}] + k_{10}[ED_{13}] - k_{14}[E][M_1] + k_{-14}[EM_1] + k_{26}[M_2] - k_{27}[M_1] \quad (20)$$

$$d[M_2]/dt = k_9[ED_{12}] + k_{12}[ED_{23}] - k_{15}[E][M_2] + k_{-15}[EM_2] - k_{26}[M_2] + k_{27}[M_1] + k_{28}[M_3] - k_{29}[M_2] \quad (21)$$

$$d[M_3]/dt = k_{11}[ED_{13}] + k_{13}[ED_{23}] - k_{16}[E][M_3] + k_{-16}[EM_3] - k_{28}[M_3] + k_{29}[M_2] \quad (22)$$

$$d[F]/dt = k_{20}[E^*] - k_{21}[E][F] + k_{-21}[EF] \quad (23)$$

Assuming pseudo-equilibrium relationships for respective enzyme complexes, the reaction rates for the enzyme complexes are approximated to zero as follows:

$$d[ET]/dt = 0 = k_1[E][T] - (k_{-1} + k_2 + k_3 + k_4)[ET] \quad (24)$$

$$d[ED_{12}]/dt = 0 = k_5[E][D_{12}] - (k_{-5} + k_8 + k_9)[ED_{12}] \quad (25)$$

$$d[ED_{13}]/dt = 0 = k_6[E][D_{13}] - (k_{-6} + k_{10} + k_{11})[ED_{13}] \quad (26)$$

$$d[ED_{23}]/dt = 0 = k_7[E][D_{23}] - (k_{-7} + k_{12} + k_{13})[ED_{23}] \quad (27)$$

$$d[EM_1]/dt = 0 = k_{14}[E][M_1] - (k_{-14} + k_{17})[EM_1] \quad (28)$$

$$d[EM_2]/dt = 0 = k_{15}[E][M_2] - (k_{-15} + k_{18})[EM_2] \quad (29)$$

$$d[EM_3]/dt = 0 = k_{16}[E][M_3] - (k_{-16} + k_{19})[EM_3] \quad (30)$$

$$\begin{aligned} d[E^*]/dt = 0 = {} & (k_2 + k_3 + k_4)[ET] + (k_8 + k_9)[ED_{12}] \\ & + (k_{10} + k_{11})[ED_{13}] + (k_{12} + k_{13})[ED_{23}] \\ & + (k_{17})[EM_1] + (k_{18})[EM_2] + (k_{19})[EM_3] - k_{20}[E^*] \end{aligned} \quad (31)$$

$$d[EF]/dt = 0 = k_{21}[E][F] - k_{-21}[EF] \quad (32)$$

The total enzyme concentration, $[E]_{tot}$ is the sum of the concentrations of the enzyme complexes and free enzyme as follows:

$$\begin{aligned} [E]_{tot} = {} & [E] + [ET] + [ED_{12}] + [ED_{13}] + [ED_{23}] + [EM_1] + [EM_2] \\ & + [EM_3] + [E^*] + [EF] \end{aligned} \quad (33)$$

Algebraic manipulation of Eqns 24–33 and their substitution into Eqns 16–23 result in the following expressions:

$$d[T]/dt = -(K_1 + K_2 + K_3)[T][E]_{tot}/\sigma \quad (34)$$

$$d[D_{12}]/dt = (K_1[T] - (K_4 + K_5)[D_{12}])[E]_{tot}/\sigma + k_{22}[D_{13}] - k_{23}[D_{12}] \quad (35)$$

$$d[D_{13}]/dt = (K_2[T] - (K_6 + K_7)[D_{13}])[E]_{tot}/\sigma - k_{22}[D_{13}] + k_{23}[D_{12}] + k_{24}[D_{23}] - k_{25}[D_{13}] \quad (36)$$

$$d[D_{23}]/dt = (K_3[T] - (K_8 + K_9)[D_{13}])[E]_{tot}/\sigma - k_{24}[D_{23}] + k_{25}[D_{13}] \quad (37)$$

$$d[M_1]/dt = (K_4[D_{12}] + K_6[D_{13}] - K_{10}[M_1])[E]_{tot}/\sigma + k_{26}[M_2] - k_{27}[M_1] \quad (38)$$

$$d[M_2]/dt = (K_5[D_{12}] + K_8[D_{23}] - K_{11}[M_2])[E]_{tot}/\sigma - k_{26}[M_2] + k_{27}[M_1] + k_{28}[M_3] - k_{29}[M_2] \quad (39)$$

$$d[M_3]/dt = (K_7[D_{13}] + K_9[D_{23}] - K_{12}[M_3])[E]_{tot}/\sigma - k_{28}[M_3] + k_{29}[M_2] \quad (40)$$

$$d[F]/dt = ((K_1 + K_2 + K_3)[T] + (K_4 + K_5)[D_{12}] + (K_6 + K_7)[D_{13}] + (K_8 + K_9)[D_{23}] + K_{10}[M_1] + K_{11}[M_2] + K_{12}[M_3])[E]_{tot}/\sigma \quad (41)$$

where the term σ and the constants are as follows:

$$\sigma = 1 + (K_1 + K_2 + K_3)[T] + (K_4 + K_5)K_{14}[D_{12}] + (K_6 + K_7)K_{15}[D_{13}] + (K_8 + K_9)K_{16}[D_{23}] + K_{10}K_{17}[M_1] + K_{11}K_{18}[M_2] + K_{12}K_{19}[M_3] + [F]/K_{20} \quad (42)$$

$$K_1 = k_1k_2/(k_{-1} + k_2 + k_3 + k_4) \quad (43)$$

$$K_2 = k_1k_3/(k_{-1} + k_2 + k_3 + k_4) \quad (44)$$

$$K_3 = k_1k_4/(k_{-1} + k_2 + k_3 + k_4) \quad (45)$$

$$K_4 = k_5k_8/(k_{-5} + k_8 + k_9) \quad (46)$$

$$K_5 = k_5k_9/(k_{-5} + k_8 + k_9) \quad (47)$$

$$K_6 = k_6k_{10}/(k_{-6} + k_{10} + k_{11}) \quad (48)$$

$$K_7 = k_6k_{11}/(k_{-6} + k_{10} + k_{11}) \quad (49)$$

$$K_8 = k_7k_{12}/(k_{-7} + k_{12} + k_{13}) \quad (50)$$

$$K_9 = k_7k_{13}/(k_{-7} + k_{12} + k_{13}) \quad (51)$$

$$K_{10} = k_{14}k_{17}/(k_{-14} + k_{17}) \quad (52)$$

$$K_{11} = k_{15}k_{18}/(k_{-15} + k_{18}) \quad (53)$$

$$K_{12} = k_{16}k_{19}/(k_{-16} + k_{19}) \quad (54)$$

$$K_{13} = (k_2 + k_3 + k_4 + k_{20})/(k_2 + k_3 + k_4)k_{20} \quad (55)$$

$$K_{14} = (k_8 + k_9 + k_{20})/(k_8 + k_9)\,k_{20} \quad (56)$$

$$K_{15} = (k_{10} + k_{11} + k_{20})/(k_{10} + k_{11})\,k_{20} \quad (67)$$

$$K_{16} = (k_{12} + k_{13} + k_{20})/(k_{12} + k_{13})\,k_{20} \quad (58)$$

$$K_{17} = (k_{17} + k_{20})/k_{17}\,k_{20} \quad (59)$$

$$K_{18} = (k_{18} + k_{20})/k_{18}\,k_{20} \quad (60)$$

$$K_{19} = (k_{19} + k_{20})/k_{19}\,k_{20} \quad (61)$$

$$K_{20} = k_{-21}/k_{21} \quad (62)$$

There are 28 unknown constants: K_i (i = 1–20), the kinetic constants for the enzymatic reaction, and k_j (j = 22–29), the constants for acyl migrations.

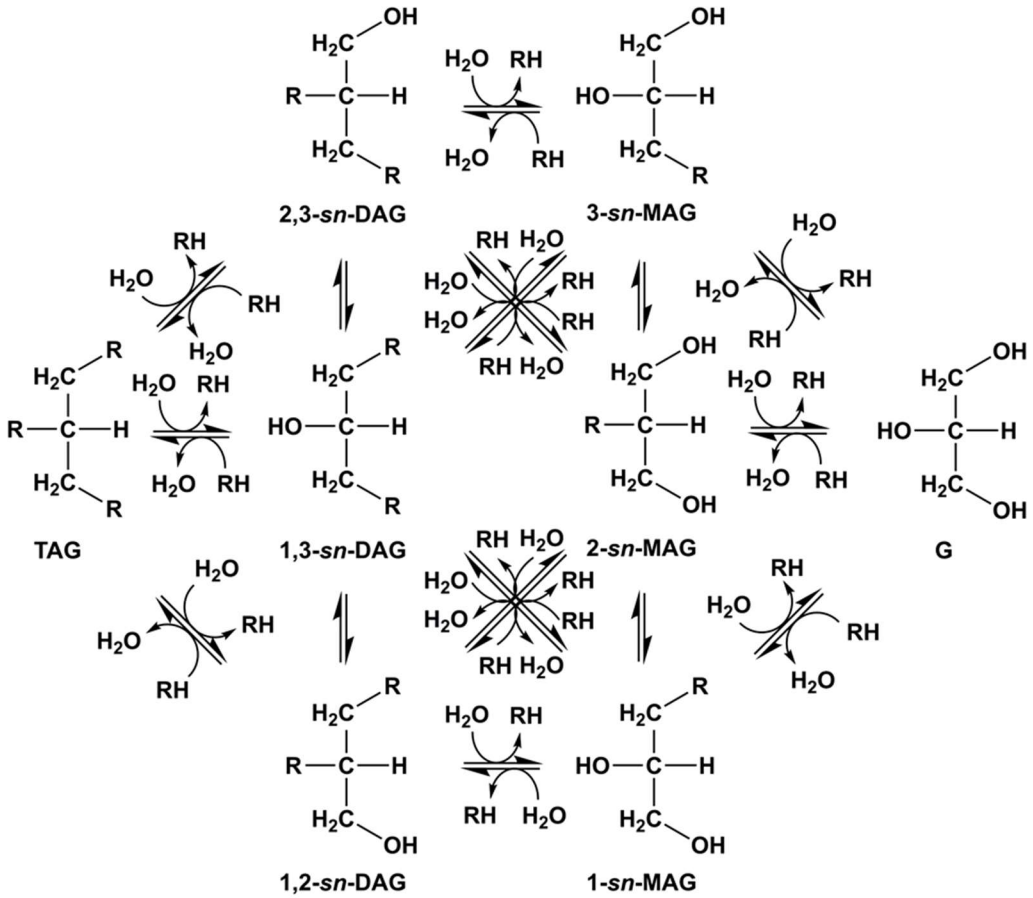

Figure II-1. Schematic diagram of lipase-catalyzed hydrolysis of triacylglycerol (TAG). Hydrolysis of TAG sequentially produces diacylglycerol (DAG), monoacylglycerol (MAG), and glycerol (G). Hydrolysis, and esterification are represented by horizontal, and diagonal arrows. Acyl migrations between DAGs and MAGs are represented by vertical arrows. R represents the fatty acyl moiety.

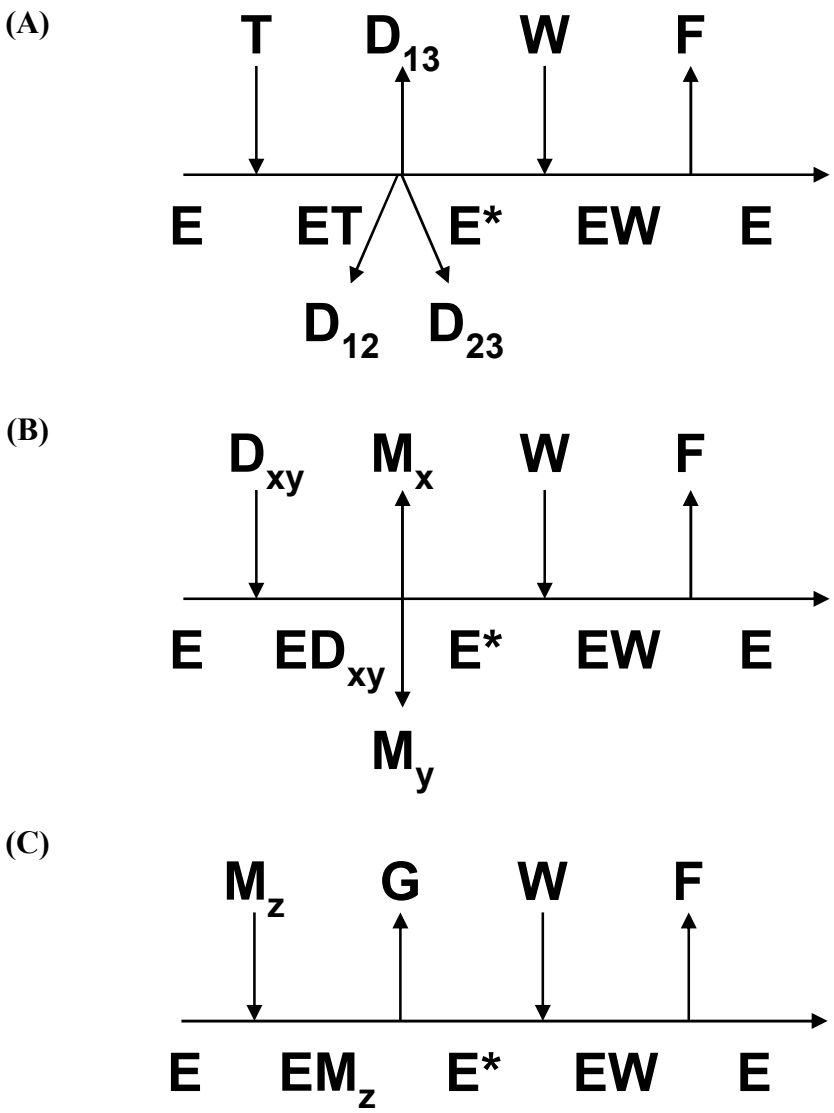

Figure II-2. Schematic diagram of the Ping-Pong Bi-Bi mechanism underlying lipase-catalyzed hydrolysis of (A) triacylglycerol, (B) diacylglycerols, and (C) monoacylglycerols with cleavage of the ester bond at respective *sn*-1, *sn*-2 and *sn*-3 positions. The (x, y) subscript denotes one of the (1, 2), (1, 3) and (2, 3) pairs, whereas z denotes 1, 2 or 3.

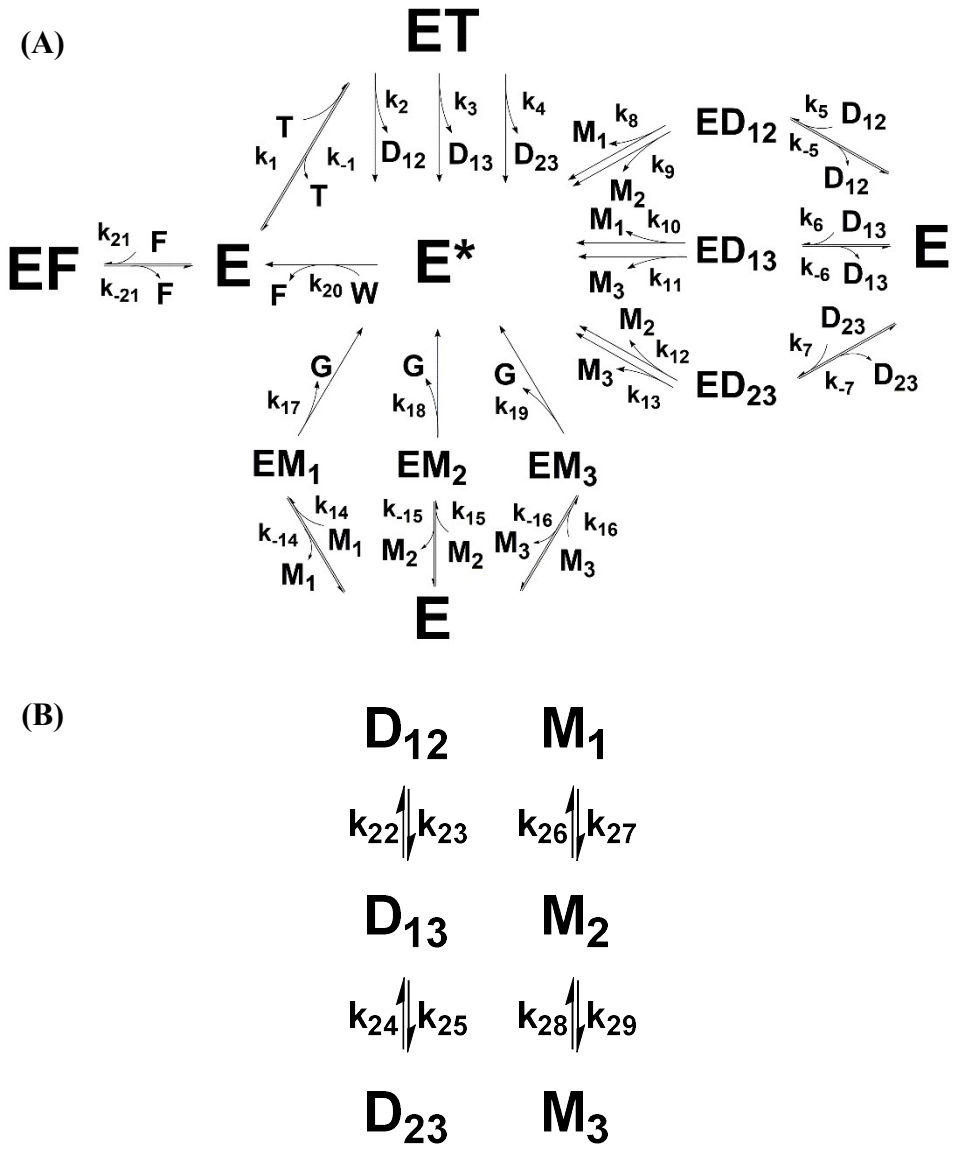

Figure II-3. Conceptual scheme of the overall reaction based on the (A) Ping-Pong Bi-Bi mechanism of lipase and (B) acyl migration for stepwise triacylgylcerol hydrolysis.

II-2-4-2. Fitting of the kinetic model

The model parameters, K_i and k_j, were estimated by fitting the experimental data through the minimization of the objective function:

$$f = 2S_1 S_2/(S_1 + S_2) \quad (63)$$

$$S_1 = \sum_k^{NOBS} \sum_l^{NCOM} (X_{kl}^{exp} - X_{kl}^{calc})^2 \quad (64)$$

$$S_2 = \sum_k^{NOBS} \sum_l^{NCOM} ((X_{kl}^{exp} - X_{kl}^{calc})/X_{kl}^{exp})^2 \quad (65)$$

where NOBS, NCOM, X_{kl}^{exp} and X_{kl}^{calc} denote the number of experimental observations, the number of components in the fitting procedure, and the experimental and calculated concentration of the component. A computational code was developed and implemented including simultaneous differential equations, Eqns 34–41, for the parameter estimation procedure with the software MATLAB R2019b. The subroutine 'ode45' was used to solve the differential equations and the 'fmincon' optimization subroutine was used to minimize the objective function (Eqn 63). When an experimental concentration of component was zero, the term involving that experimental value was excluded in the calculation to avoid division by zero.

II-3. Results and discussion

II-3-1. Separation and quantification of OA and oleoylglycerols

The chromatogram in Figure II-4A shows the separation of OA, all isomers of MOG and DOG, and TOG on the CHIRALPAK IA column. The peaks corresponding to OA, 1-*sn*- and 2-*sn*-MOG, 1,2-*sn*- and 1,3-*sn*-DOG, and TOG were identified by injecting each standard compound, while those of 3-*sn*-MOG and 2,3-*sn*-DOG were identified by comparison with racemic and enantiomeric standards. The eight molecular species were eluted in the order of OA, 2-*sn*-MOG, 3-*sn*-MOG, 1-*sn*-MOG, 2,3-*sn*-DOG, 1,2-*sn*-DOG, 1,3-*sn*-DOG, and TOG. The injection of the reaction mixture of TOG hydrolysis by PFL confirmed that the separation was not affected by other components, including AOT, which eluted at about 4.9 min (Figure II-4B). However, when injecting the reaction medium containing only olive oil, the representative of high-oleic oils, it was observed that several peaks of compounds other than TOG were present in olive oil (Figure II-4C). Since the peak at a retention time of 15.8 min had interference with 1,2-*sn*-DOG and 1,3-*sn*-DOG, it would be needed to apply further purification or separation steps to analyze high-oleic oils, including olive oil, and their lipase-catalyzed

modification process. Still, the present analytical system was available for the separation of hydrolysis products of TOG, which is an adequate substrate for the determination of stereoselectivity of lipase.

Table II-1 describes the quality of separation and quantification of the HPLC method for each analyte. The enantiomers of MOG and DOG were separated with *Rs* of more than 1.52 and α of more than 1.05 while achieving an analysis time of 20 minutes. These results were comparable to those obtained in a previous study on the simultaneous separation of oleoylglycerol isomers using tandem-column HPLC having *Rs* lower than 1.20 and 73-min run time (Deng, Nakano, & Iwasaki, 2007). Furthermore, the use of a silica column in the previous study does not fully exclude the acyl migration of MAGs and DAGs. This potential problem was mitigated in the current study by employing a single CSP column.

The selection of stationary phase and the mobile phase was based on a previous report showing that isomers of MAGs and DAGs with a variety of unsaturated fatty acid chains could be resolved on the same amylose tris-(3,5-dimethylphenylcarbamate) column, *i.e.*, CHIRALPAK IA, using a mixture of acetonitrile and methanol as the mobile phase (Itabashi & Kuksis, 2009). Enantiomeric 2,3-*sn*-DOG and 1,2-*sn*-DOG were separated with much higher resolution compared to normal-phase HPLC using acetonitrile-methanol (90:10, v/v). However, the present study examines the lipase-catalyzed

hydrolysis of TOG. Therefore, we used acetone instead of methanol, the latter showing restricted solubility toward TAGs and therefore not suitable for precise quantification of TOG.

The relative standard deviations of the retention times of all compounds were less than 1%, indicating good reproducibility. Calibration curves for each of the eight molecular species were obtained by injecting 10 μL of different concentrations of OA, 2-*sn*-MOG, 1-*sn*-MOG, 1-*rac*-MOG, 1,2-*sn*-DOG, 1,2-*rac*-DOG, 1,3-*sn*-DOG, and TOG. As shown in Table 1, all species had excellent linear fits (coefficient of determination > 0.986) based on double logarithmic plots of peak area and analyte concentration. Using these calibration curves and six replicates of each analyte, the relative standard deviation of the concentration for each analyte was determined to be in the ranges of 0.60-1.85%. These results indicate that the present analytical method is reproducible and suitable for the separation and quantitation of mixtures containing OA, MOGs, DOGs, and TOG.

(A)

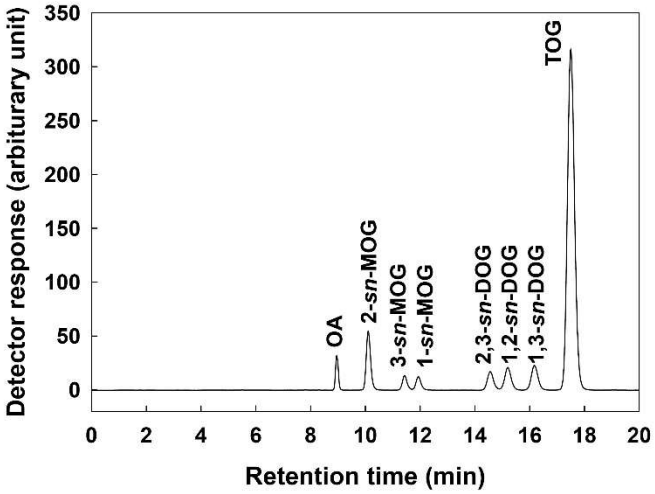
Detector response (arbituraru unit)
Retention time (min)
OA
2-sn-MOG
3-sn-MOG
1-sn-MOG
2,3-sn-DOG
1,2-sn-DOG
1,3-sn-DOG
TOG

(B)

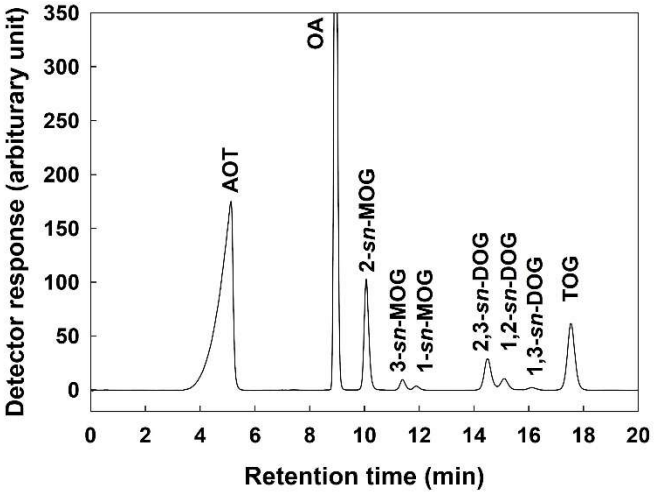
Detector response (arbituraru unit)
Retention time (min)
AOT
OA
2-sn-MOG
3-sn-MOG
1-sn-MOG
2,3-sn-DOG
1,2-sn-DOG
1,3-sn-DOG
TOG

(C)

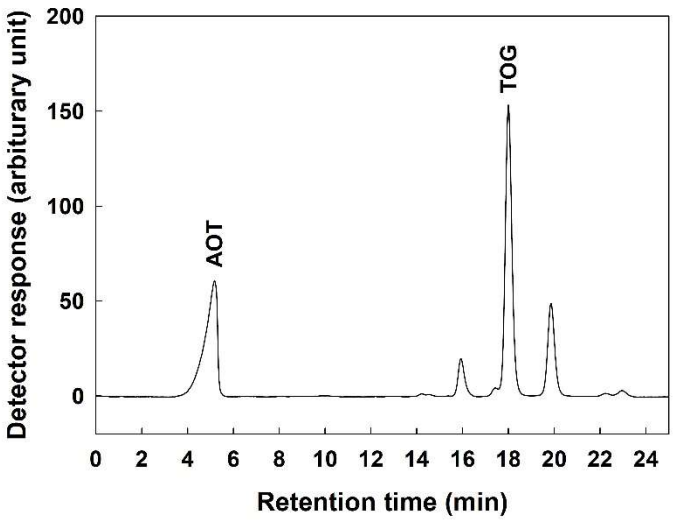

Figure II-4. Chromatographic resolution of all types of oleoylglycerols and oleic acid (OA) on a chiral stationary phase high-performance liquid chromatography system. Chromatograms were obtained by injecting (A) a mixture of standard compounds, (B) reaction mixtures of lipase-catalyzed trioleoylglycerol (TOG) hydrolysis at 12 h, and (C) reaction medium containing olive oil (17.7 mg/mL) instead of TOG.

Table II-1. Chromatographic data for oleic acid and oleoylglycerols on the chiral stationary phase HPLC system

Molecular species	Retention time (min)	α[a]	R_s[b]	RSD%, retention time (n=9)	RSD%, measurement (n=6)	Calibration range (µM)	Calibration points	Calibration curve[c]	R^2[d]
OA	8.98	-	-	0.04	0.60	137–577	6	y = 3.215 x – 2.903	0.9975
2-*sn*-MOG	10.12	1.17	4.80	0.09	1.31	26–350	8	y = 1.170 x + 1.714	0.9963
3-*sn*-MOG	11.45	1.17	4.41	0.10	1.16	27–130	6	y = 1.963 x + 1.334	0.9900
1-*sn*-MOG	11.95	1.06	1.56	0.02	1.85	32–182	7	y = 1.560 x + 1.848	0.9949
2,3-*sn*-DOG	14.68	1.28	7.02	0.13	1.65	11–145	10	y = 1.573 x + 2.781	0.9937
1,2-*sn*-DOG	15.35	1.05	1.52	0.21	1.52	34–460	10	y = 1.598 x + 2.462	0.9981
1,3-*sn*-DOG	16.34	1.08	2.23	0.12	1.60	57–430	8	y = 1.697 x + 1.834	0.9868
TOG	17.50	1.10	2.88	0.04	1.40	80–1060	10	y = 1.513 x + 2.811	0.9995

[a]Separation factor between preceding peak
[b]Resolution factor between preceding peak
[c]y = log(peak area), x = log(concentration in µM)
[d]Coefficient of determination

II-3-2. Stereoselectivity of model lipases on trioleoylglycerol

The selectivity of lipase for ester bonds at the *sn*-1, *sn*-2, and *sn*-3 positions of a prochiral substrate, which is TOG in this study, was investigated by obtaining time courses of 1,2-*sn*-DOG, 2,3-*sn*-DOG, and 1,3-*sn*-DOG during TOG hydrolysis. Figures II-5, 6, 7, and 8 show the changes in concentrations of OA, MOGs, DOGs, and TOG as a function of reaction time when PPL, CVL, PFL, and CALA were used, respectively.

In the case of PPL, it is observed that an increase in OA was accompanied by a decrease in TOG at 24 h when the degree of hydrolysis reached 41.6% (Figure II-5A). Concentrations of 2,3-*sn*-DOG and 1,2-*sn*-DOG increased to 3.03 and 2.97 mM after 2 h, respectively, and decreased thereafter. In contrast, the concentration of 1,3-*sn*-DOG was not detected until 6 h and increased to 0.47 mM after 24 h (Figure II-5B). At the early phase of hydrolysis, the ratio of 2,3-*sn*-DOG, 1,3-*sn*-DOG, and 1,2-*sn*-DOG among DOGs was 47.7%, 0%, and 52.3%, respectively. Therefore, the low difference in the ratio of 2,3-*sn*-DOG and 1,2-*sn*-DOG during the initial phase of hydrolysis indicated that PPL did not exhibit a stereopreference for the *sn*-1 or *sn*-3 position of TOG. This finding corresponds to previous reports on the stereoselectivity of PPL during hydrolysis of prochiral TAGs (Carrière, Rogalska, Cudrey, Ferrato, Laugier, & Verger, 1997; Rodriguez et al., 2008; Rogalska, Cudrey, Ferrato, & Verger, 1993). The transitory cumulation of 2,3-

sn-DOG and 1,2-*sn*-DOG indicates that the rates of their hydrolysis into MOGs exceeded those of their formation from TOG hydrolysis. Figure II-5C shows that the concentrations of 2-*sn*-MOG, 3-*sn*-MOG, and 1-*sn*-MOG increased to 7.88, 0.98, and 0.76 mM, respectively. Note that concentrations of 1-*sn*-MOG and 1-*sn*-MOG were not detected during the early phase of hydrolysis. This indicates that the main positions of hydrolysis were *sn*-3 for 2,3-*sn*-DOG and *sn*-1 for 1,2-*sn*-DOG, respectively.

The CVL-catalyzed hydrolysis of TOG exhibited initial accumulation of 2,3-*sn*-DOG and 1,2-*sn*-DOG with their maximum at 2 and 5 h, respectively, while 1,3-*sn*-DOG remained not detected until 24 h (Figure II-6B). At degree of hydrolysis 2.6%, the ratio of 2,3-*sn*-DOG, 1,3-*sn*-DOG, and 1,2-*sn*-DOG was 64.1%, 0%, and 35.9%, respectively. This result indicated that CVL exhibits a stereopreference for the *sn*-3 position of TOG, which was comparable to that of a previous report which carried out the hydrolysis of an emulsion system (Rogalska et al., 1993). Among MOGs, 2-*sn*-MOG reached its maximum of 12.10 mM at 5 h and decreased thereafter, while 3-*sn*-MOG and 1-*sn*-MOG increased to 1.13 and 1.71 mM, respectively (Figure II-6C). Therefore, it is expected that the main positions for DOG hydrolysis of CVL were as same as that of PPL.

In contrast to PPL and CVL, PFL produced all DOG isomers from the early phase of TOG hydrolysis (Figure II-7B). At degree of hydrolysis 7.6%,

the DOGs consisted of 74.1% 2,3-*sn*-DOG, 16.5% 1,3-*sn*-DOG, and 9.4% 2,3-*sn*-DOG. This indicates that the selectivity of PFL for TOG in reverse micelle is in the order of *sn*-1, *sn*-2, and *sn*-3. This result showed that PFL in the reverse micelle is capable of hydrolyzing the ester bond of TOG at the *sn*-2 position, which is in contrast to the previous report that PFL is a 1,3-regiospecific lipase on TOG in an emulsion system (Rogalska et al., 1993). However, it has also been reported that the PFL exhibited hydrolysis of the ester bond at the *sn*-2 position instead of strict 1,3-specificity in aprotic organic media at a low water content (Berger & Schneider, 1991), which is a similar condition to that of the present study. Although the effect of the organic solvent on the positional preference of lipase remains unclear, this shift in positional preference might be related to the local interaction of solvent molecules with hydrophobic residues having increased flexibility (Kamal, Yedavalli, Deshmukh, & Rao, 2013; Tejo, Salleh, & Pleiss, 2004). However, the proportion of 2,3-*sn*-DOG decreased to 47.0%, while that of 1,2-*sn*-DOG increased to 32.4% after 24 h. The decrease of a gap between the proportions of 2,3-*sn*-DOG and 1,2-*sn*-DOG indicates that PFL preferentially hydrolyzed 2,3-*sn*-DOG over 1,2-*sn*-DOG. In addition, the concentration of 2-*sn*-MOG was the highest among MOGs throughout the entire reaction time (Figure II-7C), indicating that the *sn*-3 position of 2,3-*sn*-DOG and *sn*-1 position of 1,2-*sn*-DOG were the preferred sites of hydrolysis.

The CALA-catalyzed TOG hydrolysis exhibited the most different feature from the other lipases tested. At degree of hydrolysis 11.4%, the proportions of 1,3-*sn*-DOG, 2,3-*sn*-DOG, and 1,2-*sn*-DOG were 54.9, 27.3, and 17.7%, respectively (Figure II-8B). This result was comparable to the proportion from the previous work in emulsion system, which were 68.8, 18.6, and 12.6%, respectively, indicating that CALA shows the highest selectivity on *sn*-2 position of TOG (Rogalska et al., 1993). Note that 2-*sn*-MOG, which was the most abundant MOGs in TOG hydrolysis by the other lipases, showed the lowest concentration among MOGs in CALA-mediated hydrolysis (Figure II-8C). This phenomenon is ascribed to that 2-*sn*-MOG can be produced only from hydrolysis at *sn*-3 position of 2,3-*sn*-DOG and *sn*-1 position as shown in Figure II-1. In addition, acyl migration likely affected the proportions of DOGs and MOGs. Therefore, it is necessary to apply an appropriate kinetic model to the data to quantify the integral stereoselectivity, considering the entire reaction process of TAG hydrolysis in terms of reaction rate constants.

(A)

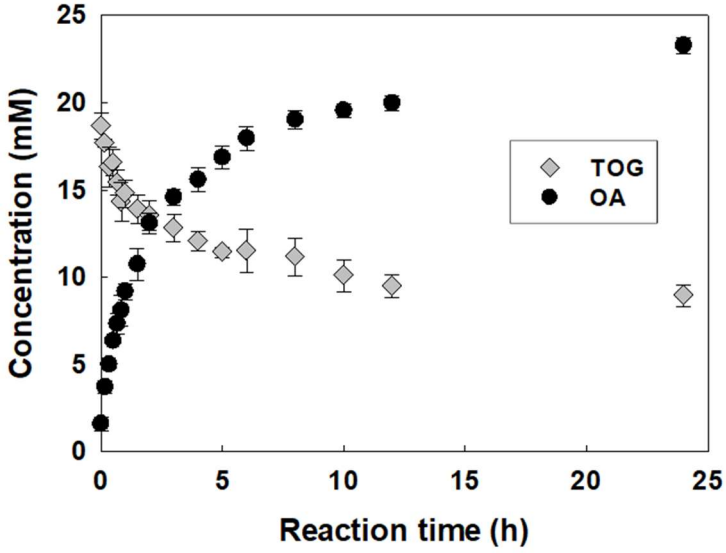
Concentration (mM)
Reaction time (h)
TOG
OA
0
5
10
15
20
25

(B)

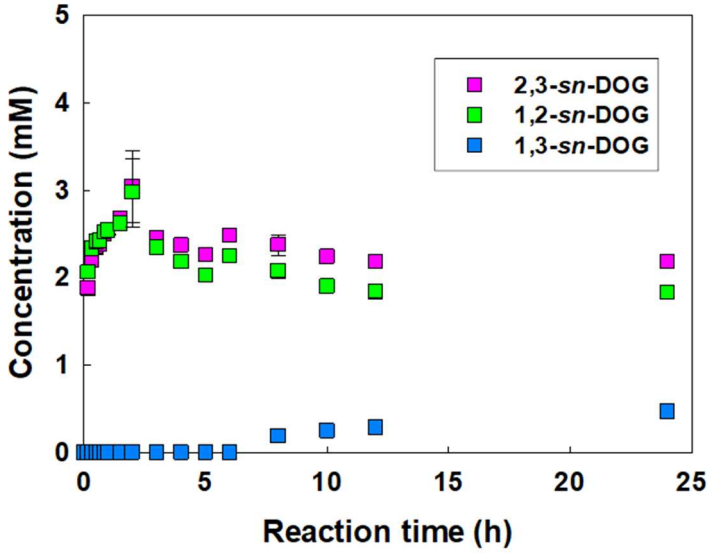
Concentration (mM)
Reaction time (h)
2,3-sn-DOG
1,2-sn-DOG
1,3-sn-DOG
0
1
2
3
4
5
0
5
10
15
20
25

(C)

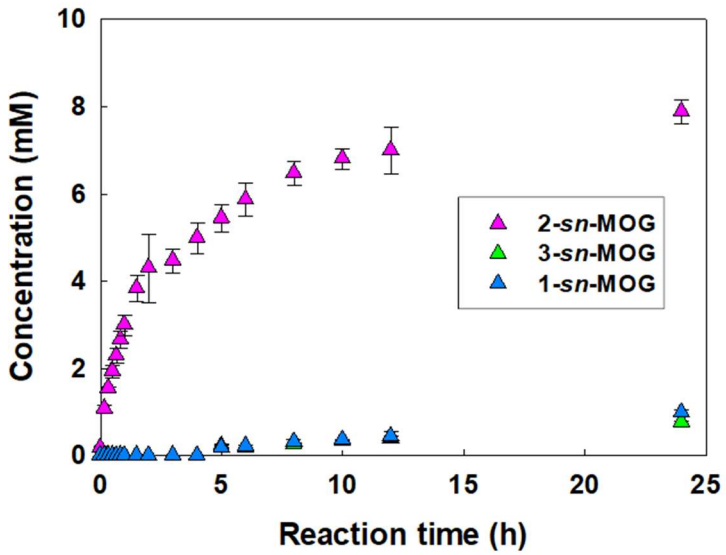

Figure. II-5. Acylglycerol species during the hydrolysis of trioleoylglycerol (TOG), catalyzed by lipase from porcine pancreas in reverse micelle. (A) TOG and oleic acid (OA), (B) dioleoylglycerol (DOG), and (C) monooleoylglycerol (MOG). The data are presented as means with standard deviations (n=3).

(A)

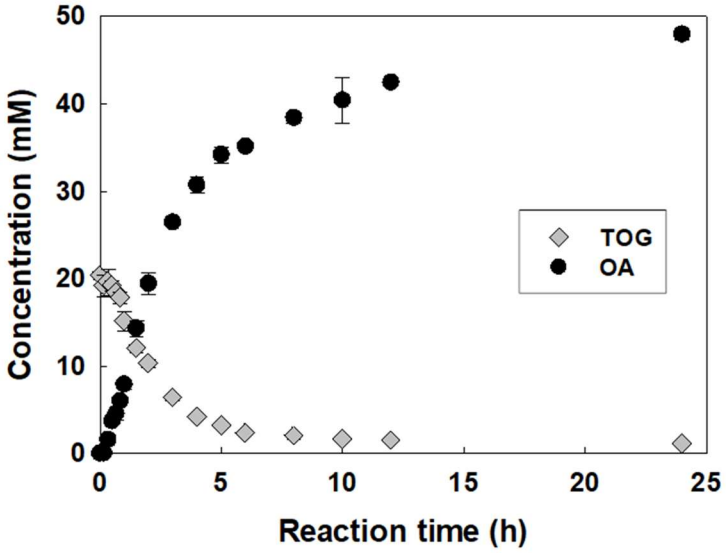
Concentration (mM)
Reaction time (h)
TOG
OA
0
10
20
30
40
50
0
5
10
15
20
25

(B)

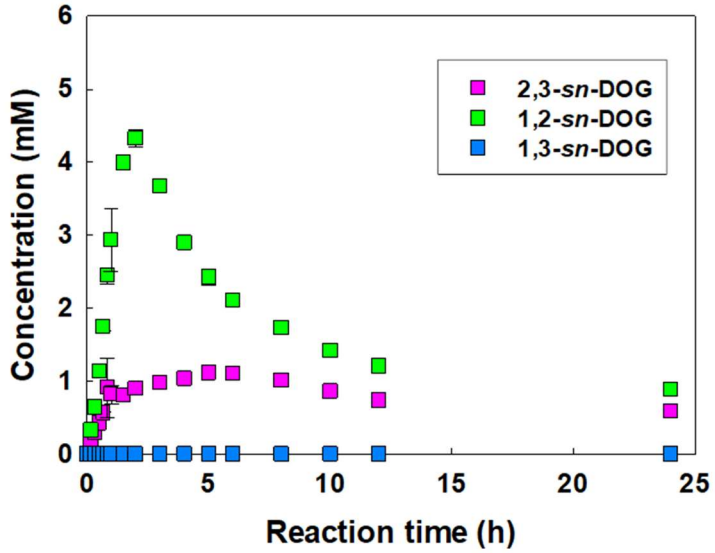
Concentration (mM)
Reaction time (h)
2,3-sn-DOG
1,2-sn-DOG
1,3-sn-DOG
0
1
2
3
4
5
6
0
5
10
15
20
25

(C)

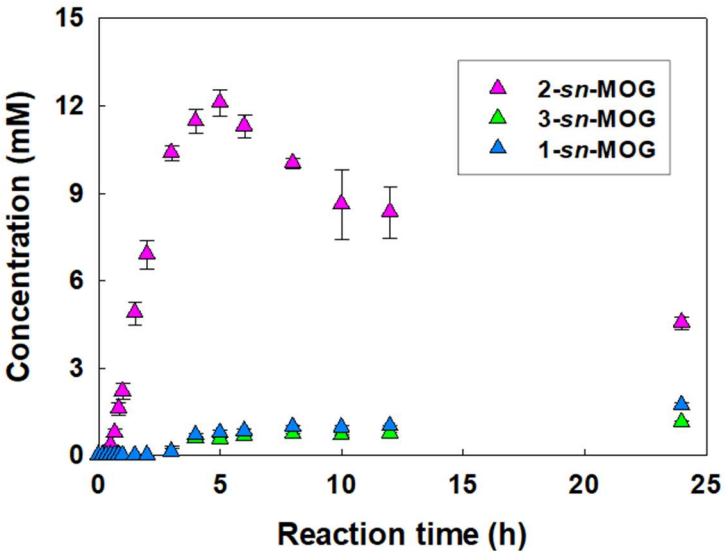

Figure II-6. Acylglycerol species during the hydrolysis of trioleoylglycerol (TOG), catalyzed by lipase from *Chromobacterium viscosum* in reverse micelle. (A) TOG and oleic acid (OA), (B) dioleoylglycerol (DOG), and (C) monooleoylglycerol (MOG). The data are presented as means with standard deviations (n=3).

(A)

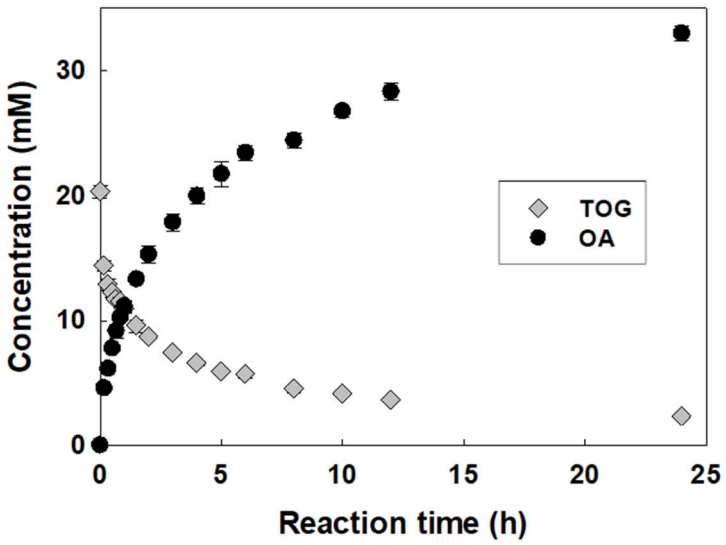
Concentration (mM)
Reaction time (h)
TOG
OA
0
10
20
30
0
5
10
15
20
25

(B)

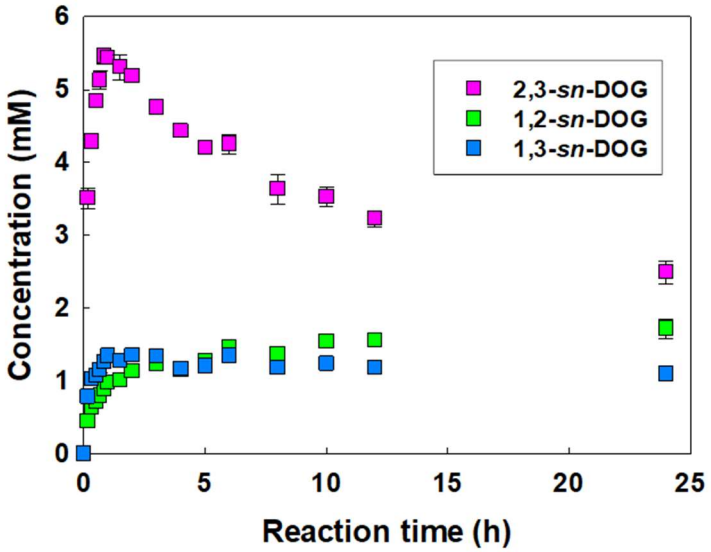
Concentration (mM)
Reaction time (h)
2,3-sn-DOG
1,2-sn-DOG
1,3-sn-DOG
0
1
2
3
4
5
6
0
5
10
15
20
25

(C)

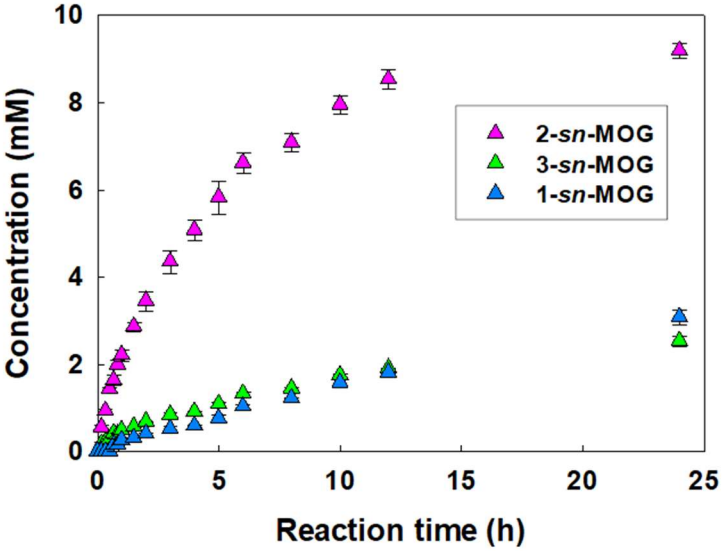

Figure II-7. Acylglycerol species during the hydrolysis of trioleoylglycerol (TOG), catalyzed by lipase from *Pseudomonas fluorescens* in reverse micelle. (A) TOG and oleic acid (OA), (B) dioleoylglycerol (DOG), and (C) monooleoylglycerol (MOG). The data are presented as means with standard deviations (n=3).

(A)

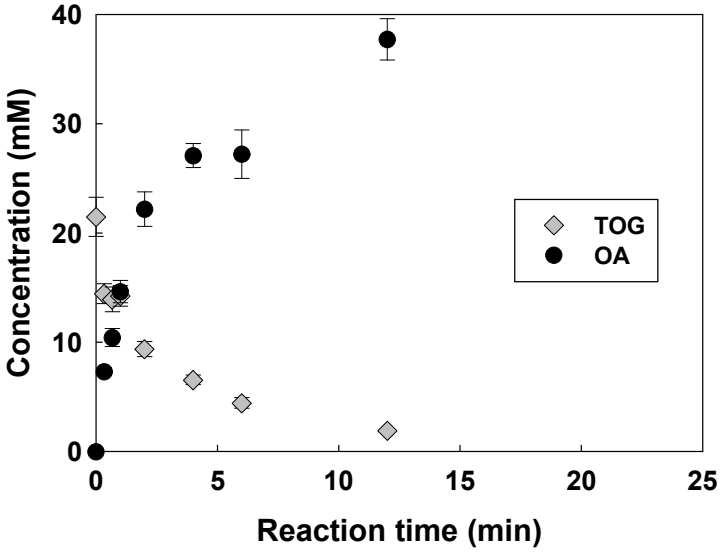
Concentration (mM)
Reaction time (min)
TOG
OA
0
10
20
30
40
0
5
10
15
20
25

(B)

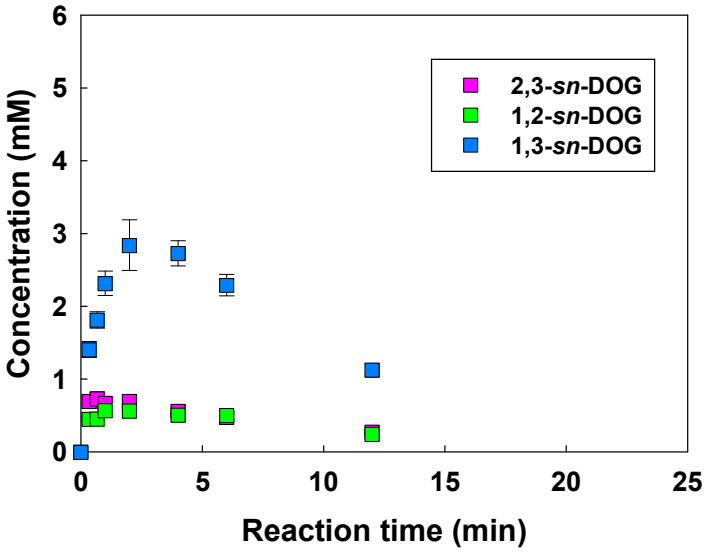
Concentration (mM)
Reaction time (min)
2,3-sn-DOG
1,2-sn-DOG
1,3-sn-DOG
0
1
2
3
4
5
6
0
5
10
15
20
25

(C)

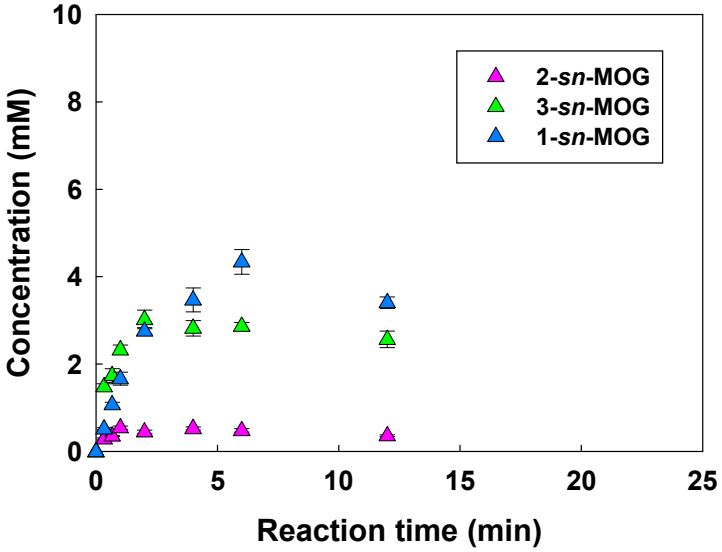

Figure II-8. Acylglycerol species during the hydrolysis of trioleoylglycerol (TOG), catalyzed by lipase A from *Candida antarctica* in reverse micelle. (A) TOG and oleic acid (OA), (B) dioleoylglycerol (DOG), and (C) monooleoylglycerol (MOG). The data are presented as means with standard deviations (n=3).

II-3-3. Integral stereoselectivity of model lipases on trioleoylglycerol from kinetic modeling

The time-course profiles of TOG hydrolysis catalyzed by PPL, CVL, and PFL with varying initial TOG concentrations are shown in Figures II-9, 10, 11, respectively. In the case of PPL, when the initial TOG concentration increased from 10 to 20 and 30 mM, the consumption of TOG and formation of OA decreased, while there were no significant differences between 20 and 30 mM (Figure II-9A). For CVL, there were less deviations in the consumption or formation rate of TOG and OA than for PPL (Figure II-10A). However, transitory cumulations of 1,2-*sn*-DOG and 2,3-*sn*-DOG were observed with a higher formation rate and maximum value according to increasing initial TOG concentration (Figure II-9B). The PFL-catalyzed reaction showed decreasing TOG consumption and OA formation rate with increasing initial TOG concentration (Figure II-10A). Accordingly, 20 mM of TOG concentration was used to obtain the time course of the hydrolysis catalyzed by CALA (Figure II-11). In all cases, the best fit of the models were in good agreement with the experimental results with satisfactory values of determination coefficient (R^2), which were calculated to be 0.96, 0.98, 0.99, and 0.97 for PPL, CVL, PFL, and CALA, respectively.

To assess differences in integral stereoselectivity among the lipases, kinetic parameters were established and estimated (Table II-2). The kinetic

constants K_1–K_3, K_4–K_9 and K_{10}–K_{12} represent the conversion rate of TAG, DAGs, and MAGs into DAGs, MAGs, and glycerol through acylation step in lipase-catalyzed hydrolysis, respectively. For PPL, the reaction rates of hydrolysis at the *sn*-1 and *sn*-3 positions of TOG respectively, K_3 and K_1, were similar and much higher than that at the *sn*-2 position, K_2. In DOG hydrolysis, K_5 and K_8 representing the conversion of respectively, the *sn*-1 position of 1,2-*sn*-DOG and the *sn*-3 position of 2,3-*sn*-DOG, were the two highest values, following the increase of 2-*sn*-MOG (Figure II-9C). It is worth noting that K_4 and K_9, representing conversion at the *sn*-2 position of 1,2-*sn*-DOG and 2,3-*sn*-DOG, respectively, were lower than K_5 and K_8, which matches the time course of 1-*sn*- and 3-*sn*-MOG (Figure II-9C) and the kinetic model-based outcome of Hermansyah et al., who reported that PPL preferred the *sn*-2 position over the *sn*-1 or *sn*-3 position of DOGs (Hermansyah, Wijanarko, Kubo, Shibasaki-Kitakawa, & Yonemoto, 2010). Although the constant associated with the conversion of *sn*-1-MOG, K_{10}, was the highest in MOG consumption, all three values were far lower than those for TOG or DOG conversion. On the other hand, CVL exhibited *sn*-3 stereoselectivity for TOG conversion based on a value of K_1 higher than K_3, with negligible K_2. Cleavage of the *sn*-1 position of 1,2-*sn*-DOG by CVL was the only significant reaction in DOG conversion judging from K_4–K_9. In accordance with the rapid decrease of 2-*sn*-MOG (Figure II-10C), K_{11} was the highest among K_{10}–K_{12}.

In the case of PFL, the selectivity for TOG appeared in the order of *sn*-1, *sn*-2, and *sn*-3 as the kinetic parameters were in the order of K_3, K_2, and K_1. Unlike PPL and CVL, the *sn*-3 position of 2,3-*sn*-DOG represented by K_8 was the most selective site, followed by the *sn*-1 and *sn*-3 positions of 1,3-*sn*-DOG, represented by K_7 and K_6, respectively. For MOG conversion by PFL, the selectivity was in the order of 2-*sn*-MOG, 1-*sn*-MOG, and 3-*sn*-MOG, judging from K_{11}, K_{10}, and K_{12}. For CALA, K_2 was the highest value followed by K_1, and K_3, indicating that the selectivity for TOG was in the order of *sn*-2, *sn*-3, and *sn*-1. The distinguishing characteristic of CALA from other lipases was revealed in DOG conversion, in which K_6 and K_7 representing the consumption of 1,3-*sn*-DOG were the top two values. In MOG conversion by CALA, the selectivity was in the order of 1-*sn*-MOG, 3-*sn*-MOG, and 2-*sn*-MOG, judging from K_{10}, K_{12}, and K_{11}.

To describe the whole process of TOG hydrolysis, the reactions catalyzed by the four lipases considering integral stereoselectivity are visually summarised in Figure II-13. The main reaction is designated as red arrows along with stepwise TOG hydrolysis. For PPL, the main pathway of reaction progress is from TOG to 1,2-*sn*-DOG and 2,3-*sn*-DOG at a similar rate, and then to 2-*sn*-MOG. For CVL, the main pathway went from TOG to 2,3-*sn*-DOG, 2-*sn*-MOG, and glycerol. In contrast to PPL and CVL, PFL exhibited significant selectivity for all *sn*-positions of TOG, with the main pathway

going from TOG to *sn*-2,3-DOG, 2-*sn*-MOG, and glycerol. For CALA, the main reaction pathway from TOG went through 1,3-*sn*-DOG, 1-*sn*-MOG, and glycerol.

The current kinetic model-based approach is necessary to analyze integral stereoselectivity because the lipase-catalyzed TAG hydrolysis consists of consecutive steps, with all three DAG and MAG isomers being potent substrates of lipase. Moreover, various acylglycerols exhibit different physicochemical characteristics depending on whether they are mixed or separated (Small, 1968), which changes the physicochemistry of the reaction and could affect the substrate recognition of lipase (Muralidhar, Chirumamilla, Marchant, Ramachandran, Ward, & Nigam, 2002) and eventually, its stereoselectivity. The previous kinetic modeling approaches for lipase-catalyzed TOG hydrolysis based on the mechanism of lipase activity considered these points (Hermansyah, Kubo, Shibasaki-Kitakawa, & Yonemoto, 2006), and fitting of the model to experimental data was improved by applying regioselectivity of the lipase (Hermansyah et al., 2010). However, there was no measurement of DAG or MAG isomers, limiting the application of such models in stereoselectivity analyses. Therefore, the present kinetic model represents the most comprehensive understanding of lipase stereoselectivity, as it considers all enzymatic hydrolysis steps and non-enzymatic acyl migrations of DOG and MOG isomers.

(A)

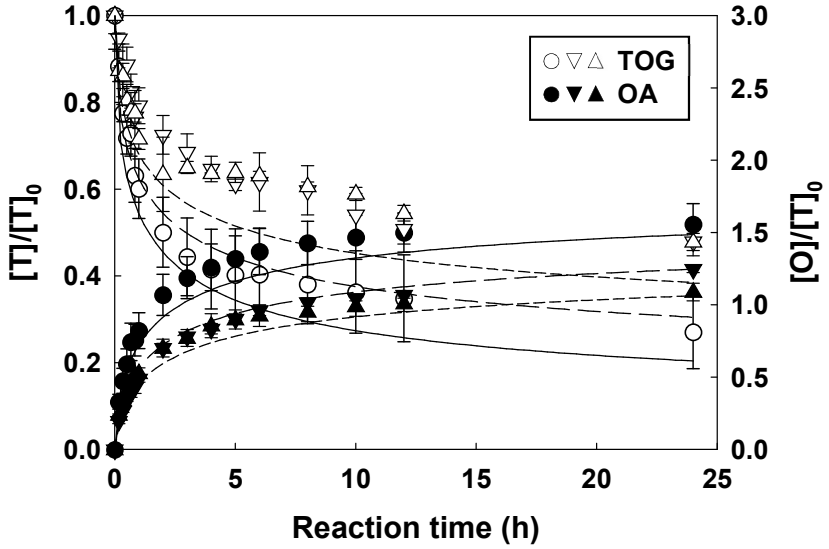
TOG
OA
[T]/[T]0
[O]/[T]0
Reaction time (h)

(B)

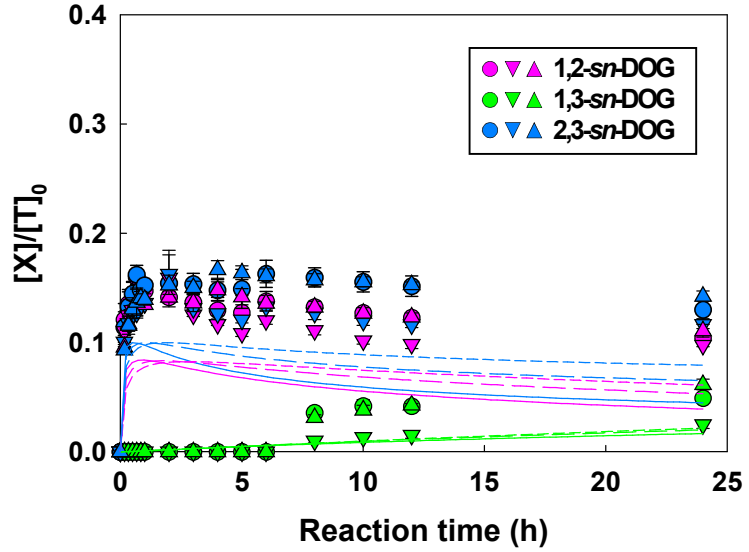
1,2-sn-DOG
1,3-sn-DOG
2,3-sn-DOG
[X]/[T]0
Reaction time (h)

(C)

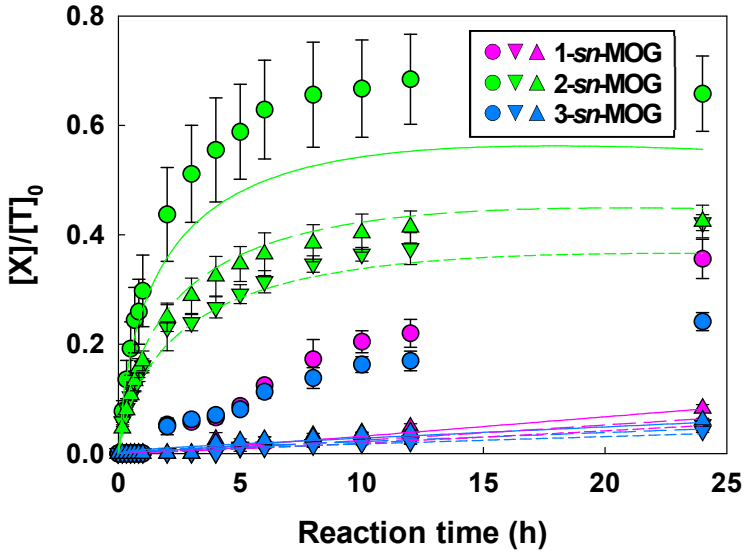

Figure II-9. Fitting of the kinetic model for trioleoylglycerol (TOG) hydrolysis when lipase from porcine pancreas was used with initial TOG concentrations of 10 mM (○, solid), 20 mM (▽, long dash), and 30 mM (△, short dash). (A) TOG and oleic acid (OA), (B) dioleoylglycerol (DOG), and (C) monooleoylglycerol (MOG).

(A)

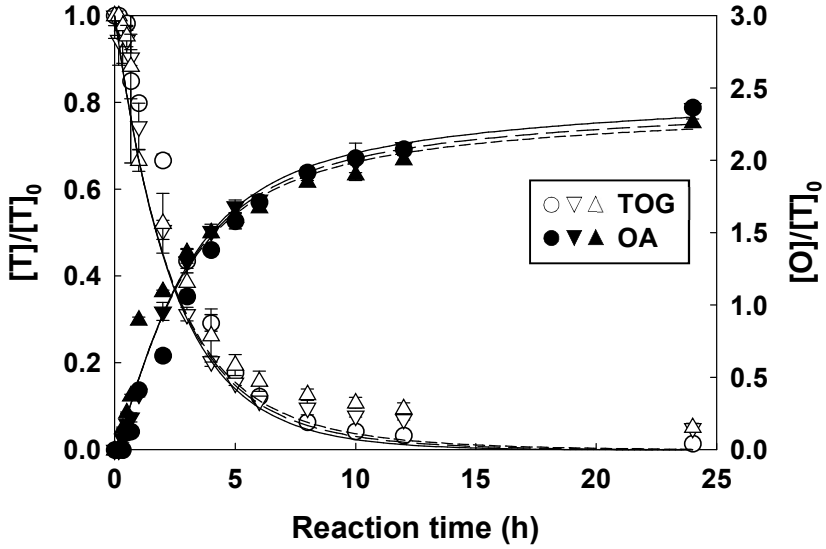
1.0
0.8
0.6
0.4
0.2
0.0
[T]/[T]0
3.0
2.5
2.0
1.5
1.0
0.5
0.0
[O]/[T]0
TOG
OA
0
5
10
15
20
25
Reaction time (h)

(B)

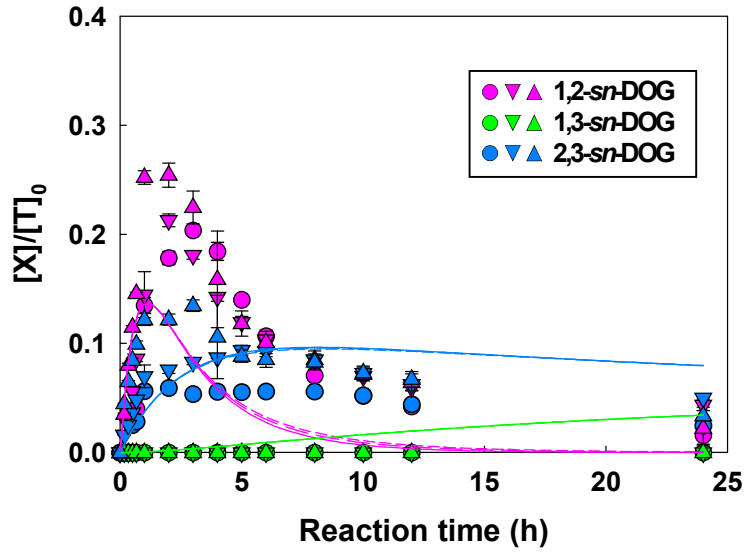
0.4
0.3
0.2
0.1
0.0
[X]/[T]0
1,2-sn-DOG
1,3-sn-DOG
2,3-sn-DOG
0
5
10
15
20
25
Reaction time (h)

(C)

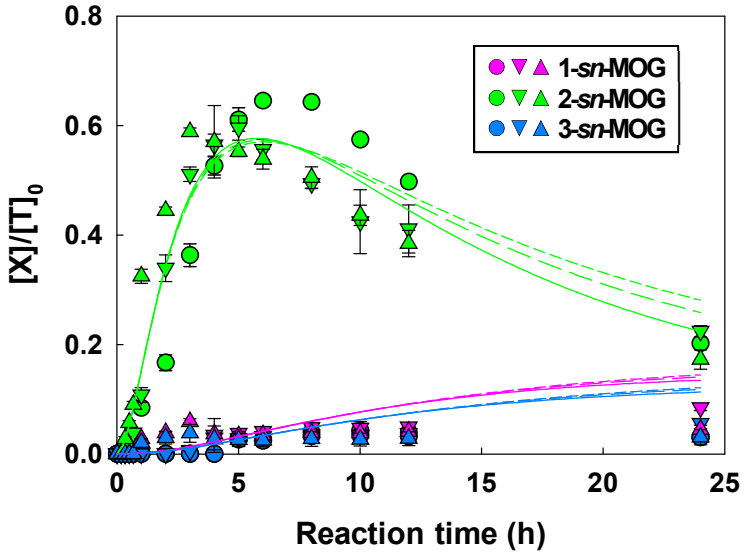

Figure II-10. Fitting of the kinetic model for trioleoylglycerol (TOG) hydrolysis when lipase from *Chromobacterium viscosum* was used with initial TOG concentrations of 10 mM (○, solid), 20 mM (▽, long dash), and 30 mM (△, short dash). (A) TOG and oleic acid (OA), (B) dioleoylglycerol (DOG), and (C) monooleoylglycerol (MOG).

(A)

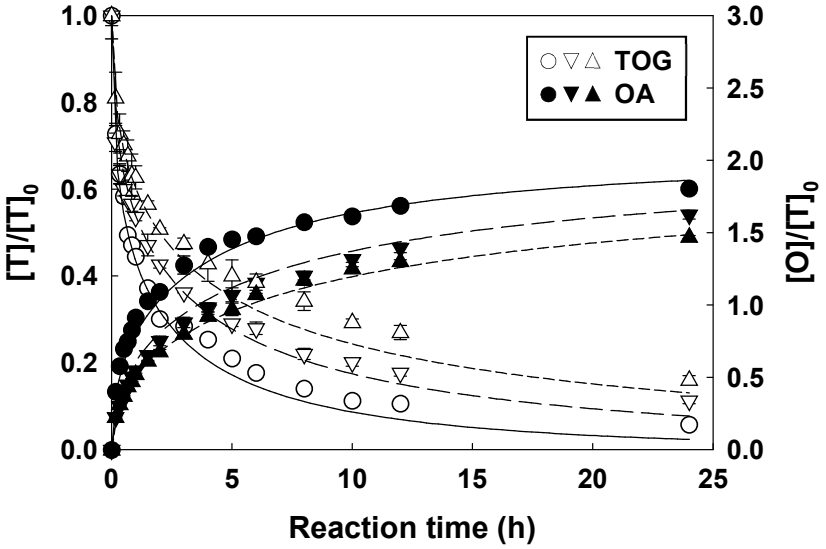
TOG
OA
[T]/[T]0
[O]/[T]0
Reaction time (h)

(B)

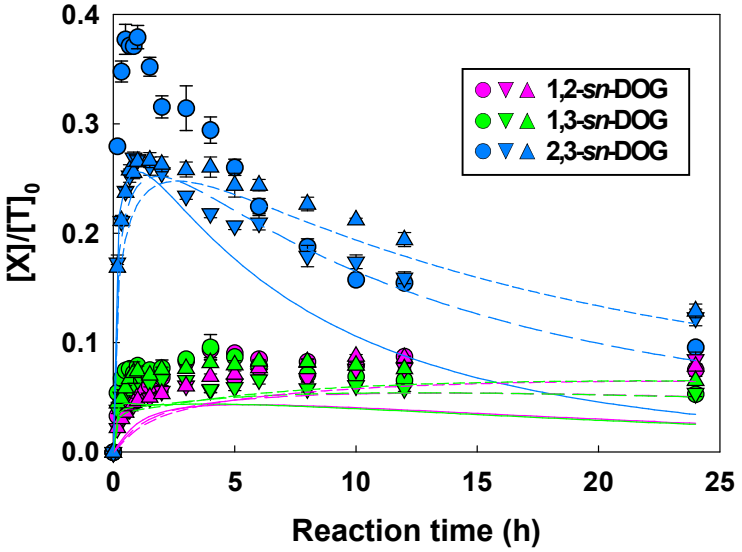
1,2-sn-DOG
1,3-sn-DOG
2,3-sn-DOG
[X]/[T]0
Reaction time (h)

(C)

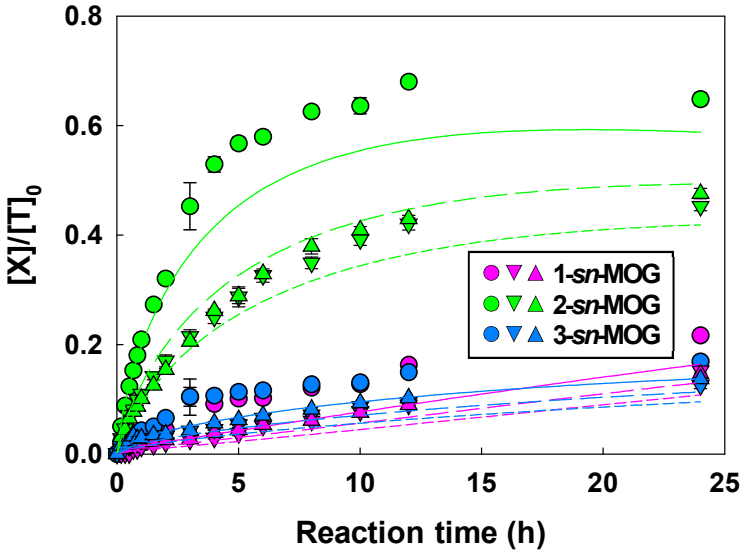

Figure II-11. Fitting of the kinetic model for trioleoylglycerol (TOG) hydrolysis when lipase from *Pseudomonas fluorescens* was used with initial TOG concentrations of 10 mM (○, solid), 20 mM (▽, long dash), and 30 mM (△, short dash). (A) TOG and oleic acid (OA), (B) dioleoylglycerol (DOG), and (C) monooleoylglycerol (MOG).

(A)

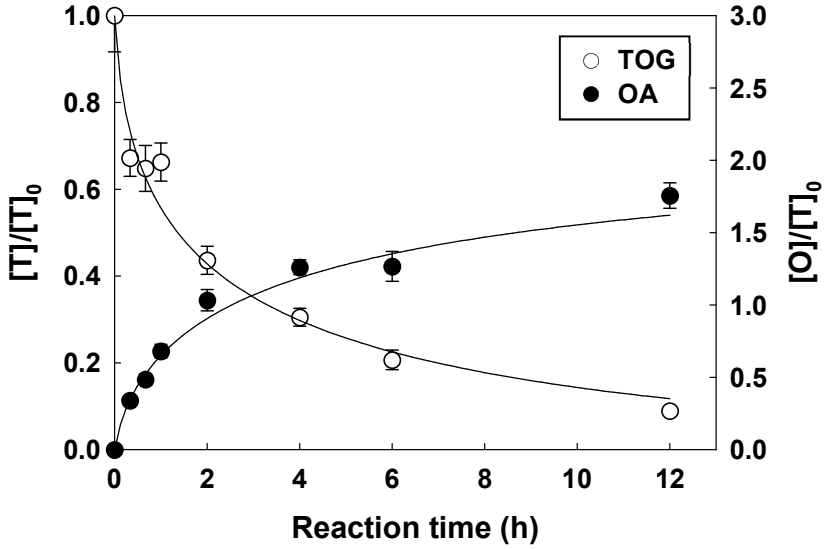
TOG
OA
[T]/[T]0
[O]/[T]0
Reaction time (h)

(B)

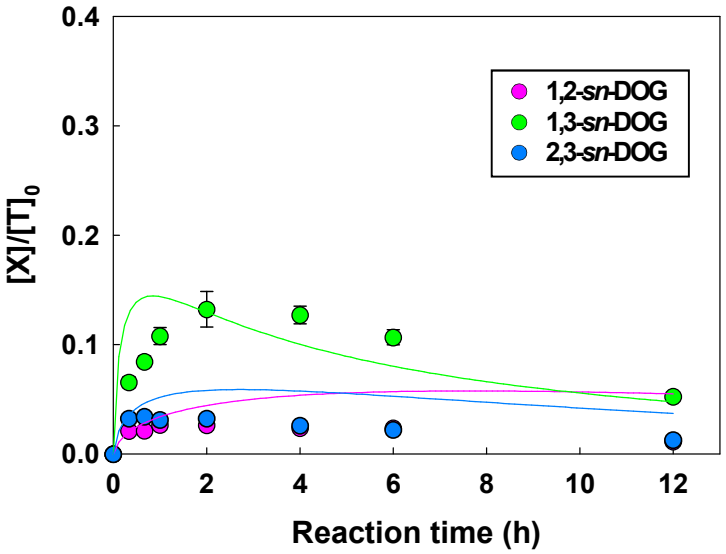
1,2-sn-DOG
1,3-sn-DOG
2,3-sn-DOG
[X]/[T]0
Reaction time (h)

(C)

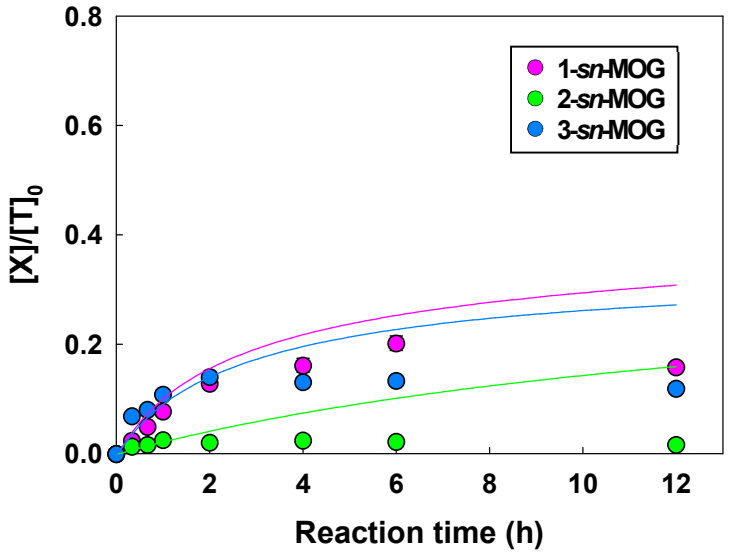

Figure II-12. Fitting of the kinetic model for trioleoylglycerol (TOG) hydrolysis when lipase A from *Candida antarctica* was used with initial TOG concentrations of 20 mM (○, solid). (A) TOG and oleic acid (OA), (B) dioleoylglycerol (DOG), and (C) monooleoylglycerol (MOG).

Table II-2. Values of kinetic parameters associated with trioleoylglycerol hydrolysis catalyzed by lipases from porcine pancreas (PPL), *Chromobacterium viscosum* (CVL), *Pseudomonas fluorescens* (PFL), and lipase A from *Candida antarctica* (CALA) estimated using the kinetic model

Kinetic constants	PPL	CVL	PFL	CALA
K_1 ($M^{-1}h^{-1}$)	7.52×10^{9}	6.70×10^{6}	3.75×10^{8}	1.00×10^{8}
K_2 ($M^{-1}h^{-1}$)	5.85×10^{3}	6.71	1.30×10^{10}	1.03×10^{9}
K_3 ($M^{-1}h^{-1}$)	1.13×10^{10}	8.63×10^{5}	5.93×10^{10}	2.12×10^{8}
K_4 ($M^{-1}h^{-1}$)	8.62×10^{08}	1.62×10^{2}	8.32×10^{06}	1.33×10^{8}
K_5 ($M^{-1}h^{-1}$)	4.81×10^{10}	3.10×10^{7}	8.55×10^{06}	3.98×10^{6}
K_6 ($M^{-1}h^{-1}$)	1.92×10^{06}	6.86×10^{2}	3.05×10^{10}	2.13×10^{9}
K_7 ($M^{-1}h^{-1}$)	2.19×10^{06}	3.22×10^{2}	6.72×10^{10}	1.93×10^{9}
K_8 ($M^{-1}h^{-1}$)	6.72×10^{10}	1.83×10^{2}	9.45×10^{10}	1.45×10^{9}
K_9 ($M^{-1}h^{-1}$)	2.44×10^{9}	1.06×10^{2}	3.66×10^{8}	6.36×10^{5}
K_{10} ($M^{-1}h^{-1}$)	6.45×10^{2}	6.87×10^{-10}	8.40×10^{4}	2.41×10^{-3}
K_{11} ($M^{-1}h^{-1}$)	5.13	1.00×10^{6}	1.77×10^{5}	3.66×10^{3}
K_{12} ($M^{-1}h^{-1}$)	4.35×10^{-1}	1.39×10^{-1}	2.23×10^{4}	1.29×10^{-3}
K_{13} (M·h)	5.96×10^{-5}	1.69×10^{-11}	8.52×10^{-5}	1.93×10^{-5}
K_{14} (M·h)	4.16×10^{-7}	2.03×10^{-11}	5.20×10^{-1}	2.23×10^{-2}
K_{15} (M·h)	5.48×10^{-3}	3.58×10^{-1}	2.15×10^{-4}	1.99×10^{-7}
K_{16} (M·h)	1.50×10^{-7}	1.75×10^{-6}	1.25×10^{-3}	2.90×10^{-6}
K_{17} (M·h)	8.75×10^{6}	3.19×10^{7}	2.13×10^{4}	4.26×10^{5}
K_{18} (M·h)	9.56×10^{6}	3.88×10^{-11}	3.69×10^{1}	7.17×10^{2}
K_{19} (M·h)	8.17×10^{6}	1.79×10^{3}	3.78×10^{5}	9.90×10^{5}

Table II-2. (*continued*)

Kinetic constants	PPL	CVL	PFL	CALA
K_{20}	7.82×10^{7}	1.04×10^{6}	6.15×10^{7}	5.34×10^{5}
k_{22} (h^{-1})	7.11×10^{-6}	2.05×10^{-3}	8.68×10^{-1}	2.75×10^{-2}
k_{23} (h^{-1})	1.26×10^{-2}	2.06×10^{-3}	8.72×10^{-1}	4.82×10^{-2}
k_{24} (h^{-1})	3.95×10^{-6}	2.19×10^{-2}	3.05×10^{-2}	4.97×10^{-2}
k_{25} (h^{-1})	1.77×10^{-6}	2.18×10^{-2}	2.25×10^{-2}	3.34×10^{-2}
k_{26} (h^{-1})	6.28×10^{-3}	1.81×10^{-2}	8.66×10^{-3}	5.00×10^{-2}
k_{27} (h^{-1})	1.93×10^{-6}	1.81×10^{-2}	7.49×10^{-4}	3.10×10^{-2}
k_{28} (h^{-1})	4.73×10^{-5}	1.45×10^{-2}	2.09×10^{-4}	1.86×10^{-2}
k_{29} (h^{-1})	3.40×10^{-3}	1.45×10^{-2}	4.42×10^{-4}	1.87×10^{-2}

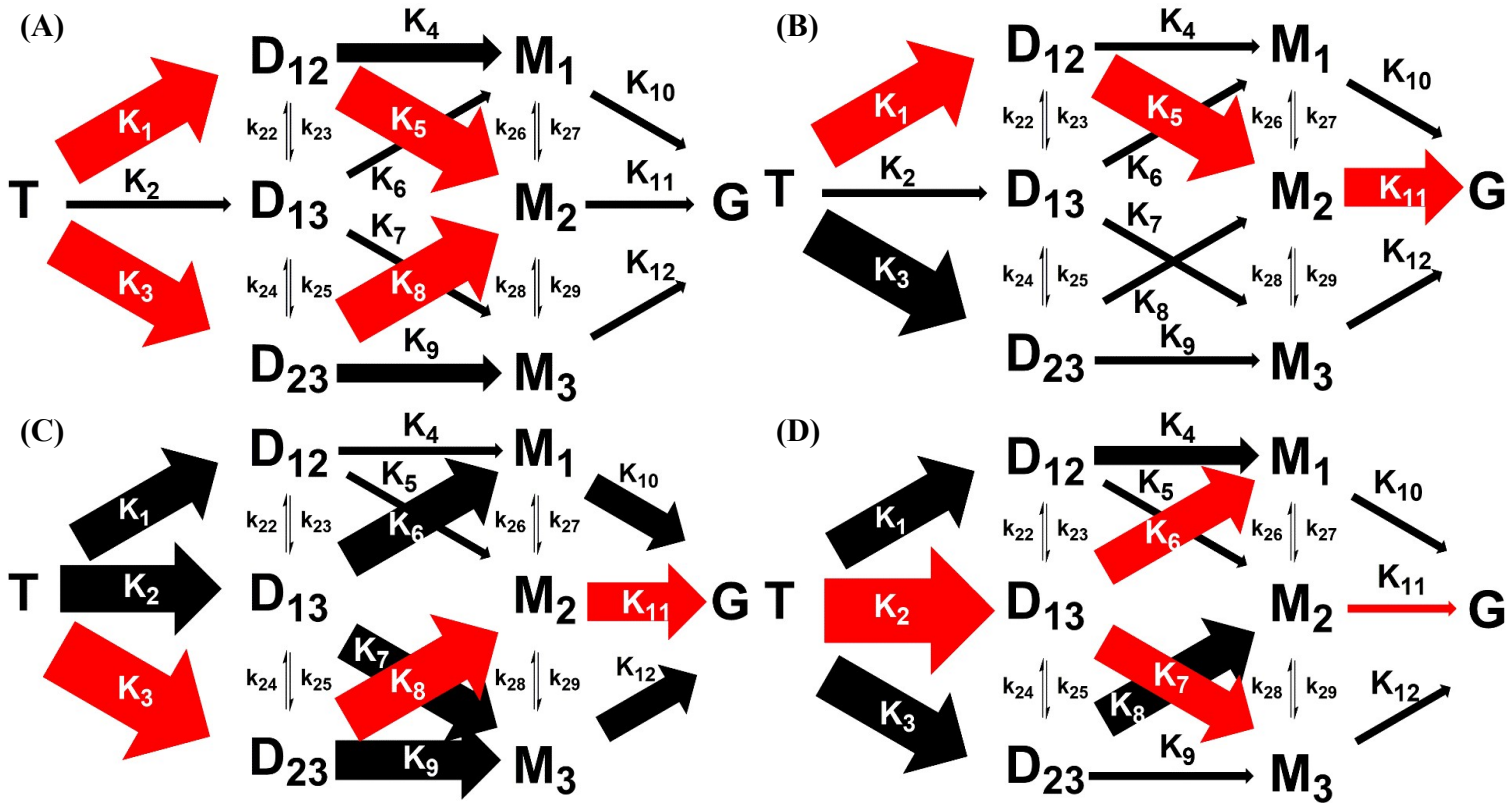

Figure II-13. Summary of trioleoylgylcerol hydrolysis catalyzed by lipases from (A) porcine pancreas, (B) *Chromobacterium viscosum*, (C) *Pseudomonas fluorescens*, and (D) lipase A from *Candida antarctica* considering integral stereoselectivity.

II-4. Conclusions

In this chapter, a simple analytical method for the separation and quantification of OA, enantiomeric and regioisomeric MOGs and DOGs, and TOG using an HPLC system equipped with the CSP column was established and validated. The applicability of the method for analysis of the integral stereoselectivity, to express the innate ability of the lipase concerning all of the hydrolysis steps, was demonstrated using TOG hydrolysis catalyzed by four model lipases. With short analysis times and excellent resolution of all hydrolysates, this method was shown to be useful for a rapid and accurate evaluation of integral stereoselectivity. Also, a kinetic model describing the integral stereoselectivity of lipase was constructed based on the Ping-Pong Bi-Bi mechanism, selectivity for all positions of acylglycerols, and acyl migration of DOG and MOG isomers, and applied to assess experimental results from four model lipases. With varying initial substrate concentrations, the model provided a good description of stepwise TOG hydrolysis by lipases with different selectivities. The kinetic constants from the model could be used to predict the stereoselective nature of lipases comprehensively and quantitatively while considering the total reaction scheme of lipase-catalyzed

TAG hydrolysis. Therefore, integral stereoselectivity derived from the present kinetic model would provide solutions for the effective selection, screening, and development of lipases to produce specific DAG or MAG isomers, which will be important for the production of lipids with enantiomerically specific structures.

II-5. References

Berger, M., & Schneider, M. P. (1991). Regioselectivity of lipases in organic solvents. *Biotechnology Letters, 13*(5), 333-338.

Carrière, F., Rogalska, E., Cudrey, C., Ferrato, F., Laugier, R., & Verger, R. (1997). *In vivo* and *in vitro* studies on the stereoselective hydrolysis of tri- and diglycerides by gastric and pancreatic lipases. *Bioorganic & Medicinal Chemistry, 5*(2), 429-435.

Deng, L., Nakano, H., & Iwasaki, Y. (2007). Direct separation of regioisomers and enantiomers of monoacylglycerols by tandem column high-performance liquid chromatography. *Journal of Chromatography A, 1165*(1), 93-99.

Donot, F., Cazals, G., Gunata, Z., Egron, D., Malinge, J., Strub, C., . . . Schorr-Galindo, S. (2013). Analysis of neutral lipids from microalgae by HPLC-ELSD and APCI-MS/MS. *Journal of Chromatography B, 942-943*, 98-106.

Goto, M., Goto, M., Nakashio, F., Yoshizuka, K., & Inoue, K. (1992). Hydrolysis of triolein by lipase in a hollow fiber reactor. *Journal of Membrane Science, 74*(3), 207-214.

Hermansyah, H., Kubo, M., Shibasaki-Kitakawa, N., & Yonemoto, T. (2006). Mathematical model for stepwise hydrolysis of triolein using *Candida rugosa* lipase in biphasic oil–water system. *Biochemical Engineering Journal, 31*(2), 125-132.

Hermansyah, H., Wijanarko, A., Kubo, M., Shibasaki-Kitakawa, N., & Yonemoto, T. (2010). Rigorous kinetic model considering positional specificity of lipase for enzymatic stepwise hydrolysis of triolein in biphasic oil–water system. *Bioprocess and Biosystems Engineering, 33*(7), 787-796.

Itabashi, Y., & Kuksis, A. (2009, May 3-6). Direct enantiomer separation of mono- and diacylglycerols by reversed-phase HPLC on polysaccharide-type chiral stationary phases. 100 th AOCS Annual Meeting & Expo, Orlando.

Kamal, M. Z., Yedavalli, P., Deshmukh, M. V., & Rao, N. M. (2013). Lipase in aqueous-polar organic solvents: activity, structure, and stability. *Protein Science, 22*(7), 904-915.

Muralidhar, R. V., Chirumamilla, R. R., Marchant, R., Ramachandran, V. N., Ward, O. P., & Nigam, P. (2002). Understanding lipase stereoselectivity. *World Journal of Microbiology and Biotechnology, 18*(2), 81-97.

Paiva, A. L., Balcão, V. M., & Malcata, F. X. (2000a). Kinetics and

mechanisms of reactions catalyzed by immobilized lipases. *Enzyme and Microbial Technology, 27*(3), 187-204.

Paiva, A. L., Balcão, V. M., & Malcata, F. X. (2000b). Kinetics and mechanisms of reactions catalyzed by immobilized lipases. *Enzyme and Microbial Technology, 27*(3), 187-204.

Prazeres, D. M. F., Lemos, F., Garcia, F. A. P., & Cabral, J. M. S. (1993). Modeling lipolysis in a reversed micellar system: Part I. Conventional batch reactor. *Biotechnology and Bioengineering, 42*(6), 759-764.

Rodriguez, J. A., Mendoza, L. D., Pezzotti, F., Vanthuyne, N., Leclaire, J., Verger, R., . . . Fotiadu, F. (2008). Novel chromatographic resolution of chiral diacylglycerols and analysis of the stereoselective hydrolysis of triacylglycerols by lipases. *Analytical Biochemistry, 375*(2), 196-208.

Rogalska, E., Cudrey, C., Ferrato, F., & Verger, R. (1993). Stereoselective hydrolysis of triglycerides by animal and microbial lipases. *Chirality, 5*(1), 24-30.

Small, D. M. (1968). A classification of biologic lipids based upon their interaction in aqueous systems. *Journal of the American Oil Chemists Society, 45*(3), 108.

Stolyhwo, A., Martin, M., & Guiochon, G. (1987). Analysis of lipid classes by HPLC with the evaporative light scattering detector. *Journal of Liquid*

Chromatography, 10(6), 1237-1253.

Tejo, B. A., Salleh, A. B., & Pleiss, J. (2004). Structure and dynamics of *Candida rugosa* lipase: the role of organic solvent. *Journal of Molecular Modeling, 10*(5), 358-366.

Chapter III

Determination of integral stereoselectivity on triacylglycerol of various fatty acids

III-1. Introduction

The selectivity of lipase plays an important role in its application in the food industry such as the production of structured lipids since it enables the specific composition of the fatty acid (FA) compositions of the product in contrast to chemical catalysts (Xu, 2000). It is also reported that the stereoselectivity of lipase is highly affected by the chain length of substrate (Holmberg, Szmulik, Norin, & Hult, 1989; Pan, Kawamoto, Fukui, Sonomoto, & Tanaka, 1990). Therefore, the integral stereoselectivity of lipase could vary depending on the type of FA in the triacylglycerol (TAG) used as a substrate, which should be considered for the practical application of the lipase.

This chapter aimed to evaluate the integral stereoselectivity of lipases on TAG of varying FAs and compare them. For this purpose, the simultaneous separation and quantification methods of TAG, DAG, MAG isomers, and FA with acyl moiety of saturated FA (C14:0, C16:0, C18:0) and unsaturated FA, linoleate (C18:2), were established based on two conditions of high-performance liquid chromatography (HPLC) equipped with evaporative light-scattering detector (ELSD). Applying the kinetic model established in chapter II, the integral stereoselectivity of the four model lipases was determined on TAG of aforementioned FAs.

III-2. Materials and methods

III-2-1. Materials

1,2-Dimyristoyl-*rac*-glycerol (1,2-*rac*-DMG, > 99%), 1,2-dimyristoyl-*sn*-glycerol (1,2-*sn*-DMG, > 99%), 1,3-dimyristoyl-*sn*-glycerol (1,3-*sn*-DMG, > 99%), 1-myristoyl-*rac*-glycerol (1-*rac*-MMG, > 99%), 2-myristoyl-*sn*-glycerol (2-*sn*-MMG, > 99%), 1,2-distearoyl-*rac*-glycerol (1,2-*rac*-DSG, > 99%), 1,2-distearoyl-*sn*-glycerol (1,2-*sn*-DSG, > 98%), 1,3-distearoyl-*sn*-glycerol (1,3-*sn*-DSG, > 99%), 1-stearoyl-*rac*-glycerol (1-*rac*-MSG, > 99%), 2-stearoyl-*sn*-glycerol (2-*sn*-MSG, > 99%), trilinoleoylglycerol (TLG, > 98%), 1,2-dilinoleoyl-*rac*-glycerol (1,2-*rac*-DLG, > 99%), 1,2-dilinoleoyl-*sn*-glycerol (1,2-*sn*-DLG, > 99%), 1-linoleoyl-*rac*-glycerol (1-*rac*-MLG, > 99%), 2-linoleoyl-*sn*-glycerol (2-*sn*-MLG, > 99%) were purchased from Larodan Fine Chemicals AB (Malmö, Sweden). Tripalmitoylglycerol (TPG, > 99%), 1,2-Dipalmitoyl-*rac*-glycerol (1,2-*rac*-DPG, > 99%), 1,2-dipalmitoyl-*sn*-glycerol (1,2-*sn*-DPG, > 99%), 1,3-dipalmitoyl-*sn*-glycerol (1,3-*sn*-DPG, > 99%), 1-palmitoyl-*rac*-glycerol (1-*rac*-MPG, > 99%), 3-palmitoyl-*sn*-glycerol (3-*sn*-MPG, > 99%), 2-palmitoyl-*sn*-glycerol (2-*sn*-MPG, > 99%), palmitic acid (PA, > 99%), tristearoylglycerol (TSG, > 99%), stearic acid (SA,

> 99%), myristic acid (MA, > 99%), linoleic acid (LA, > 99%), bis(2-ethylhexyl) sulfosuccinate sodium salt (Aerosol-OT, AOT, > 99%), and Trizma base (Tris, > 99%) were purchased from Sigma-Aldrich (St. Louis, MO, USA). 1,3-Dilinoleoyl-*sn*-glycerol (1,3-*sn*-DLG, > 99%) were purchased from Cayman Chemical (Ann Arbor, MI, USA). 1-Stearoyl-*sn*-glycerol (1-*sn*-MSG, 95%) was purchased from Santa Cruz Biotechnology (Dallas, TX, USA). 1-Linoleoyl-*sn*-glycerol (1-*sn*-MLG, > 95%) was purchased from Toronto Research Chemicals (Ontario, Canada). Trimyristoylglycerol (TMG, > 97%) was purchased from Tokyo Chemical Industry (Tokyo, Japan). Trifluoroacetic acid (guaranteed reagent grade), hydrochloric acid (HCl), and ethanol (HPLC grade) were purchased from Samchun Pure Chemicals (Gyeonggi-do, Republic of Korea). Acetonitrile, ethyl acetate, *n*-hexane, and isooctane (J.T. Baker, Phillipsburg, NJ, USA) were of HPLC grade. Purified lipase from porcine pancreas (PPL), *Chromobacterium viscosum* (CVL), *Pseudomonas fluorescence* (PFL), and lipase A from *Candida antarctica* were purchased from Sigma-Aldrich. All other chemicals were of extra pure grade and used without further purification.

III-2-2. Chromatographic resolution of fatty acid and acylglycerols of various acyl chain

As in the case of oleic acid and oleoylglycerols, a chiral stationary phase (CSP) column, CHIRALPAK IA (amylose tris-(3,5-dimethylphenylcarbamate) immobilized on 5 μm silica gel, 250 × 4.6 mm; Daicel Chemical Ind., Osaka, Japan), was used for the simultaneous separation of PA, enantiomers and regioisomers of MPG and DPG, and TPG. In the case of fatty acids and 7 acylglycerol species with acyl moiety of MA, SA, and LA, CHIRALCEL OZ-3 column (cellulose tris-(3-chloro-4-methylphenylcarbamate) immobilized on 3 μm silica gel, 250 × 4.6 mm; Daicel Chemical Ind.) was used. The HPLC system consisted of a Waters Alliance e2695 separation module (Waters Co., Milford, MA, USA) and an Alltech ELSD 2000 instrument (Alltech Co., Deerfield, MA, USA). For separation of PA and 7 palmitoylglycerols, the column was eluted with acetonitrile-ethyl acetate-trifluoroacetic acid (90:10:0.1, v/v/v) at a flow rate of 1.0 mL/min. The drift pipe temperature and nitrogen flow rate were 70°C and 1.8 L/min, respectively. On the other hand, the mobile phase condition for resolution of fatty acids and 7 acylglycerol species with acyl moiety of MA, SA, and LA was *n*-hexane-ethanol-trifluoroacetic acid (98:2:0.1, v/v/v) with a flow rate of 1.0 mL/min, while drift pipe temperature and nitrogen flow rate were 46°C and 1.7 L/min, respectively.

The column temperature was maintained at 30°C in all cases. An aliquot (10 μL) of a sample containing authentic standards dissolved in ethyl acetate was injected into the HPLC system and the peaks were detected with the ELSD. With the analytical condition above, the separation of analytes was characterized by separation factor (α) and resolution factor (Rs), which were calculated from the chromatograms as follows:

$$\alpha = \frac{t_{R2} - t_D}{t_{R1} - t_D}$$

$$R_s = \frac{(t_{R2} - t_{R1})}{w_1 + w_2}$$

where t_R is retention time, t_D is delay time, and w is peak width. An indexed 1 and 2 refers to the former and the latter of two adjacent peaks.

III-2-3. Hydrolysis of triacylglycerols in the reverse micelle

To prepare the reverse micelle containing model lipases, each freeze-dried lipase powder was solubilized in 50 mM Tris-HCl buffer (pH 7.0, CALA; pH 7.7, PPL; pH 8.0, CVL and PFL). The IOT solution containing a substrate (1.964 mL) was pre-incubated in a water bath at 37°C with magnetic stirring at 500 rpm. Lipase-catalyzed hydrolysis was initiated by adding 36 μL of a lipase solution and vortex-mixing for 1 min. The final concentrations of AOT and the *R*-value ($[H_2O]/[AOT]$) of the reverse micelle were 100 mM and 10, respectively. The final concentrations of TMG, TPG, TSG, and TLG were 20 mM, 12.4 mM, 5 mM, and 20 mM, respectively. At various time points up to 12 h, aliquots (50 μL) of the reactant were collected and diluted with 550 μL of ethyl acetate, for TPG, and 700 μL of *n*-hexane-ethanol (90:10, v/v), for TMG, TSG, and TLG, respectively. Then, the mixtures were vortexed for 30 s and filtered through a 0.45 μm PTFE syringe filter. After filtration, 10 μL of each filtrate was injected into the HPLC system for analysis of FA and seven acylglycerols.

III-2-4. Kinetic modeling of lipase-catalyzed triacylglycerol hydrolysis

From the time course of TAG, DAG and MAG isomers, and FA with acyl moiety of MA, PA, SA, and LA, K_i (i = 1–20), the kinetic constants for the enzymatic reaction, and k_j (j = 22–29), the constants for acyl migrations, were estimated by fitting the experimental data as described previously in the section II-2-4, chapter II.

III-3. Results and discussion

III-3-1. Separation and quantification of fatty acid and acylglycerols of various acyl chain

Since the HPLC-ELSD analysis with CHIRALPAK IA column and mobile phase of acetonitrile-acetone-trifluoroacetic acid (90:10:0.1, v/v/v) was not able to separate the enantiomeric DAG other than dioleoylglycerol (data not shown), two additional separation condition was applied for simultaneous resolution of the acylglycerols and fatty acids. For TPG and its hydrolysates, the resolution was achieved on the same CHIRALPAK IA column but the acetone in the mobile phase was changed to ethyl acetated as shown in Figure III-1B. The eight molecular species were eluted in the order of PA, 2-*sn*-MPG, 3-*sn*-MPG, 1-*sn*-MPG, TPG, 2,3-*sn*-DOG, 1,2-*sn*-DOG, and 1,3-*sn*-DOG, which was similar with that of TOG and its hydrolysates except that the TAG component was middle of MAGs and DAGs. However, for resolution of TMG, TSG, TLG, and their hydrolysates, the CHIRALCEL OZ-3 column was used with mobile phase of *n*-hexane-ethanol-trifluoroacetic acid, which is a typical normal phase condition. In these cases, the elution order of the compounds was TAG, FA, 2,3-*sn*-DAG, 1,2-*sn*-DAG, 1,3-*sn*-

DAG, 1-*sn*-MAG, 3-*sn*-MAG, 2-*sn*-MAG (Figure III-1A, C, and D).

Tables III-1, 2, 3, and 4 describe the quality of separation and quantification of the HPLC methods for acylglycerols and fatty acids with acyl moiety of MA, PA, SA, and LA, respectively. It is worth noting that the retention times of TMG and TLG and their hydrolysates were almost the same for each of their classes, while those of TSG and its hydrolysates were shorter. This trend was ascribed to the equivalent carbon number rule, which states that the acylglycerols elute in the order of the chain length subtracting twice the number of double bonds (Fotia, Potortì, La Torre, Di Bella, & Saitta, 2021; Podlaha & Töregård, 1982). The enantiomers of DMG, DPG, and DLG were separated with R_s of more than 1.6 and α of more than 1.14 while achieving an analysis time of 35 min. The lowest R_s was observed for the separation of 1,2-*sn*-DSG and 1,3-*sn*-DSG with a value of 1.31. In the case of DPG and MPG, R_s of more than 1.69 with 20-min run time. These results were comparable to those obtained in a previous study on the separation of enantiomeric MPG, MSG, and MLG using phenylcarbamate derivatives of cellulose as CSP having *Rs* of 3.05, 2.91, and 3.49 in run time above 35 min (Fotia et al., 2021). The general model explaining the mechanism of resolution of these chiral compounds on CSP is a three-point interaction model, which states that the difference in steric fitness between three functional groups of stereocenter carbon of the analyte enantiomers and CSP determines the elution

order (Dalgliesh, 1952). The polysaccharide-based CSPs, however, are thought to display chiral recognition through the complex conformationally-driven process with non-covalent molecular interactions such as hydrogen bonding and π- π interaction (Booth, Wahnon, & Wainer, 1997; Wainer, 1987). Therefore, the concise interpretation of the reason for the chiral discrimination of DAG and MAG enantiomers on these columns is challenging. Still, the current data are worthy as another example of the resolution of acylglycerols on amylose- and cellulose-based CSP with phenylcarbamate functional groups.

The relative standard deviations of the retention times of all compounds were less than 1% except that of 2-*sn*-MLG (1.25%), indicating good reproducibility. Calibration curves for each of the molecular species were obtained as double logarithmic plots of peak area and analyte concentration by injecting 10 μL of different concentrations of FA, MAGs, DAGs, and TAG. As shown in Tables III-1, 2, 3, and 4, all species had excellent linear fits (coefficient of determination > 0.986). Using these calibration curves and six replicates of each analyte, the relative standard deviations of the concentration for each analyte were determined to be in the ranges of 0.17-1.45%. These results indicate that the present analytical method is reproducible and suitable for the separation and quantitation of mixtures containing FA, MAGs, DAGs, and TAG with an acyl moiety of MA, PA, SA, and LA.

(A)

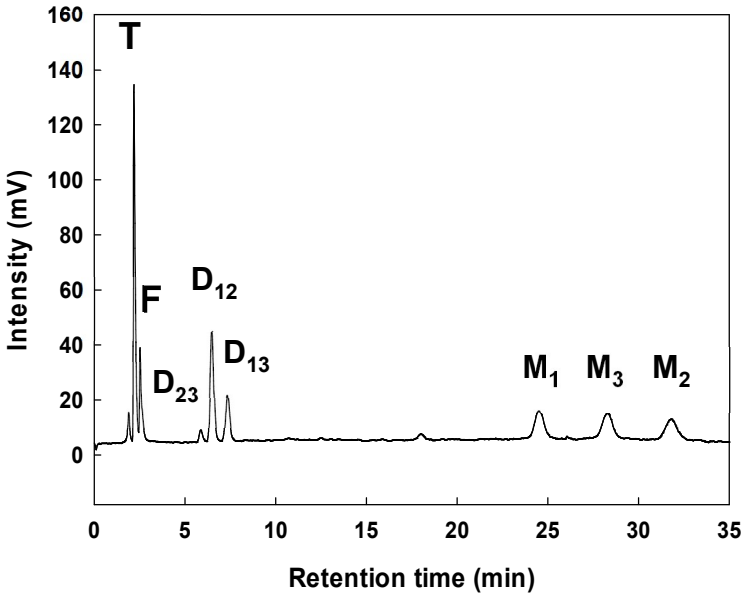
T
F
D12
D13
D23
M1
M3
M2
Intensity (mV)
Retention time (min)
160
140
120
100
80
60
40
20
0
0
5
10
15
20
25
30
35

(B)

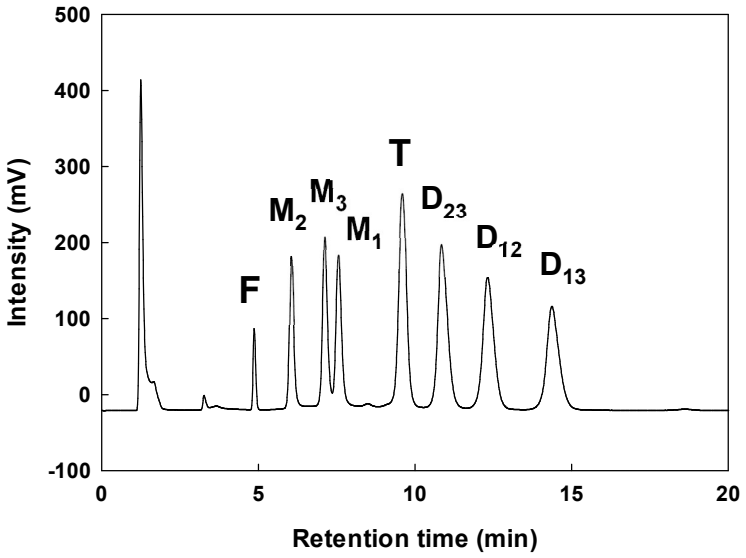
T
M2
M3
M1
F
D23
D12
D13
Intensity (mV)
Retention time (min)
500
400
300
200
100
0
-100
0
5
10
15
20

(C)

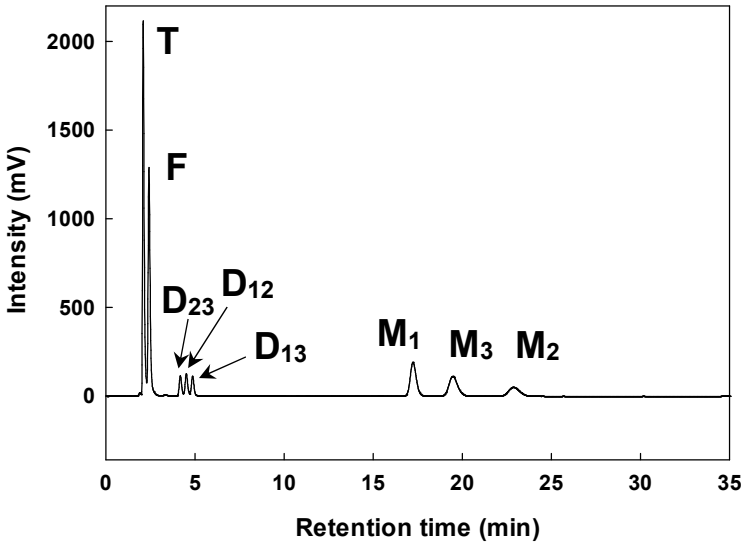

(D)

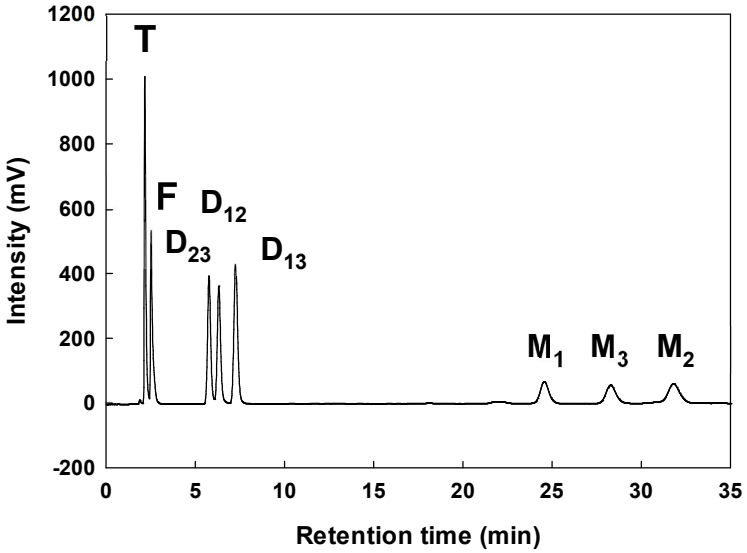

Figure III-1. Chromatographic resolution of all types of acylglycerols and fatty acid on a chiral stationary phase HPLC system according to fatty acyl chain moieties: (A) myristic, (B) palmitic, (C) stearic and (D) linoleic acid.

Table III-1. Chromatographic data for myristic acid and myristoylglycerols on the chiral stationary phase HPLC system

Molecular species	Retention time (min)	α[a]	R_s[b]	RSD%, retention time (n=9)	RSD%, measurement (n=6)	Calibration range (μM)	Calibration points	Calibration curve[c]	R^2[d]
TMG	2.20	-	-	0.10	0.76	26-345	10	y = 1.275 x + 3.716	0.9977
MA	2.52	1.87	1.99	0.22	0.48	82-1095	10	y = 2.772 x – 1.749	0.9937
2,3-*sn*-DMG	5.86	5.66	12.79	0.14	0.33	37-487	10	y = 1.359 x + 3.140	0.9966
1,2-*sn*-DMG	6.48	1.15	1.71	0.12	0.52	37-487	10	y = 1.356 x + 3.151	0.9976
1,3-*sn*-DMG	7.33	1.18	2.15	0.13	0.31	37-487	10	y = 1.369 x + 3.050	0.9967
1-*sn*-MMG	24.54	4.11	25.32	0.16	1.28	62-826	10	y = 1.371 x + 2.453	0.9968
3-*sn*-MMG	28.28	1.16	3.76	0.18	0.90	62-826	10	y = 1.396 x + 2.368	0.9957
2-*sn*-MMG	31.83	1.13	3.11	0.37	1.04	83-826	9	y = 1.404 x + 2.227	0.9892

[a]Separation factor between preceding peak
[b]Resolution factor between preceding peak
[c]y = log(peak area), x = log(concentration in μM)
[d]Coefficient of determination

Table III-2. Chromatographic data for palmitic acid and palmitoylglycerols on the chiral stationary phase HPLC system

Molecular species	Retention time (min)	α[a]	R_s[b]	RSD%, retention time (n=9)	RSD%, measurement (n=6)	Calibration range (µM)	Calibration points	Calibration curve[c]	R^2[d]
PA	4.89	-	-	0.10	0.47	170-1316	5	y = 3.463 x – 4.130	0.9984
2-*sn*-MPG	6.09	1.10	5.82	0.08	0.87	16-1626	10	y = 1.586 x + 1.978	0.9987
3-*sn*-MPG	7.16	1.30	4.29	0.09	0.82	12-1200	10	y = 1.502 x + 2.307	0.9991
1-*sn*-MPG	7.62	1.08	1.69	0.07	1.02	16-1650	10	y = 1.467 x + 2.175	0.9917
TPG	9.64	1.31	5.82	0.07	0.65	13-1239	10	y = 1.532 x + 2.576	0.9984
2,3-*sn*-DPG	11.03	1.16	3.04	0.09	0.40	27-1770	9	y = 1.499 x + 2.418	0.9977
1,2-*sn*-DPG	12.45	1.14	2.52	0.11	0.26	16-1605	10	y = 1.529 x + 2.344	0.9983
1,3-*sn*-DPG	14.65	1.20	3.48	0.11	0.24	45-1628	8	y = 1.581 x + 2.125	0.9976

[a]Separation factor between preceding peak
[b]Resolution factor between preceding peak
[c]y = log(peak area), x = log(concentration in µM)
[d]Coefficient of determination

Table III-3. Chromatographic data for stearic acid and stearoylglycerols on the chiral stationary phase HPLC system

Molecular species	Retention time (min)	α[a]	R_s[b]	RSD%, retention time (n=9)	RSD%, measurement (n=6)	Calibration range (μM)	Calibration points	Calibration curve[c]	R^2[d]
TSG	2.08	-	-	0.13	0.48	23-310	10	y = 1.300 x + 3.722	0.9958
SA	2.41	2.15	1.84	0.60	1.45	40-2340	9	y = 1.051 x + 3.808	0.9959
2,3-*sn*-DSG	4.25	3.80	8.40	0.52	0.17	33-440	10	y = 1.603 x + 2.582	0.9953
1,2-*sn*-DSG	4.57	1.15	1.40	0.30	0.26	33-440	10	y = 1.600 x + 2.590	0.9952
1,3-*sn*-DSG	4.97	1.12	1.31	0.29	0.23	33-440	10	y = 1.566 x + 2.654	0.9953
1-*sn*-MSG	17.82	5.00	37.04	0.61	0.28	48-640	10	y = 1.698 x + 1.424	0.9866
3-*sn*-MSG	20.25	1.15	2.85	0.25	0.32	50-656	10	y = 1.695 x + 1.413	0.9867
2-*sn*-MSG	22.76	1.14	2.14	0.76	0.31	57-756	10	y = 1.846 x + 1.084	0.9870

[a]Separation factor between preceding peak
[b]Resolution factor between preceding peak
[c]y = log(peak area), x = log(concentration in μM)
[d]Coefficient of determination

Table III-4. Chromatographic data for linoleic acid and linoleoylglycerols on the chiral stationary phase HPLC system

Molecular species	Retention time (min)	α[a]	R_s[b]	RSD%, retention time (n=9)	RSD%, measurement (n=6)	Calibration range (μM)	Calibration points	Calibration curve[c]	R^{2}[d]
TLG	2.18	-	-	0.20	0.64	12-426	8	y = 1.268 x + 3.830	0.9986
LA	2.57	1.94	2.17	0.50	0.39	72-2567	8	y = 1.108 x + 3.268	0.9863
2,3-*sn*-DLG	5.77	5.53	13.00	0.51	0.30	23-810	8	y = 1.384 x + 3.135	0.9986
1,2-*sn*-DLG	6.32	1.14	1.64	0.50	0.46	23-810	8	y = 1.380 x + 3.147	0.9985
1,3-*sn*-DLG	7.26	1.21	2.59	0.51	0.27	26-932	8	y = 2.031 x + 1.762	0.9968
1-*sn*-MLG	24.55	4.17	26.93	0.55	1.19	40-1410	8	y = 1.298 x + 2.843	0.9980
3-*sn*-MLG	28.28	1.16	3.88	0.55	0.83	40-1410	8	y = 1.295 x + 2.831	0.9980
2-*sn*-MLG	31.81	1.13	3.15	1.25	0.92	110-1410	6	y = 2.203 x + 0.372	0.9945

[a]Separation factor between preceding peak
[b]Resolution factor between preceding peak
[c]y = log(peak area), x = log(concentration in μM)
[d]Coefficient of determination

III-3-2. Kinetic modeling of model lipases on triacylglycerols of various fatty acids

To assess the differences of integral stereoselectivity on various substrates, kinetic parameters were estimated from the time course of TAG hydrolysis with varying FA, i.e. MA, PA, SA, and LA, catalyzed by PPL, CVL, PFL, and CALA. As established in chapter II, the kinetic constants K_1–K_3, K_4–K_9, and K_{10}–K_{12} represent the conversion of TAG, DAGs, and MAGs, respectively.

III-3-2-1. Lipase from porcine pancreas

Figures III-2, 3, 4, and 5 show the time courses of PPL-catalyzed hydrolysis of TAG with acyl moiety of MA, PA, SA, and LA, respectively. As same as the case of TOG hydrolysis, the concentration of 2,3-*sn*-DAG and 1,2-*sn*-DAG increased to a similar level for all substrates. Also, the concentration of 1,3-*sn*-DAG was very low, which was under the LOD until 12 h hydrolysis of TMG and TPG. From subsequent hydrolysis of DAGs, 2-*sn*-MAG showed the most rapid increase followed by 1-*sn*-MAG and 3-*sn*-MAG. Therefore, PPL showed a consistent pattern of time courses of TAG, DAGs, MAGs, and FA.

The kinetic constants for PPL were shown in Table III-5. For TAG conversion, K_2 was smaller than K_1 and K_3 by over 500-fold, while K_1 and K_3

showed differences in the range of 1.0 to 2.0-fold. Also, the *sn*-1 position of 1,2-*sn*-DAG and the *sn*-3 position of 2,3-*sn*-DAG were the two most selective positions as K_5 and K_8 were the highest values in DAG hydrolysis for all substrates except TMG, in which K_8 was slightly lower than K_6. The differences between these values and K_4 or K_9 were much lower than that of K_6 and K_7 for TAGs other than TOG, in which the opposite relationship was present. In the MAG hydrolysis, the highest values were different among substrates. However, these values were far lower than those for TAG or DAG conversion, as a steady increase of 2-*sn*-MAG indicates. Therefore, the TAG hydrolysis catalyzed by PPL can be summarized as shown in Figure III-6. For PPL, it is obvious that the main pathway of reaction progress is from TAG to 1,2-*sn*-DAG and 2,3-*sn*-DAG at a similar rate, and then to 2-*sn*-MAG when acyl moieties are MA, PA, SA, OA, and LA.

(A)

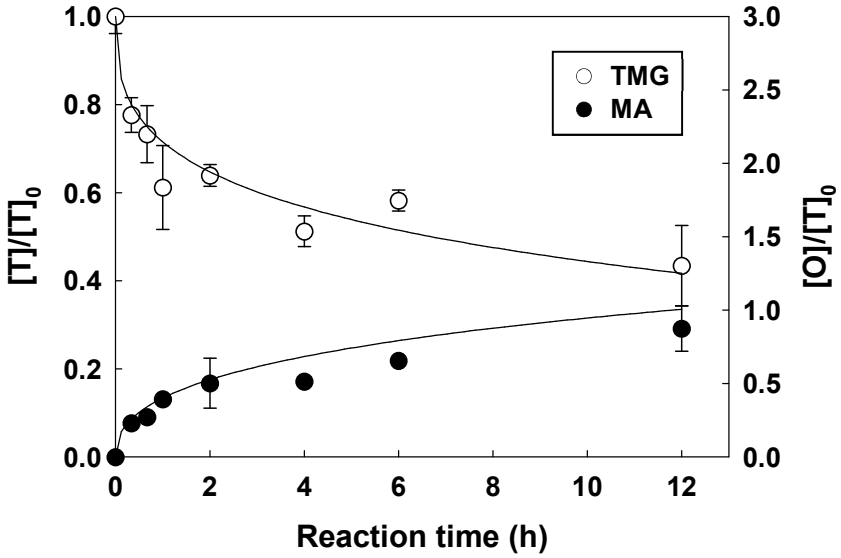
TMG
MA
[T]/[T]0
[O]/[T]0
Reaction time (h)

(B)

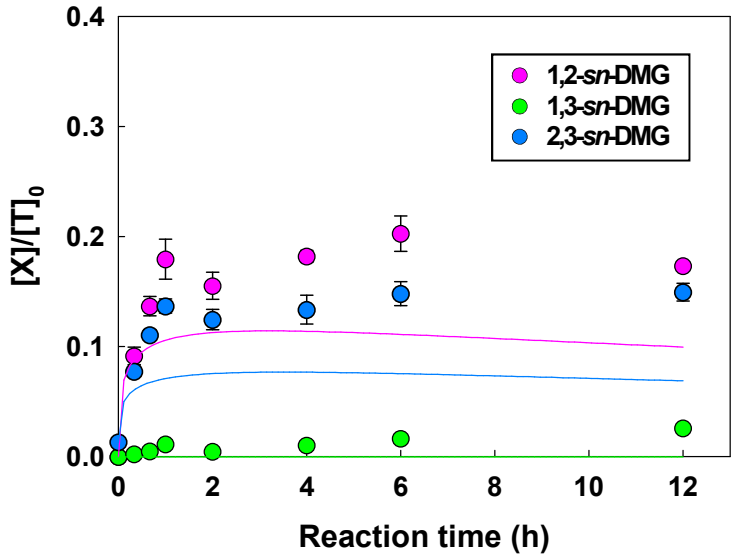
1,2-sn-DMG
1,3-sn-DMG
2,3-sn-DMG
[X]/[T]0
Reaction time (h)

(C)

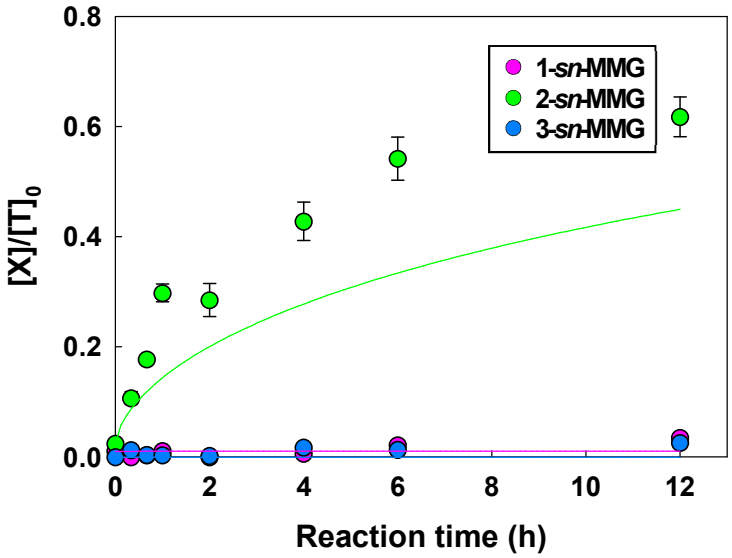

Figure III-2. Fitting of the kinetic model for trimyristoylglycerol (TMG) hydrolysis when lipase from porcine pancreas was used. (A) TMG and myristic acid (MA); (B) dimyristoylglycerol (DMG) isomers; (C) monomyristoylglycerol (MMG) isomers.

(A)

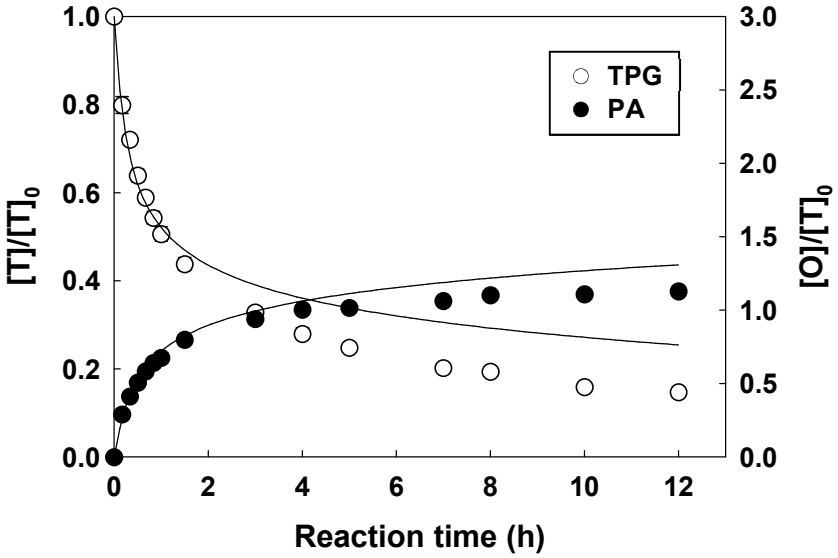
TPG
PA
[T]/[T]0
[O]/[T]0
Reaction time (h)

(B)

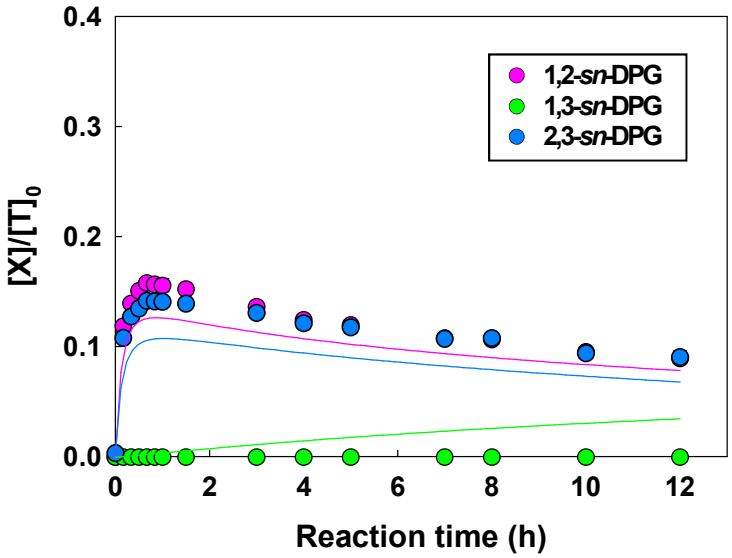
1,2-sn-DPG
1,3-sn-DPG
2,3-sn-DPG
[X]/[T]0
Reaction time (h)

(C)

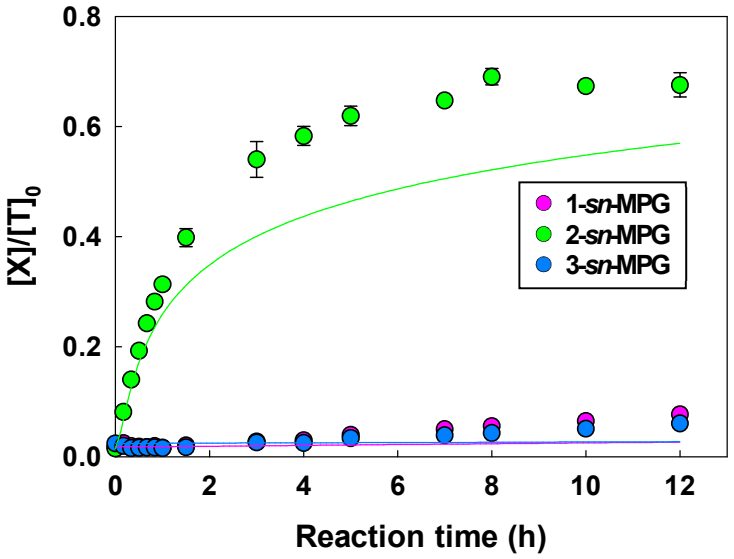

Figure III-3. Fitting of the kinetic model for tripalmitoylglycerol (TPG) hydrolysis when lipase from porcine pancreas was used. (A) TPG and palmitic acid (PA); (B) dipalmitoylglycerol (DPG) isomers; (C) monopalmitoylglycerol (MPG) isomers.

(A)

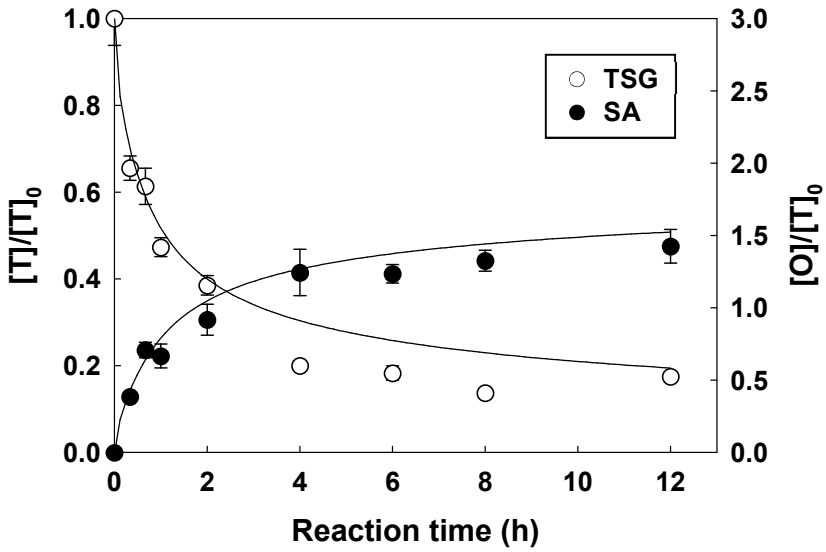
TSG
SA
[T]/[T]0
[L]/[O]0
Reaction time (h)

(B)

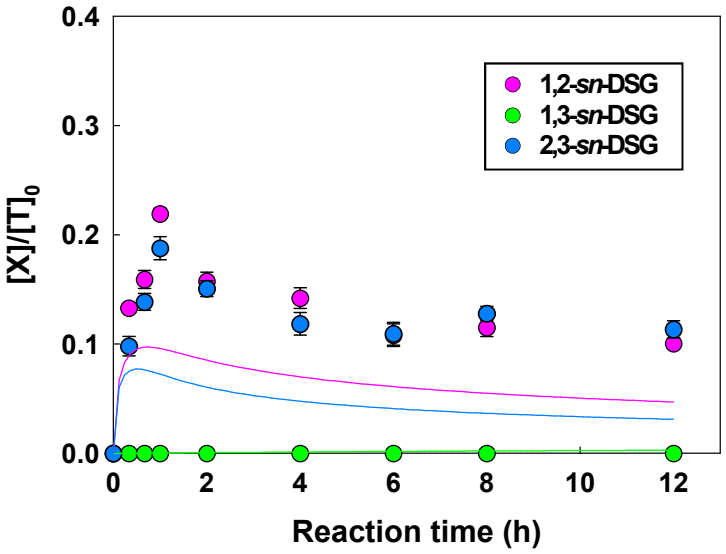
1,2-sn-DSG
1,3-sn-DSG
2,3-sn-DSG
[X]/[T]0
Reaction time (h)

(C)

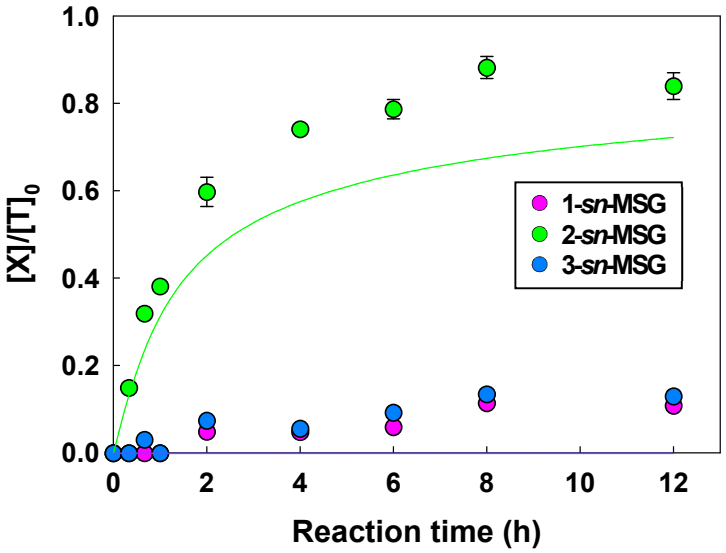

Figure III-4. Fitting of the kinetic model for tristearoylglycerol (TSG) hydrolysis when lipase from porcine pancreas was used. (A) TSG and stearic acid (SA); (B) distearoylglycerol (DSG) isomers; (C) monostearoylglycerol (MSG) isomers.

(A)

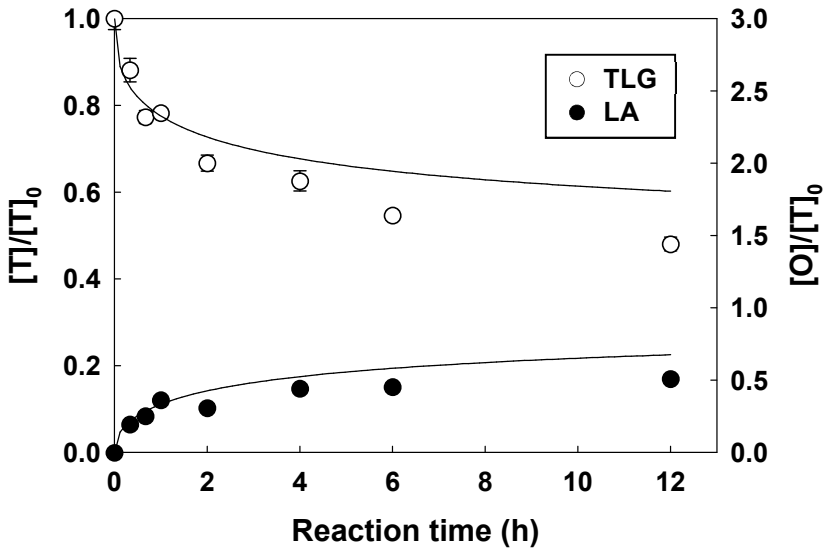
TLG
LA
[T]/[T]0
[L]/[T]0
Reaction time (h)

(B)

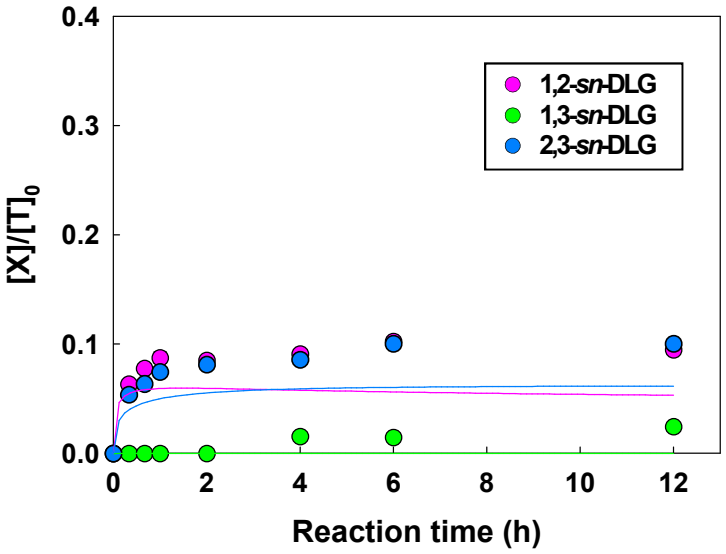
1,2-sn-DLG
1,3-sn-DLG
2,3-sn-DLG
[X]/[T]0
Reaction time (h)

(C)

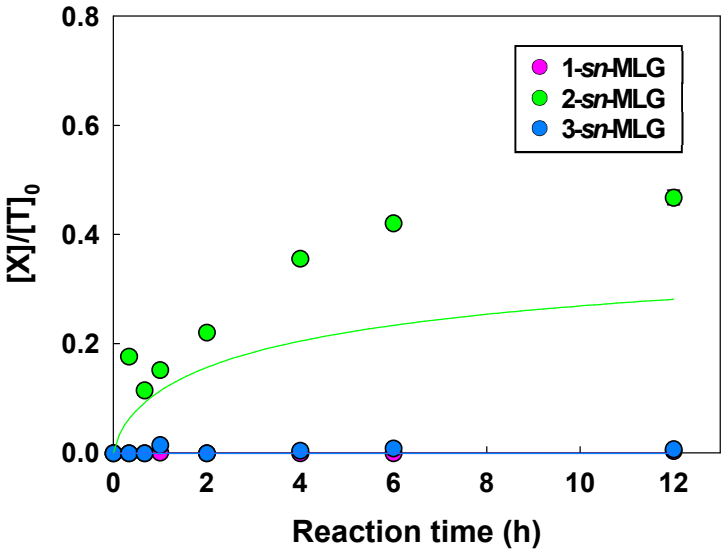

Figure III-5. Fitting of the kinetic model for trilinoleoylglycerol (TLG) hydrolysis when lipase from porcine pancreas was used. (A) TLG and linoleic acid (LA); (B) dilinoleoylglycerol (DLG) isomers; (C) monolinoleoylglycerol (MLG) isomers.

Table III-5. Values of kinetic parameters associated with triacylglycerol hydrolysis catalyzed by lipases from porcine pancreas estimated using the kinetic model

Kinetic constants	C14:0	C16:0	C18:0	C18:1	C18:2
K_1 ($M^{-1}h^{-1}$)	1.92×10^{10}	2.35×10^{10}	8.24×10^{9}	7.52×10^{9}	7.96×10^{9}
K_2 ($M^{-1}h^{-1}$)	2.00×10^{7}	1.38×10^{5}	7.90×10^{4}	5.85×10^{3}	1.00×10^{5}
K_3 ($M^{-1}h^{-1}$)	1.10×10^{10}	1.78×10^{10}	8.22×10^{9}	1.13×10^{10}	3.92×10^{9}
K_4 ($M^{-1}h^{-1}$)	6.26×10^{5}	6.88×10^{5}	1.30×10^{5}	8.62×10^{8}	3.27×10^{5}
K_5 ($M^{-1}h^{-1}$)	9.97×10^{10}	9.82×10^{10}	4.84×10^{10}	4.81×10^{10}	9.98×10^{10}
K_6 ($M^{-1}h^{-1}$)	2.87×10^{10}	2.98×10^{10}	9.42×10^{8}	1.92×10^{6}	1.55×10^{10}
K_7 ($M^{-1}h^{-1}$)	9.74×10^{9}	1.06×10^{10}	5.90×10^{8}	2.19×10^{6}	2.27×10^{10}
K_8 ($M^{-1}h^{-1}$)	8.33×10^{10}	8.13×10^{10}	6.74×10^{10}	6.72×10^{10}	3.71×10^{10}
K_9 ($M^{-1}h^{-1}$)	5.61×10^{6}	6.95×10^{5}	1.85×10^{6}	2.44×10^{9}	1.29×10^{6}
K_{10} ($M^{-1}h^{-1}$)	5.31×10^{-2}	4.48	2.53×10^{5}	6.45×10^{2}	2.39×10^{5}
K_{11} ($M^{-1}h^{-1}$)	1.76×10^{4}	2.45×10^{4}	5.10×10^{-1}	5.13	1.16×10^{1}
K_{12} ($M^{-1}h^{-1}$)	7.21×10^{4}	1.77×10^{-2}	5.95×10^{4}	4.35×10^{-1}	3.31×10^{5}
K_{13} ($M\cdot h$)	2.39×10^{-7}	1.57×10^{-4}	7.34×10^{-6}	5.96×10^{-5}	1.83×10^{-5}
K_{14} ($M\cdot h$)	4.65×10^{-7}	4.89×10^{-5}	1.60×10^{-3}	4.16×10^{-7}	6.24×10^{-5}
K_{15} ($M\cdot h$)	2.68×10^{-1}	2.91×10^{-1}	6.52×10^{-3}	5.48×10^{-3}	2.06×10^{-1}
K_{16} ($M\cdot h$)	1.00×10^{-6}	1.75×10^{-4}	1.66×10^{-3}	1.50×10^{-7}	2.79×10^{-4}
K_{17} ($M\cdot h$)	1.01×10^{7}	1.05×10^{7}	8.93×10^{6}	8.75×10^{6}	5.00×10^{7}
K_{18} ($M\cdot h$)	1.12×10^{1}	9.27	9.56×10^{6}	9.56×10^{6}	4.24×10^{6}
K_{19} ($M\cdot h$)	4.77×10^{7}	4.68×10^{7}	8.20×10^{6}	8.17×10^{6}	2.24×10^{7}
K_{20}	1.44×10^{7}	1.45×10^{7}	7.82×10^{7}	7.82×10^{7}	4.67×10^{7}

Table III-5. (*continued)*

Kinetic constants	C14:0	C16:0	C18:0	C18:1	C18:2
k_{22} (h^{-1})	6.65×10^{-7}	7.20×10^{-3}	3.88×10^{-3}	7.11×10^{-6}	3.80×10^{-6}
k_{23} (h^{-1})	1.33×10^{-6}	1.89×10^{-2}	3.96×10^{-3}	1.26×10^{-2}	7.69×10^{-6}
k_{24} (h^{-1})	1.97×10^{-6}	2.48×10^{-2}	4.54×10^{-4}	3.95×10^{-6}	9.16×10^{-6}
k_{25} (h^{-1})	9.88×10^{-7}	2.19×10^{-5}	3.71×10^{-4}	1.77×10^{-6}	4.61×10^{-6}
k_{26} (h^{-1})	2.61×10^{-6}	2.89×10^{-6}	4.34×10^{-6}	6.28×10^{-3}	4.07×10^{-6}
k_{27} (h^{-1})	1.35×10^{-6}	1.50×10^{-6}	2.17×10^{-6}	1.93×10^{-6}	2.04×10^{-6}
k_{28} (h^{-1})	1.26×10^{-8}	1.33×10^{-6}	7.87×10^{-6}	4.73×10^{-5}	2.15×10^{-6}
k_{29} (h^{-1})	2.53×10^{-8}	2.53×10^{-6}	1.58×10^{-5}	3.40×10^{-3}	4.29×10^{-6}

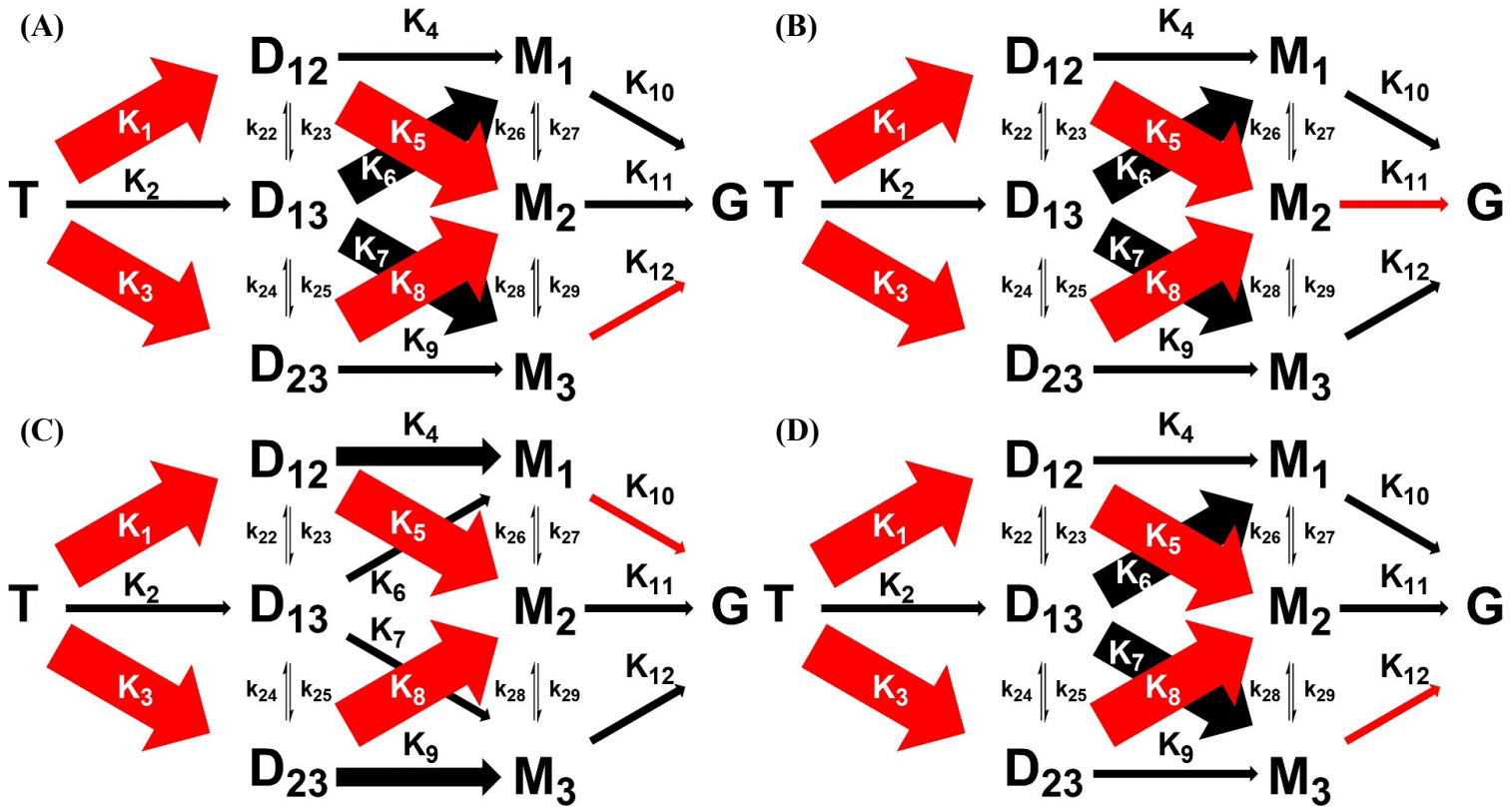

Figure III-6. Summary of triacylglycerol (TAG) hydrolysis catalyzed by lipases from porcine pancreas considering integral stereoselectivity according to fatty acyl chain moiety: (A) myristic, (B) palmitic, (C) stearic and (D) linoleic acid.

III-3-2-2. ***Lipase from Chromobacterium viscosum***

Figures III-7, 8, 9, and 10 show the time courses of CVL-catalyzed hydrolysis of TAG with acyl moiety of MA, PA, SA, and LA, respectively. As in the case of TOG hydrolysis by CVL, the concentration of 1,2-*sn*-DAG was higher than that of 2,3-*sn*-DAG from the initial phase of hydrolysis, which indicates the *sn*-3 stereoselectivity of CVL. In TMG hydrolysis, 1,3-*sn*-DAG was observed from the initial phase of hydrolysis in contrast to the situation in the hydrolysis of TPG, TSG, and TLG (Figures III-7B, 8B, 9B, and 10B). In addition, 2-*sn*-MAG increased to the maximum value in the range of 60-80% and decreased under 15% initial TAG concentration while both 1-*sn*-MAG and 3-*sn*-MAG remained in a value under 20% (Figures III-7C, 8C, 9C, and 10C).

The kinetic parameters of CVL were then compared among the substrates (Table III-6). In all substrates, the value of K_1 was higher than K_3 by 2.2 to 8.2-fold. However, the differences between K_1 and K_2 were smallest for TMG by 820-fold, while those for TPG, TSG, and TLG were over 14,500-fold. In DAG hydrolysis, cleavage on the *sn*-1 position of 1,2-*sn*-DAG was the most significant reaction as indicated by the highest K_5 among K_4 to K_9. However, K_{11} was not the highest among K_{10} to K_{12} in contrast to the rapid decrease of 2-*sn*-MAG (Figures III-7C, 8C, 9C, and 10C). Collectively, as

summarized in Figure III-11, the main pathway of hydrolysis reaction catalyzed by CVL is from TAG to 1,2-*sn*-DAG, 2-*sn*-MAG, and glycerol.

(A)

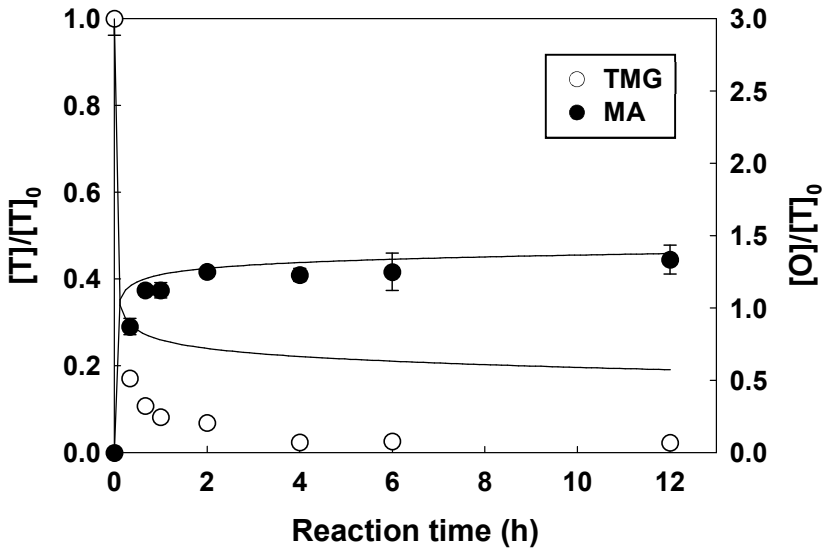
TMG
MA
[T]/[T]0
[L]/[O]0
Reaction time (h)

(B)

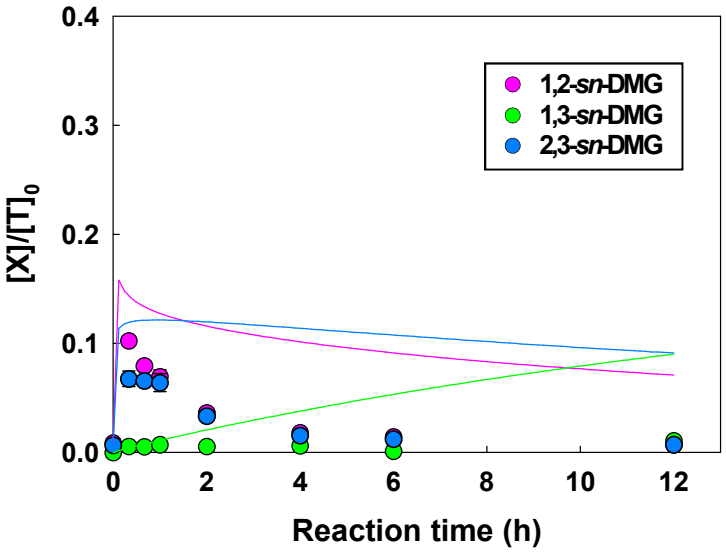
1,2-sn-DMG
1,3-sn-DMG
2,3-sn-DMG
[X]/[T]0
Reaction time (h)

(C)

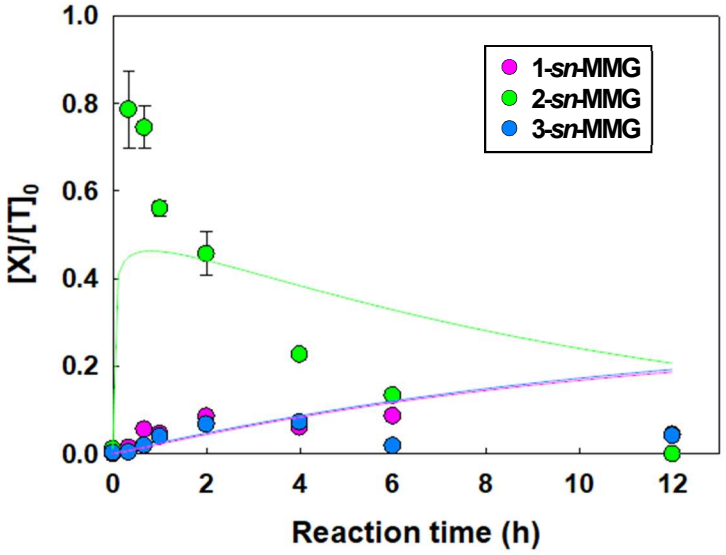

Figure III-7. Fitting of the kinetic model for trimyristoylglycerol (TMG) hydrolysis when lipase from *Chromobacterium viscosum* was used. (A) TMG and myristic acid (MA); (B) dimyristoylglycerol (DMG) isomers; (C) monomyristoylglycerol (MMG) isomers.

(A)

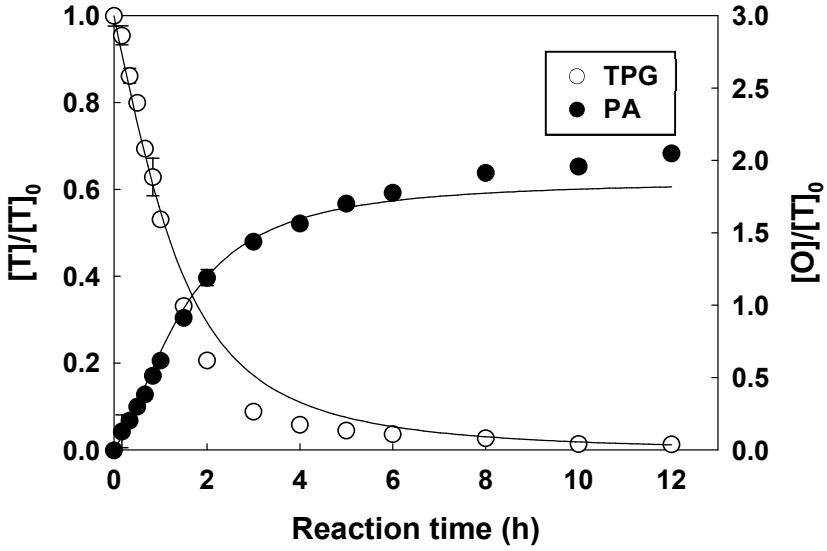
TPG
PA
[T]/[T]0
[L]/[O]0
Reaction time (h)

(B)

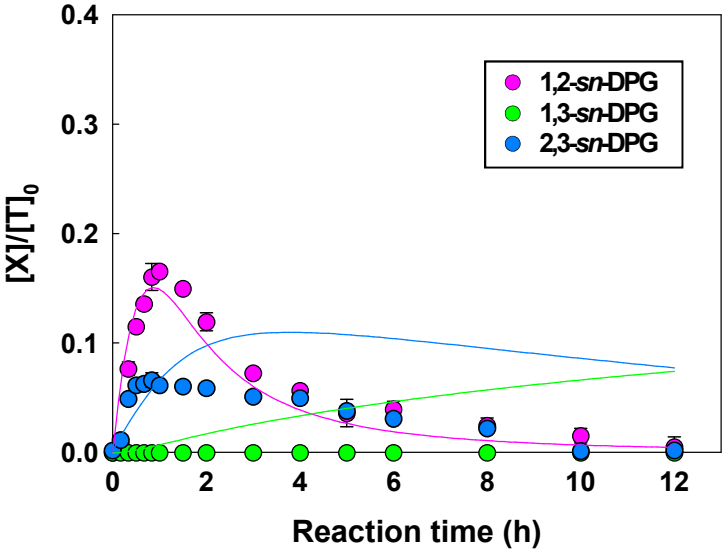
1,2-sn-DPG
1,3-sn-DPG
2,3-sn-DPG
[X]/[T]0
Reaction time (h)

(C)

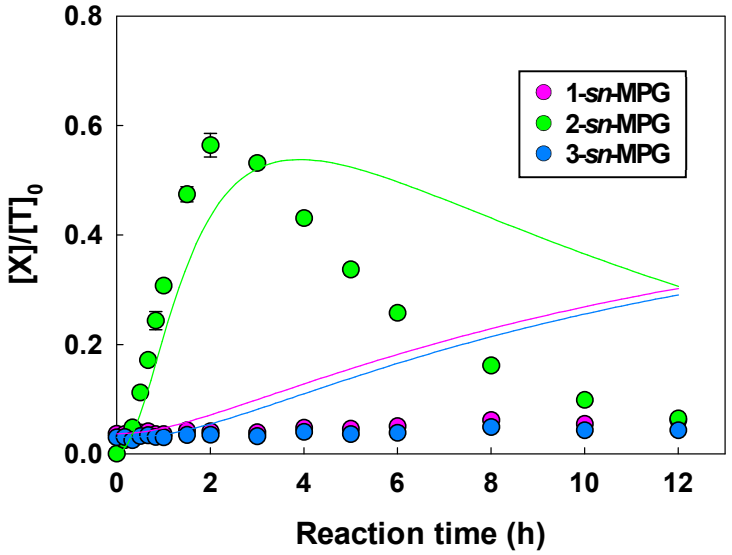

Figure III-8. Fitting of the kinetic model for tripalmitoylglycerol (TPG) hydrolysis when lipase from *Chromobacterium viscosum* was used. (A) TPG and palmitic acid (PA); (B) dipalmitoylglycerol (DPG) isomers; (C) monopalmitoylglycerol (MPG) isomers.

(A)

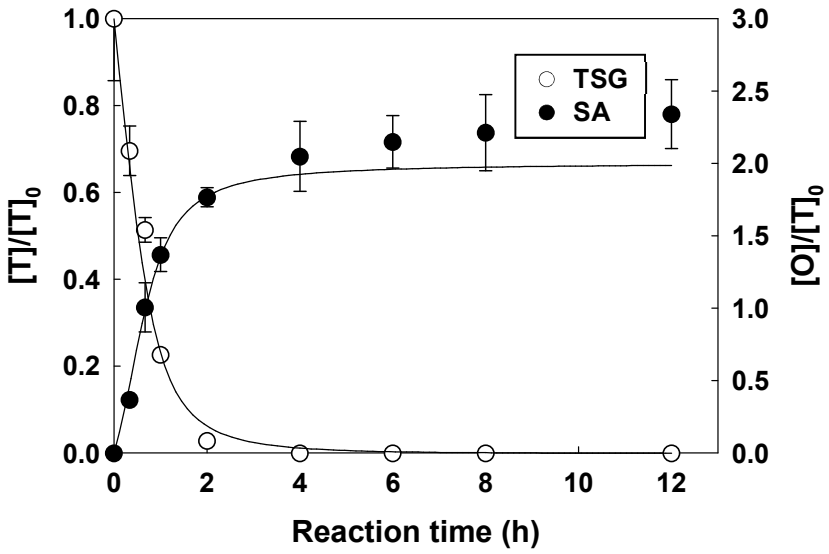
TSG
SA
[T]/[T]0
[O]/[T]0
Reaction time (h)

(B)

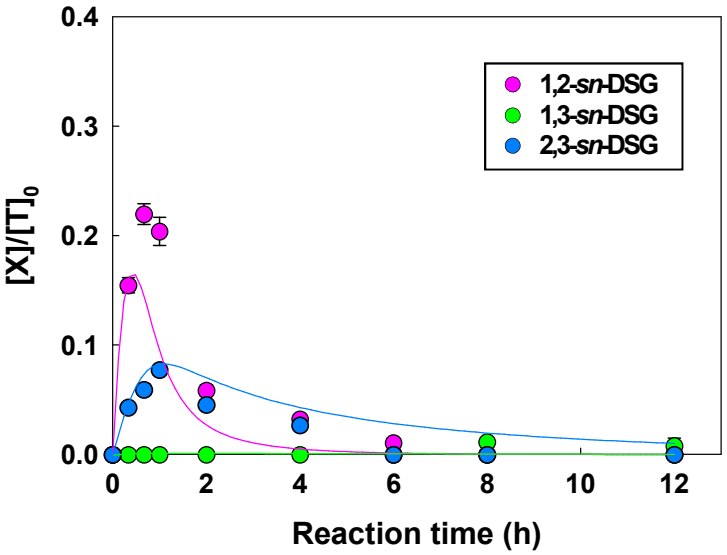
1,2-sn-DSG
1,3-sn-DSG
2,3-sn-DSG
[X]/[T]0
Reaction time (h)

(C)

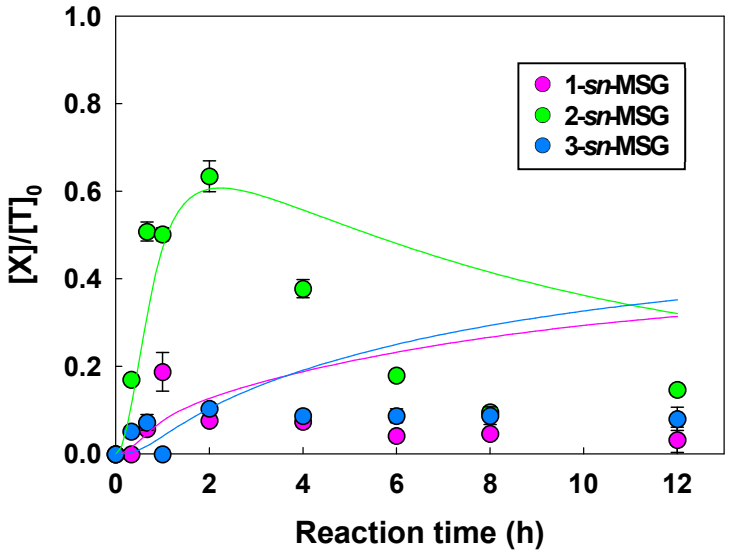

Figure III-9. Fitting of the kinetic model for tristearoylglycerol (TSG) hydrolysis when lipase from *Chromobacterium viscosum* was used. (A) tristearoylglycerol (TSG) and stearic acid (SA); (B) distearoylglycerol (DSG) isomers; (C) monostearoylglycerol (MSG) isomers.

(A)

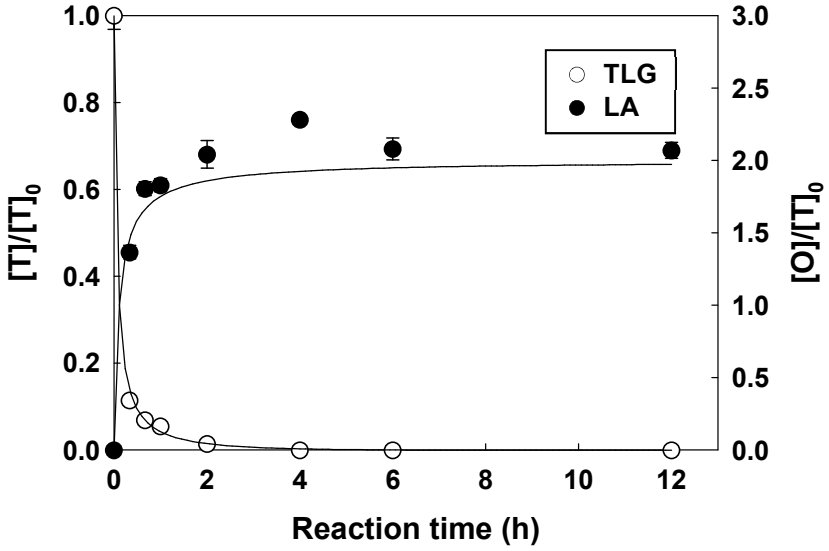
TLG
LA
[T]/[T]0
[L]/[O]0
Reaction time (h)

(B)

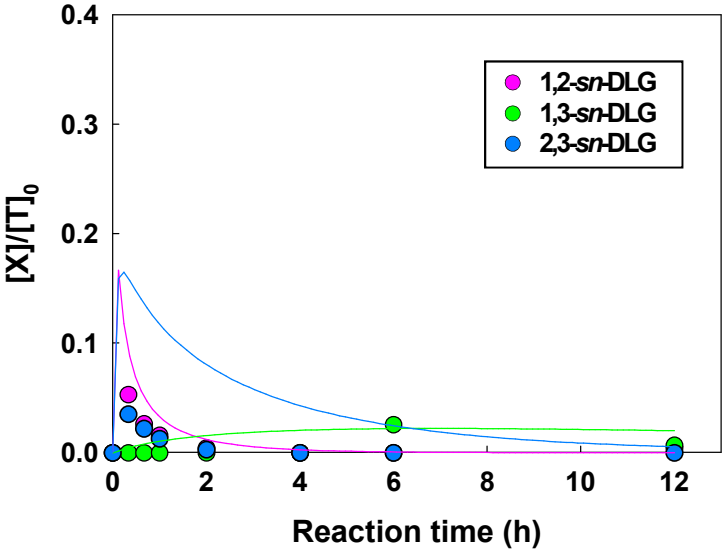
1,2-sn-DLG
1,3-sn-DLG
2,3-sn-DLG
[X]/[T]0
Reaction time (h)

(C)

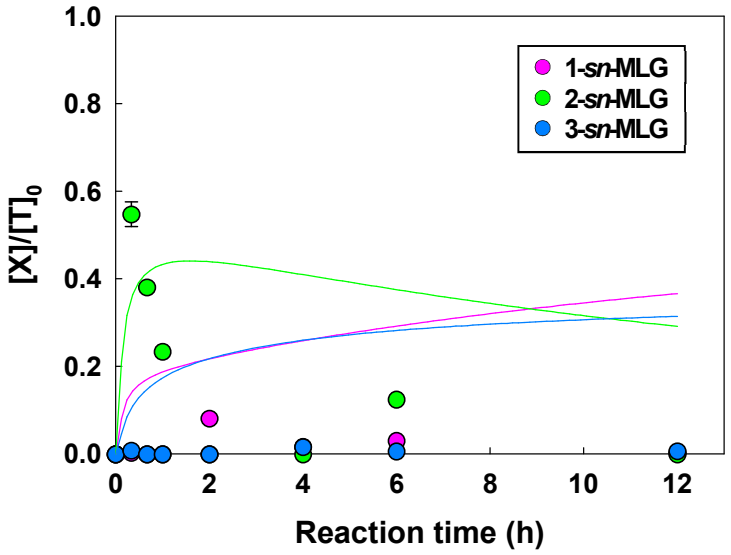

Figure III-10. Fitting of the kinetic model for trilinoleoylglycerol (TLG) hydrolysis when lipase from *Chromobacterium viscosum* was used. (A) TLG and linoleic acid (LA); (B) dilinoleoylglycerol (DLG) isomers; (C) monolinoleoylglycerol (MLG) isomers.

Table III-6. Values of kinetic parameters associated with triacylglycerol hydrolysis catalyzed by lipases from *Chromobacterium viscosum* estimated using the kinetic model

Kinetic constants	C14:0	C16:0	C18:0	C18:1	C18:2
K_1 ($M^{-1}h^{-1}$)	3.43×10^{10}	2.14×10^{10}	2.07×10^{9}	6.70×10^{6}	1.02×10^{9}
K_2 ($M^{-1}h^{-1}$)	4.19×10^{7}	1.47×10^{6}	3.95×10^{4}	6.71	2.26×10^{3}
K_3 ($M^{-1}h^{-1}$)	7.13×10^{9}	3.75×10^{9}	3.59×10^{8}	8.63×10^{5}	4.57×10^{8}
K_4 ($M^{-1}h^{-1}$)	2.82×10^{6}	2.27×10^{9}	8.31×10^{8}	1.62×10^{2}	7.39×10^{8}
K_5 ($M^{-1}h^{-1}$)	9.87×10^{10}	8.07×10^{10}	6.32×10^{9}	3.10×10^{7}	1.94×10^{9}
K_6 ($M^{-1}h^{-1}$)	3.00×10^{7}	2.60×10^{6}	2.03×10^{9}	6.86×10^{2}	3.72×10^{7}
K_7 ($M^{-1}h^{-1}$)	1.19×10^{7}	1.34×10^{6}	1.54×10^{9}	3.22×10^{2}	2.64×10^{4}
K_8 ($M^{-1}h^{-1}$)	2.70×10^{9}	1.72×10^{7}	9.23×10^{5}	1.83×10^{2}	2.00×10^{4}
K_9 ($M^{-1}h^{-1}$)	3.20×10^{8}	1.09×10^{9}	8.46×10^{8}	1.06×10^{2}	6.03×10^{8}
K_{10} ($M^{-1}h^{-1}$)	5.39×10^{-1}	1.07×10^{4}	2.18×10^{-3}	6.87×10^{-10}	3.44×10^{-4}
K_{11} ($M^{-1}h^{-1}$)	1.14×10^{-3}	6.78×10^{3}	2.30×10^{-5}	1.00×10^{6}	5.45×10^{-8}
K_{12} ($M^{-1}h^{-1}$)	1.49×10^{-2}	3.07×10^{3}	1.71×10^{3}	1.39×10^{-1}	1.61×10^{5}
K_{13} ($M\cdot h$)	8.52×10^{-9}	4.51×10^{-6}	5.29×10^{-6}	1.69×10^{-11}	2.85×10^{-7}
K_{14} ($M\cdot h$)	1.30×10^{-8}	3.87×10^{-9}	5.41×10^{-9}	2.03×10^{-11}	1.25×10^{-9}
K_{15} ($M\cdot h$)	1.91×10^{-2}	8.94×10^{-1}	3.06×10^{-4}	3.58×10^{-1}	8.88×10^{-3}
K_{16} ($M\cdot h$)	9.63×10^{-7}	8.66×10^{-7}	9.66×10^{-8}	1.75×10^{-6}	2.73×10^{-9}
K_{17} ($M\cdot h$)	8.26×10^{7}	8.36×10^{-1}	1.03×10^{5}	3.19×10^{7}	6.74×10^{3}
K_{18} ($M\cdot h$)	1.04×10^{6}	4.92×10^{-2}	8.04×10^{5}	3.88×10^{-11}	8.93×10^{6}
K_{19} ($M\cdot h$)	4.96×10^{6}	4.27×10^{1}	5.84×10^{1}	1.79×10^{3}	1.56×10^{-5}
K_{20}	1.38×10^{6}	3.73×10^{6}	1.76×10^{6}	1.04×10^{6}	2.08×10^{6}

Table III-6. (*continued*)

Kinetic constants	C14:0	C16:0	C18:0	C18:1	C18:2
k_{22} (h^{-1})	7.12×10^{-3}	5.80×10^{-3}	1.34×10^{-2}	2.05×10^{-3}	1.31×10^{-5}
k_{23} (h^{-1})	4.32×10^{-2}	4.77×10^{-2}	1.56×10^{-2}	2.06×10^{-3}	5.00×10^{-2}
k_{24} (h^{-1})	3.76×10^{-2}	4.99×10^{-2}	2.08×10^{-2}	2.19×10^{-2}	5.00×10^{-2}
k_{25} (h^{-1})	7.25×10^{-3}	4.24×10^{-4}	1.55×10^{-2}	2.18×10^{-2}	2.84×10^{-2}
k_{26} (h^{-1})	4.92×10^{-2}	5.00×10^{-2}	5.00×10^{-2}	1.81×10^{-2}	5.00×10^{-2}
k_{27} (h^{-1})	8.33×10^{-3}	7.55×10^{-5}	2.26×10^{-2}	1.81×10^{-2}	1.39×10^{-2}
k_{28} (h^{-1})	4.95×10^{-3}	7.81×10^{-5}	1.81×10^{-2}	1.45×10^{-2}	2.00×10^{-6}
k_{29} (h^{-1})	4.87×10^{-2}	5.00×10^{-2}	5.00×10^{-2}	1.45×10^{-2}	6.69×10^{-3}

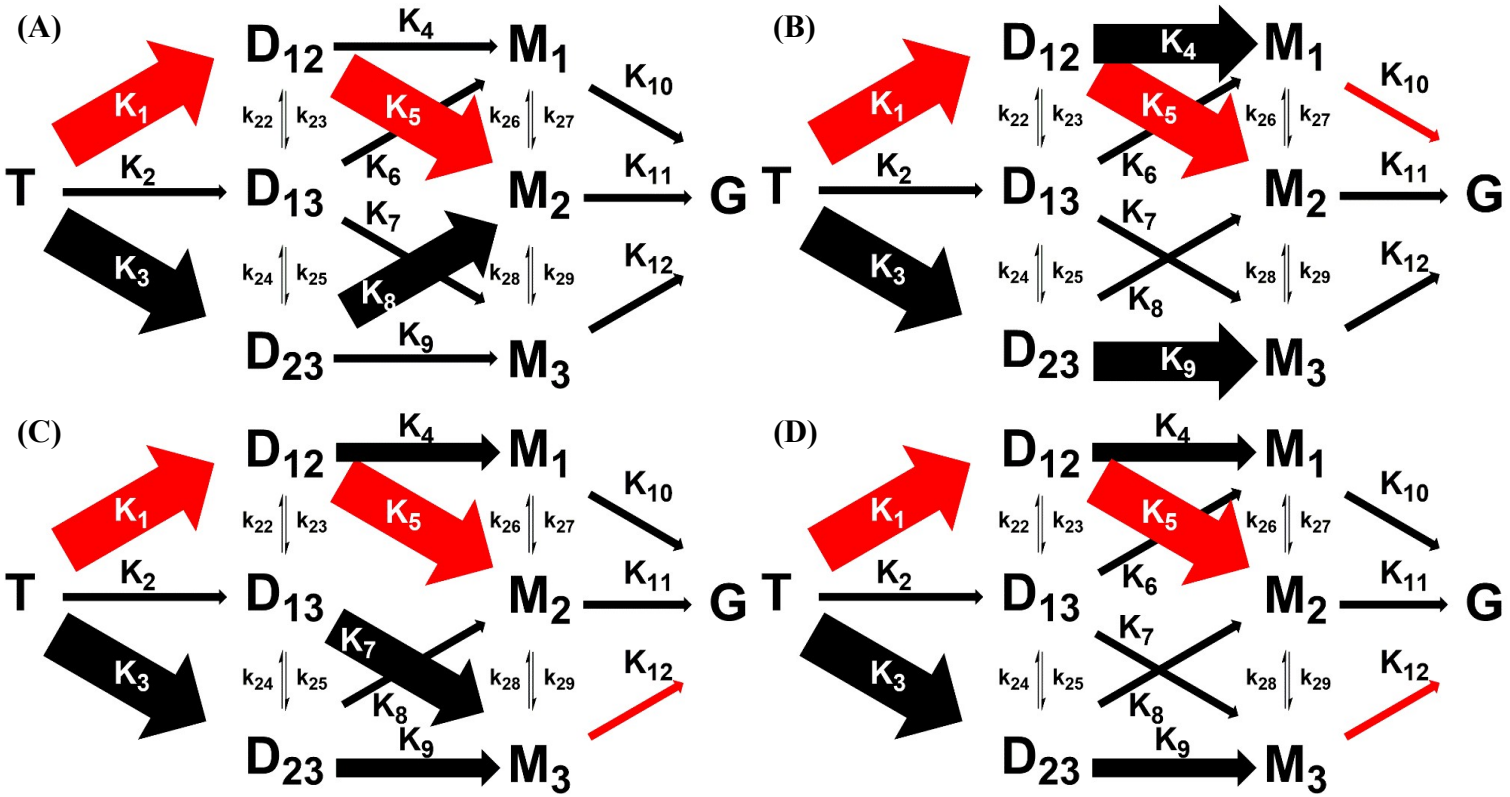

Figure III-11. Summary of TAG hydrolysis catalyzed by lipases from *Chromobacterium viscosum* considering integral stereoselectivity according to fatty acyl chain moiety: (A) myristic, (B) palmitic, (C) stearic and (D) linoleic acid.

III-3-2-3. ***Lipase from Pseudomonas fluorescens***

In contrast to PPL and CVL, in the case of PFL, DAG isomers were present from the initial phase of the reaction in the order of 2,3-*sn*-DAG, 1,2-*sn*-DAG, and 1,3-*sn*-DAG, which indicates the selectivity for ester bonds of TAG in the order of *sn*-1, *sn*-3, and *sn*-2 (Figures III-12B, 13B, 14B, and 15B). The difference observed for TPG hydrolysis was that 1,3-*sn*-DAG was not present for 12 h of reaction. The rapid increase in 2-*sn*-MAG accompanied by a gradual increase in 1-*sn*-MAG and 3-*sn*-MAG is consistent with the profile observed on TOG hydrolysis (Figures III-12C, 13C, 14C, and 15C).

The integral stereoselectivity of PFL determined by kinetic modeling is shown in Table III-7. In TAG hydrolysis, the kinetic parameters were in the order of K_3, K_2, and K_1, which indicates the selectivity of PFL for TMG, TPG, TSG, and TLG is in the order of *sn*-1, *sn*-3, and *sn*-2. Meanwhile, the fold differences between K_3 and K_2 were the highest for TPG (1.91×10^8-fold), while those for the other TAG were in the range of 9.9 to 49.9-fold. These fold differences match with the time course of DAG (Figures III-12B, 13B, 14B, and 15B). In DAG hydrolysis, the *sn*-3 position of 2,3-*sn*-DAG represented by K_8 was the most selective site with acyl moiety of MA, PA, and LA, while K_9 indicating the *sn*-3 position of 1,3-*sn*-DAG was the highest value with acyl moiety of SA. For MAG hydrolysis, PFL was selective on MAGs in the order

of 2-*sn*-MAG, 1-*sn*-MAG, and 3-*sn*-MAG, judging from K_{11}, K_{10}, and K_{12} with acyl moiety of SA, while K_{10} was the highest among these three with acyl moiety of MA, PA, and LA. However, the values for MAG hydrolysis were much smaller than those for TAG and DAG hydrolysis, which cause minor impacts on the overall profile of acylglycerols. The summarized main pathway of the hydrolysis reaction is shown in Figure III-16. The main pathway for reaction catalyzed by PFL is from TAG to 2,3-*sn*-DAG and 2-*sn*-MAG for TMG, TPG, TSG, and TLG.

(A)

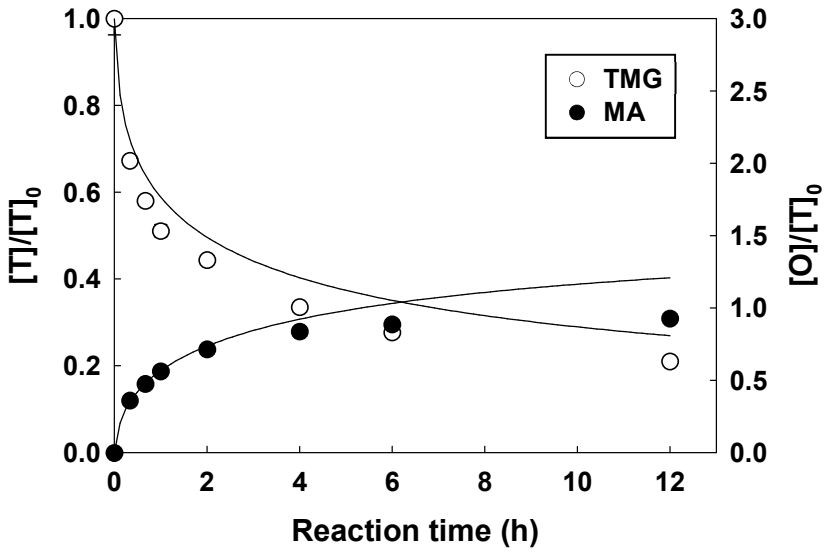
TMG
MA
[T]/[T]0
[L]/[O]0
Reaction time (h)

(B)

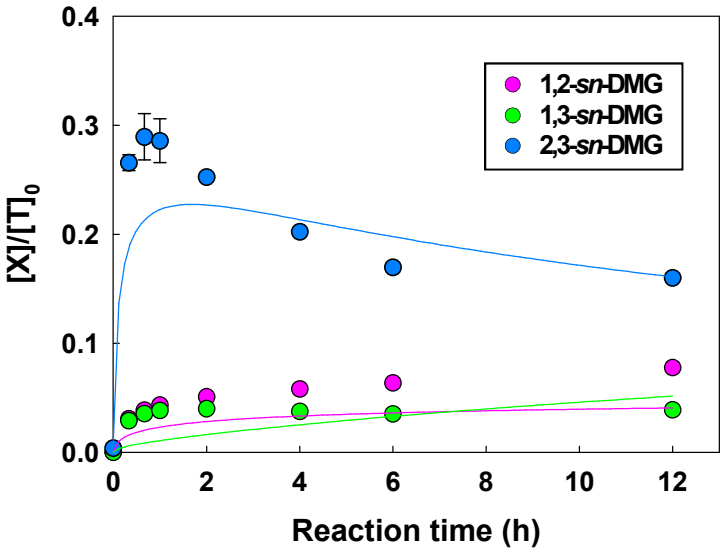
1,2-sn-DMG
1,3-sn-DMG
2,3-sn-DMG
[X]/[T]0
Reaction time (h)

(C)

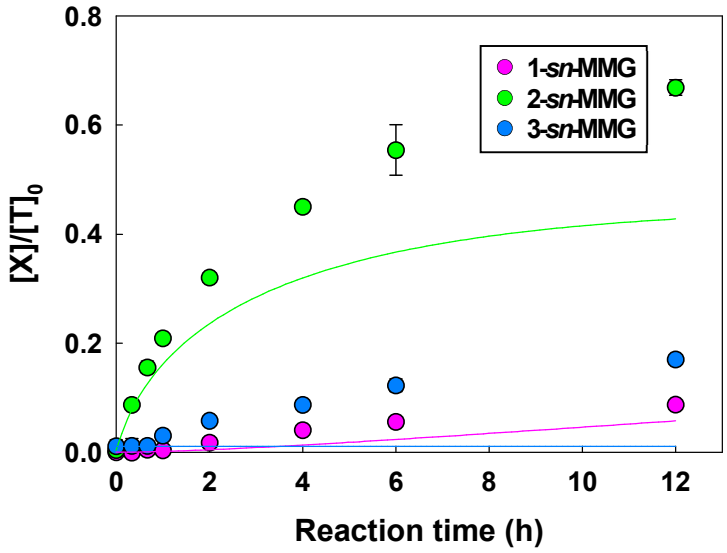

Figure III-12. Fitting of the kinetic model for trimyristoylglycerol (TMG) hydrolysis when lipase from *Pseudomonas fluorescens* was used. (A) TMG and myristic acid (MA); (B) dimyristoylglycerol (DMG) isomers; (C) monomyristoylglycerol (MMG) isomers.

(A)

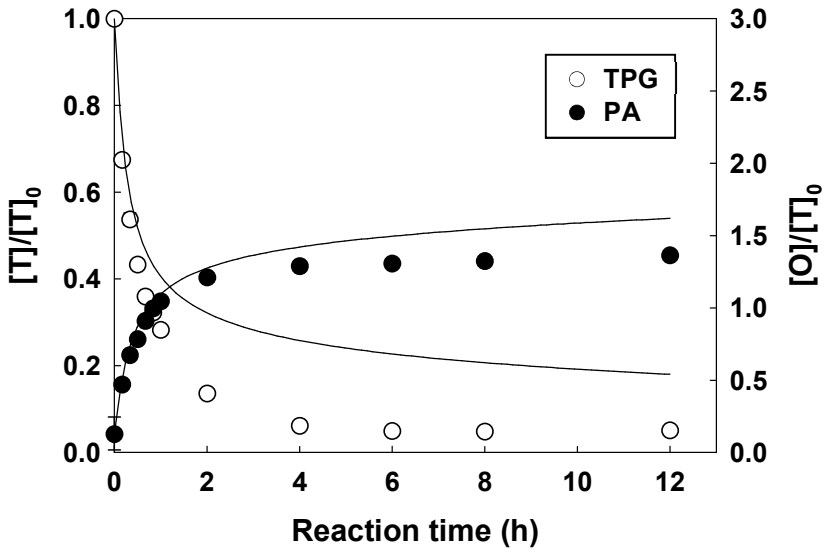
TPG
PA
[T]/[T]0
[L]/[O]0
Reaction time (h)

(B)

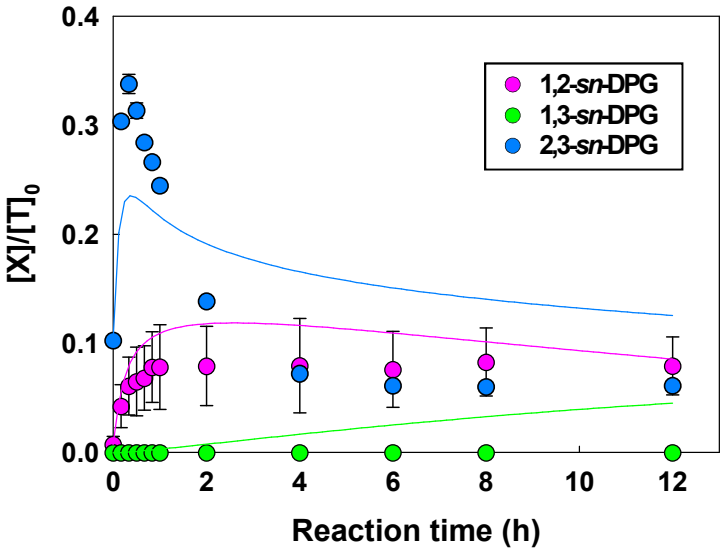
1,2-sn-DPG
1,3-sn-DPG
2,3-sn-DPG
[X]/[T]0
Reaction time (h)

(C)

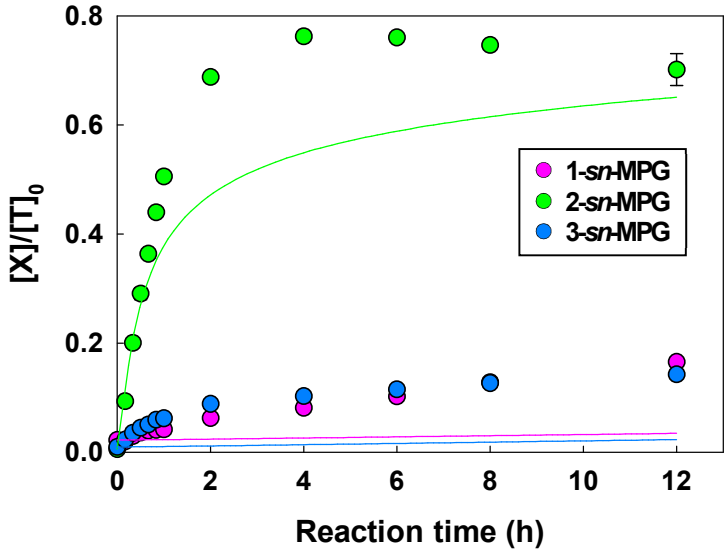

Figure III-13. Fitting of the kinetic model for tripalmitoylglycerol (TPG) hydrolysis when lipase from *Pseudomonas fluorescens* was used. (A) TPG and palmitic acid (PA); (B) dipalmitoylglycerol (DPG) isomers; (C) monopalmitoylglycerol (MPG) isomers.

(A)

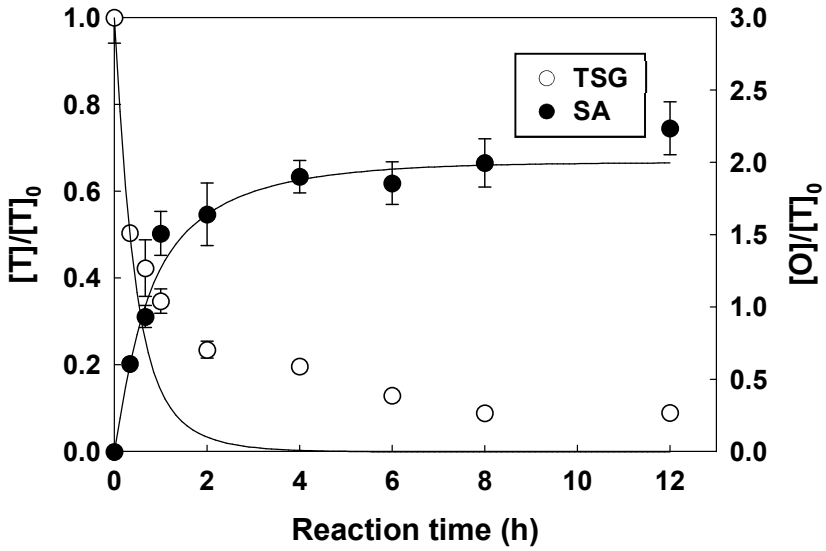
TSG
SA
[T]/[T]0
[L]/[O]0
Reaction time (h)

(B)

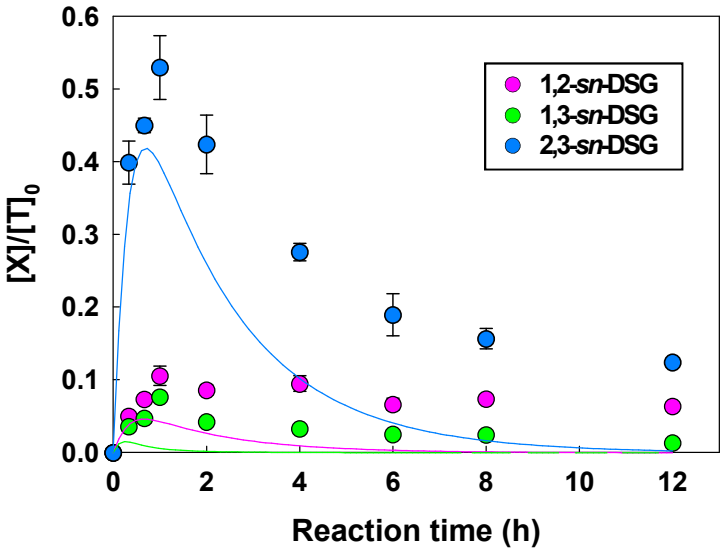
1,2-sn-DSG
1,3-sn-DSG
2,3-sn-DSG
[X]/[T]0
Reaction time (h)

(C)

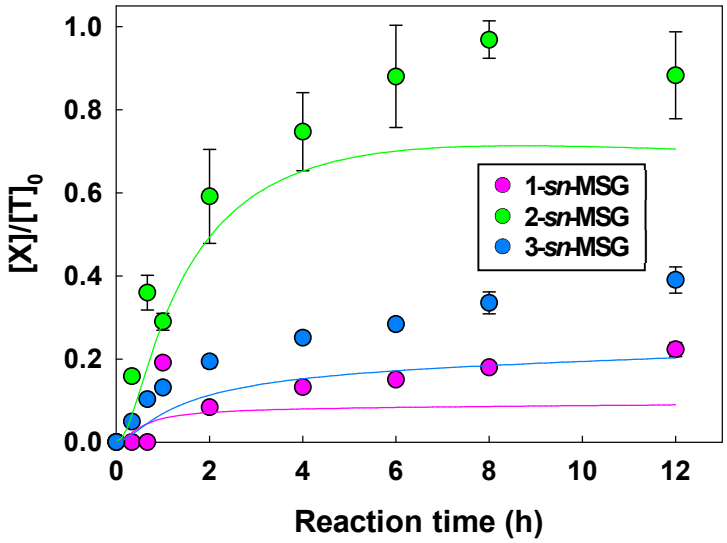

Figure III-14. Fitting of the kinetic model for tristearoylglycerol (TSG) hydrolysis when lipase from *Pseudomonas fluorescens* was used. (A) TSG and stearic acid (SA); (B) distearoylglycerol (DSG) isomers; (C) monostearoylglycerol (MSG) isomers.

(A)

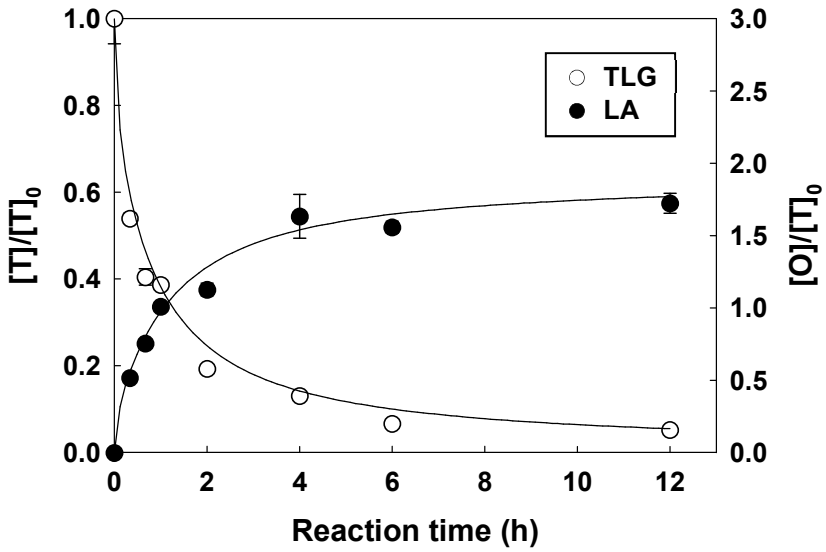
TLG
LA
[T]/[T]0
[L]/[T]0
Reaction time (h)

(B)

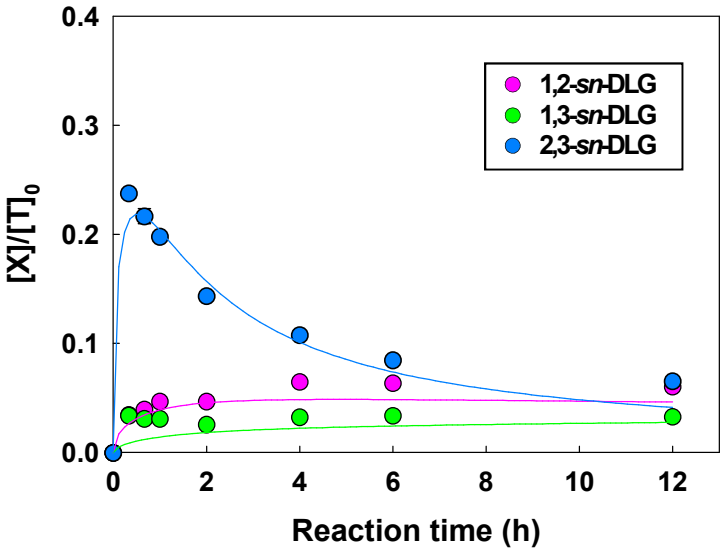
1,2-sn-DLG
1,3-sn-DLG
2,3-sn-DLG
[X]/[T]0
Reaction time (h)

(C)

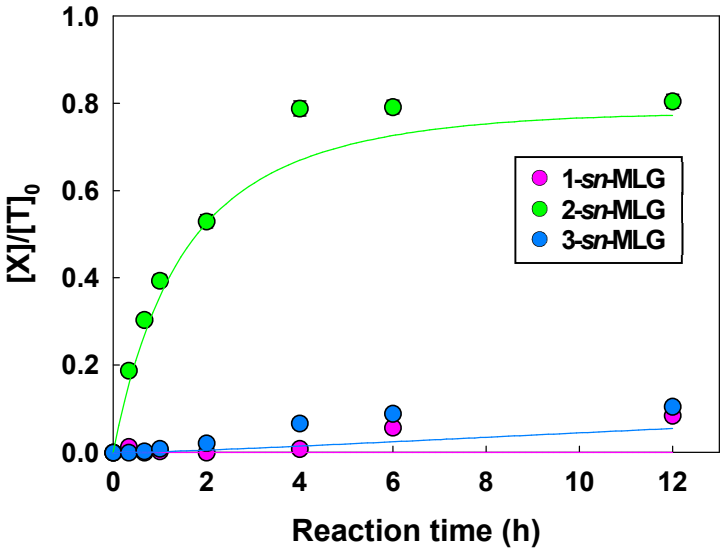

Figure III-15. Fitting of the kinetic model for trilinoleoylglycerol (TLG) hydrolysis when lipase from *Pseudomonas fluorescens* was used. (A) TLG and linoleic acid (LA); (B) dilinoleoylglycerol (DLG) isomers; (C) monolinoleoylglycerol (MLG) isomers.

Table III-7. Values of kinetic parameters associated with triacylglycerol hydrolysis catalyzed by lipases from *Pseudomonas fluorescens* estimated using the kinetic model

Kinetic constants	C14:0	C16:0	C18:0	C18:1	C18:2
K_1 ($M^{-1}h^{-1}$)	5.68×10^{7}	8.05×10^{9}	2.82×10^{8}	3.75×10^{8}	4.64×10^{8}
K_2 ($M^{-1}h^{-1}$)	1.90×10^{7}	1.92×10^{4}	2.48×10^{8}	1.30×10^{10}	1.43×10^{8}
K_3 ($M^{-1}h^{-1}$)	9.49×10^{8}	3.67×10^{10}	2.46×10^{9}	5.93×10^{10}	6.11×10^{9}
K_4 ($M^{-1}h^{-1}$)	1.55×10^{5}	1.03×10^{5}	4.40×10^{7}	8.32×10^{6}	1.71×10^{1}
K_5 ($M^{-1}h^{-1}$)	4.52×10^{5}	1.11×10^{5}	1.51×10^{9}	8.55×10^{6}	9.60×10^{8}
K_6 ($M^{-1}h^{-1}$)	1.73×10^{5}	3.46×10^{10}	7.64×10^{9}	3.05×10^{10}	4.95×10^{1}
K_7 ($M^{-1}h^{-1}$)	1.89×10^{5}	3.60×10^{10}	1.93×10^{9}	6.72×10^{10}	6.93×10^{8}
K_8 ($M^{-1}h^{-1}$)	2.06×10^{9}	8.87×10^{10}	1.16×10^{9}	9.45×10^{10}	1.42×10^{10}
K_9 ($M^{-1}h^{-1}$)	1.33×10^{4}	6.68×10^{5}	2.45×10^{8}	3.66×10^{8}	2.59×10^{5}
K_{10} ($M^{-1}h^{-1}$)	1.64×10^{3}	3.06×10^{2}	3.86×10^{2}	8.40×10^{4}	4.16×10^{5}
K_{11} ($M^{-1}h^{-1}$)	3.70×10^{2}	7.50×10^{-3}	5.45×10^{3}	1.77×10^{5}	1.54×10^{-3}
K_{12} ($M^{-1}h^{-1}$)	3.61×10^{2}	2.60×10^{1}	3.95×10^{1}	2.23×10^{4}	3.34×10^{5}
K_{13} ($M\cdot h$)	5.76×10^{-8}	4.14×10^{-5}	1.87×10^{-3}	8.52×10^{-5}	5.12×10^{-6}
K_{14} ($M\cdot h$)	1.80×10^{-3}	4.54×10^{-1}	4.30×10^{-3}	5.20×10^{-1}	1.35×10^{-1}
K_{15} ($M\cdot h$)	7.48×10^{-4}	6.24×10^{-1}	4.39×10^{-3}	2.15×10^{-4}	2.62×10^{-1}
K_{16} ($M\cdot h$)	1.17×10^{-7}	3.66×10^{-7}	6.78×10^{-4}	1.25×10^{-3}	4.92×10^{-4}
K_{17} ($M\cdot h$)	1.65×10^{5}	2.60×10^{6}	3.13×10^{4}	2.13×10^{4}	7.93×10^{7}
K_{18} ($M\cdot h$)	5.00×10^{4}	2.54×10^{6}	2.08×10^{3}	3.69×10^{1}	1.10×10^{7}
K_{19} ($M\cdot h$)	2.87	3.67×10^{7}	3.81×10^{5}	3.78×10^{5}	6.45
K_{20}	3.39×10^{5}	4.58×10^{7}	5.29×10^{5}	6.15×10^{7}	2.04×10^{7}

Table III-7. (*continued*)

Kinetic constants	C14:0	C16:0	C18:0	C18:1	C18:2
k_{22} (h^{-1})	3.16×10^{-3}	2.54×10^{-5}	5.09×10^{-3}	8.68×10^{-1}	1.95×10^{-3}
k_{23} (h^{-1})	3.19×10^{-3}	5.50×10^{-2}	1.16×10^{-2}	8.72×10^{-1}	5.67×10^{-3}
k_{24} (h^{-1})	1.66×10^{-2}	7.38×10^{-4}	1.08×10^{-2}	3.05×10^{-2}	1.02×10^{-2}
k_{25} (h^{-1})	2.61×10^{-3}	1.55×10^{-5}	6.45×10^{-3}	2.25×10^{-2}	4.39×10^{-3}
k_{26} (h^{-1})	1.57×10^{-2}	3.23×10^{-5}	1.25×10^{-3}	8.66×10^{-3}	2.82×10^{-7}
k_{27} (h^{-1})	1.56×10^{-2}	1.69×10^{-5}	3.82×10^{-4}	7.49×10^{-4}	1.41×10^{-7}
k_{28} (h^{-1})	1.91×10^{-6}	8.95×10^{-5}	2.67×10^{-3}	2.09×10^{-4}	4.96×10^{-3}
k_{29} (h^{-1})	3.71×10^{-6}	1.59×10^{-4}	6.45×10^{-3}	4.42×10^{-4}	6.62×10^{-3}

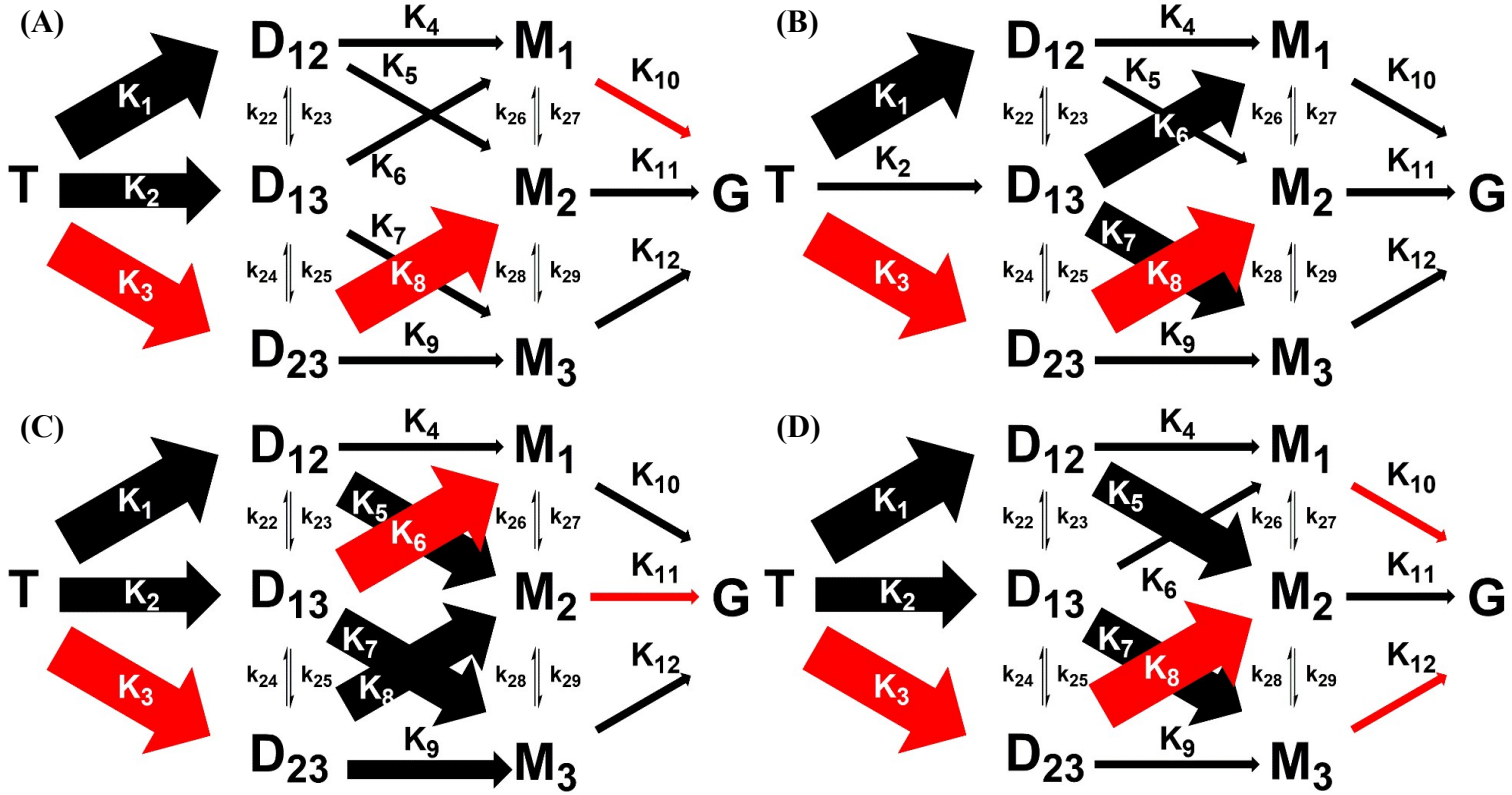

Figure III-16. Summary of triacylglycerol (TAG) hydrolysis catalyzed by lipase from *Pseudomonas fluorescens* considering integral stereoselectivity according to fatty acyl chain moiety: (A) myristic, (B) palmitic, (C) stearic and (D) linoleic acid.

III-3-2-4. ***Lipase A from Candida antarctica***

In the case of CALA, the time courses of DAGs showed the most significant differences according to the acyl moiety. In Figure III-17B, 18B, and 19B, the proportions of 2,3-*sn*-DAG, 1,2-*sn*-DAG, and 1,3-*sn*-DAG with acyl moiety of saturated FA at the early stage of hydrolysis were in the range of 40.0-43.9, 36.0-40.5, and 15.6-24.4%, respectively. However, 1,3-*sn*-DAG showed the highest proportion of 55.9% in DAG for TLG hydrolysis, followed by 23.5 % of 2,3-*sn*-DAG and 20.6% of 1,2-*sn*-DAG (Figure III-20B). Also, in contrast to the other lipases tested, 2-*sn*-MAG was not the highest among MAG in CALA-catalyzed reaction for all substrates (Figure III-17C, 18C, 19C, and 20C). However, some discrepancies in the data and the fitted curve of DAGs and MAGs during the CALA-catalyzed reaction were observed. Considering relatively low concentration of DAGs and MAGs measured in saturated FA species, variation in the substrate concentration would be required to improve the fitness of the present kinetic modelling. Also, since the equations for rate constants of the present kinetic model do not include the concept of interface, which is expressed as adsorption isotherm, further works for improvement would be application of the interface to the concentration of enzymes, substrate, and products with varying R-values.

As shown in Table III-8, the kinetic parameters for TAG hydrolysis were

in the order of K_3, K_1, and K_2 for TMG, TPG, and TSG, indicating CALA exhibits the lowest selectivity for the *sn*-2 position of TAG with saturated FA. This was inverted for the case of TLG hydrolysis, where K_2 is the highest value followed by K_3 and K_1 as same as the TOG hydrolysis. The fold differences between K_3 and K_1 were in the range of 1.4-1.6. Also, the top two values in DAG hydrolysis were toward the 1,2-*sn*-DAG and 2,3-*sn*-DAG with acyl moiety of MA, PA, and SA, while 1,3-*sn*-DAG was the most selective substrate when TLG was used. For MAG hydrolysis, the highest value was K_{10} for TMG, K_{12} for TPG and TSG, but K_{11} for TLG. However, all these values were lower than those for DAG and TAG hydrolysis.

TAG hydrolysis reactions catalyzed by the CALA are visually summarised in Figure III-21. In the hydrolysis of TAGs with saturated FA, which are TMG, TPG, and TSG in this study, CALA exhibited significant selectivity for all *sn*-positions of TAG, with the main pathway going from TAG to 1,2-*sn*-DAG and 2,3-*sn*-DAG at a similar rate, and then to 2-*sn*-MAG. In contrast, the main pathway of the reaction process for TLG was from TAG to 1,3-*sn*-DAG, 1-*sn*-MAG, and 3-*sn*-MAG at a similar rate.

These obvious differences in integral stereoselectivity among substrates depending on the presence of a double bond might be ascribed to the unique structural feature of CALA. It is known that the selectivity of lipase is

primarily determined by the structural fitness between the enzyme and the substrate (Vaysse, Ly, Moulin, & Dubreucq, 2002). With the lid in the position of open form, CALA is known to have a wide area on the catalytic residue for access to the TAG, which enables the FA chain at the *sn*-2 position to bind at the tunnel-like acyl binding site (Ericsson et al., 2008). In addition, the acyl binding tunnel of CALA shows a very good fit with long and stretched FA, which makes *trans*-FA or saturated FA to be preferred over *cis*-FA (Borgdorf & Warwel, 1999; Brundiek, Padhi, Kourist, Evitt, & Bornscheuer, 2012; Ericsson et al., 2008). Therefore, it is expected that the conformation of TAG with *sn*-2 FA on the acyl binding site is preferred over those with *sn*-1 or *sn*-3 FA on the acyl binding site to form a stable complex when unsaturated *cis*-FAs such as OA and LA are used. Conversely, when saturated FAs with more fitness to the tunnel of CALA, the *sn*-2 selectivity on TAG could be lowered since the conformation of TAG with *sn*-1 or *sn*-3 FA on the acyl binding site have less difference in stability.

On the other hand, it is thought that PPL, CVL, and PFL did not show major conversion of integral stereoselectivity on TAG of different FAs, because they have the acyl binding site with funnel-like structure in common instead of a long stretched tunnel (Pleiss, Fischer, & Schmid, 1998). In the case of PPL, the β9 loop was suggested as the primary acyl binding site of *sn*-1 or *sn*-3 FA, and the lid domain play as the secondary position for FA of TAG

at the opposite direction, leaving *sn*-2 acyl chain nonhydrolyzable by remaining in the center position interacting with hydrophobic matrix (Carrière, Withers-Martinez, van Tilbeurgh, Roussel, Cambillau, & Verger, 1998). Therefore, the integral stereoselectivity of the lipase needs to be analyzed for each substrate of FA to understand the lipases with a unique structure such as CALA. Also, it is needed to conduct the docking simulation based on molecular dynamics for elucidation of these differences in the integral stereoselectivities in further works.

(A)

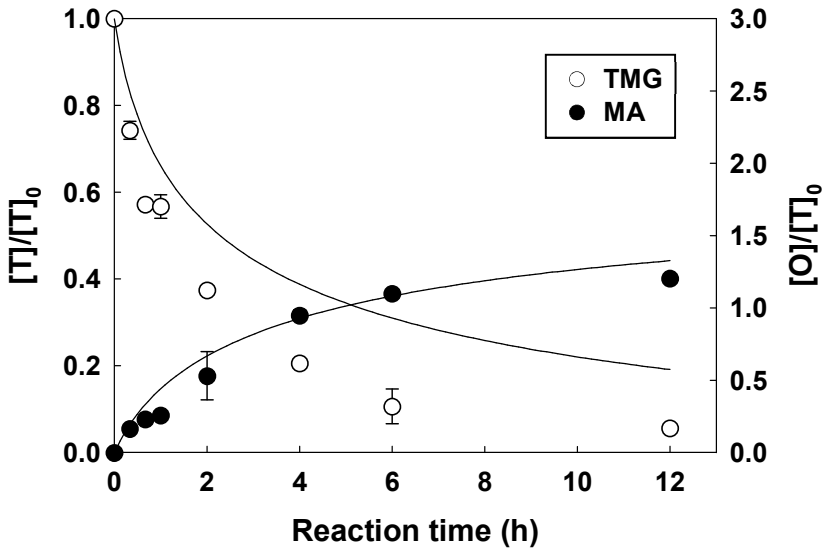
TMG
MA
[T]/[T]0
[O]/[T]0
Reaction time (h)

(B)

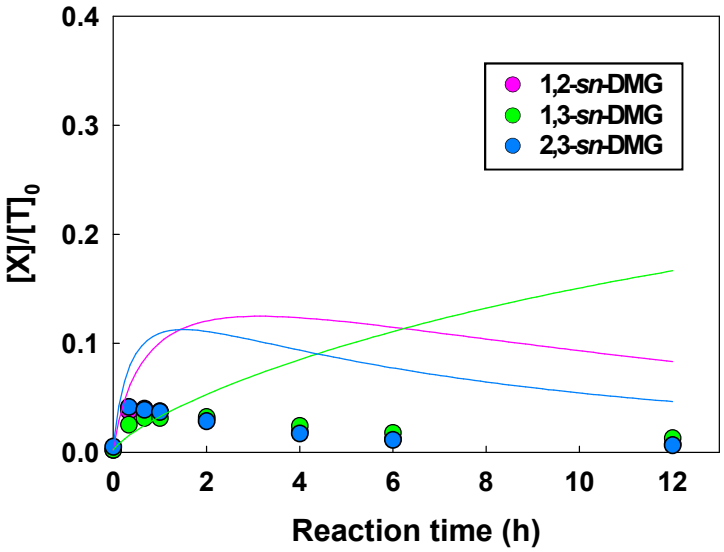
1,2-sn-DMG
1,3-sn-DMG
2,3-sn-DMG
[X]/[T]0
Reaction time (h)

(C)

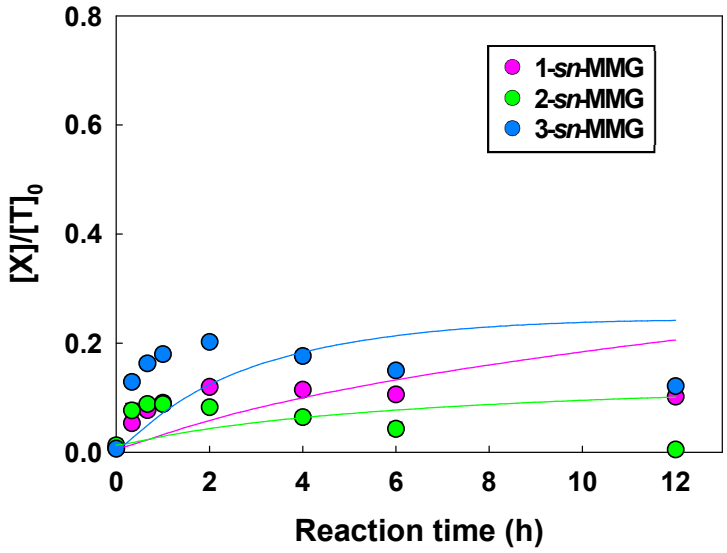

Figure III-17. Fitting of the kinetic model for trimyristoylglycerol (TMG) hydrolysis when lipase A from *Candida antarctica* was used. (A) TMG and myristic acid (MA); (B) dimyristoylglycerol (DMG) isomers; (C) monomyristoylglycerol (MMG) isomers.

(A)

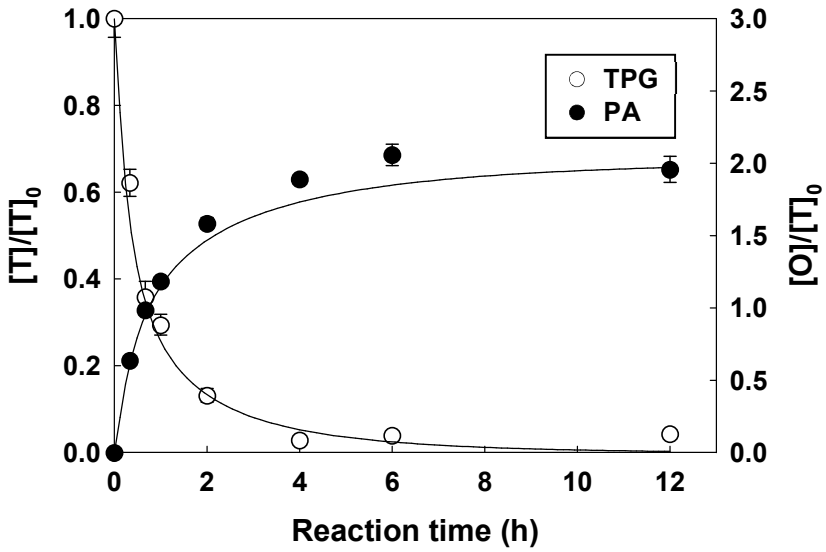
TPG
PA
[T]/[T]0
[L]/[O]0
Reaction time (h)

(B)

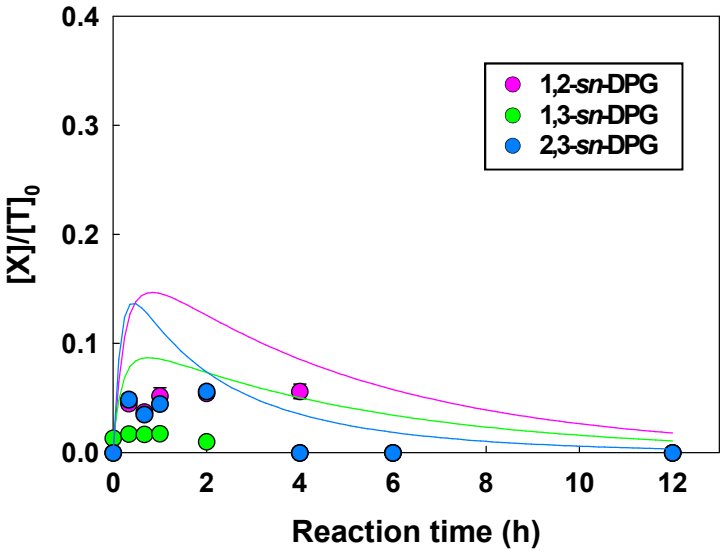
1,2-sn-DPG
1,3-sn-DPG
2,3-sn-DPG
[X]/[T]0
Reaction time (h)

(C)

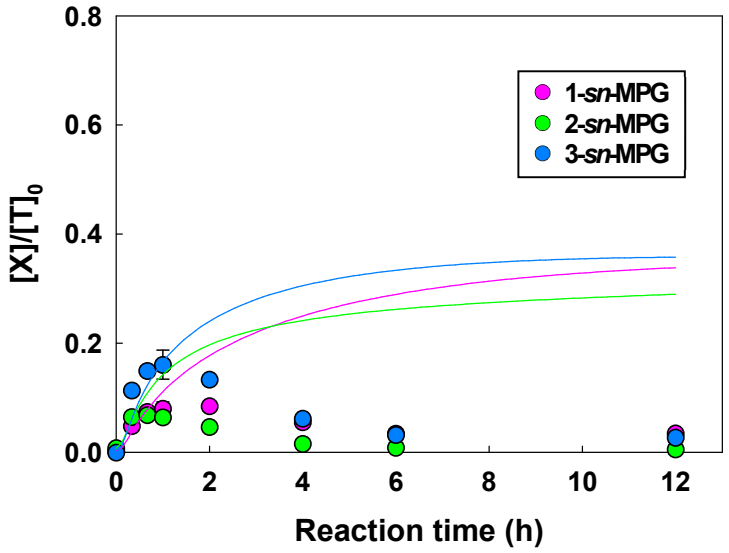

Figure III-18. Fitting of the kinetic model for tripalmitoylglycerol (TPG) hydrolysis when lipase A from *Candida antarctica* was used. (A) TPG and palmitic acid (PA); (B) dipalmitoylglycerol (DPG) isomers; (C) monopalmitoylglycerol (MPG) isomers.

(A)

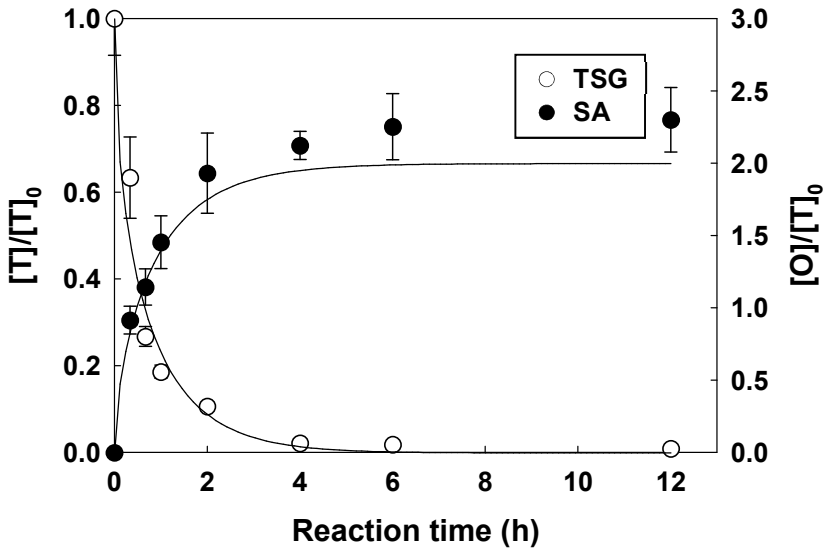
TSG
SA
[T]/[T]0
[L]/[T]0
Reaction time (h)

(B)

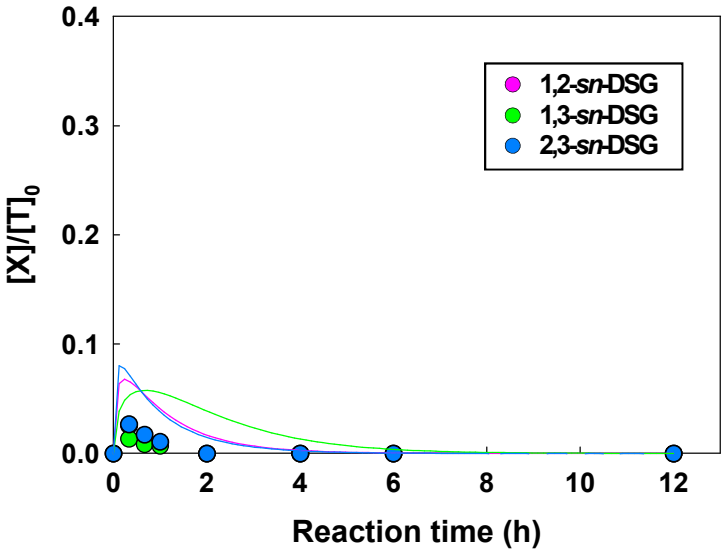
1,2-sn-DSG
1,3-sn-DSG
2,3-sn-DSG
[X]/[T]0
Reaction time (h)

(C)

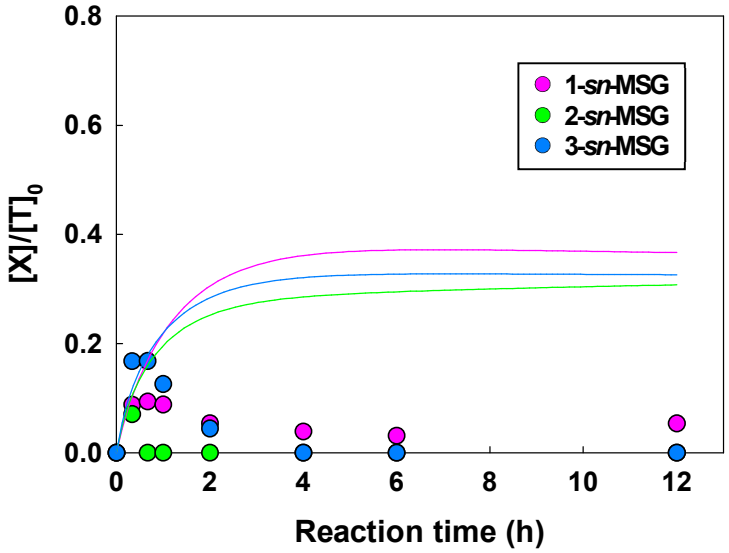

Figure III-19. Fitting of the kinetic model for tristearoylglycerol (TSG) hydrolysis when lipase from A from *Candida antarctica* was used. (A) TSG and stearic acid (SA); (B) distearoylglycerol (DSG) isomers; (C) monostearoylglycerol (MSG) isomers.

(A)

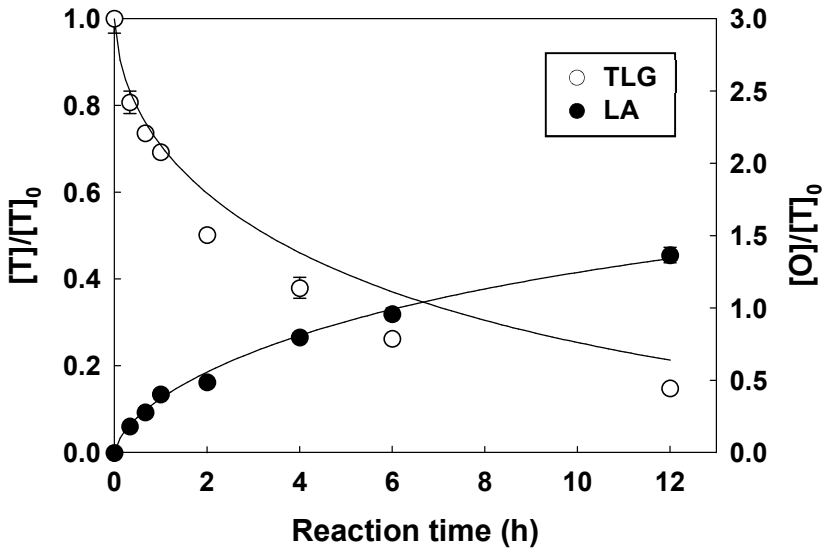
TLG
LA
[T]/[T]0
[L]/[O]0
Reaction time (h)

(B)

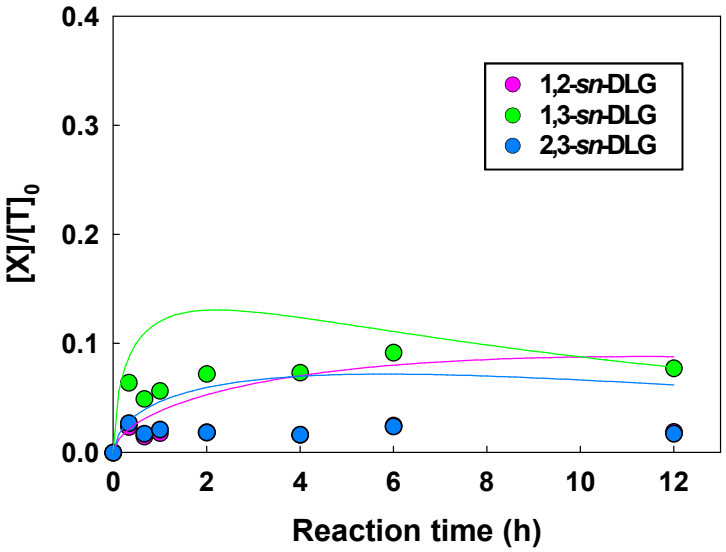
1,2-sn-DLG
1,3-sn-DLG
2,3-sn-DLG
[X]/[T]0
Reaction time (h)

(C)

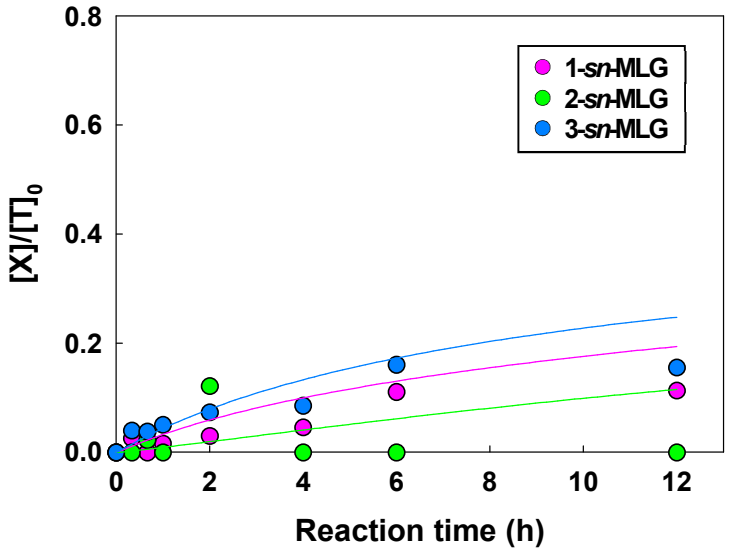

Figure III-20. Fitting of the kinetic model for trilinoleoylglycerol (TLG) hydrolysis when lipase A from *Candida antarctica* was used. (A) TLG and linoleic acid (LA); (B) dilinoleoylglycerol (DLG) isomers; (C) monolinoleoylglycerol (MLG) isomers.

Table III-8. Values of kinetic parameters associated with triacylglycerol hydrolysis catalyzed by lipase A from *Candida antarctica* estimated using the kinetic model

Kinetic constants	C14:0	C16:0	C18:0	C18:1	C18:2
K_1 ($M^{-1}h^{-1}$)	1.63×10^{9}	2.82×10^{10}	2.73×10^{9}	1.00×10^{8}	1.83×10^{8}
K_2 ($M^{-1}h^{-1}$)	2.98×10^{8}	1.62×10^{10}	1.14×10^{9}	1.03×10^{9}	9.84×10^{8}
K_3 ($M^{-1}h^{-1}$)	2.47×10^{9}	4.18×10^{10}	4.38×10^{9}	2.12×10^{8}	2.66×10^{8}
K_4 ($M^{-1}h^{-1}$)	4.18×10^{9}	5.09×10^{10}	1.90×10^{10}	1.33×10^{8}	7.12×10^{7}
K_5 ($M^{-1}h^{-1}$)	9.48×10^{5}	3.37×10^{9}	3.42×10^{9}	3.98×10^{6}	2.15×10^{7}
K_6 ($M^{-1}h^{-1}$)	1.97×10^{7}	1.78×10^{10}	4.82×10^{9}	2.13×10^{9}	1.79×10^{9}
K_7 ($M^{-1}h^{-1}$)	7.31×10^{5}	4.83×10^{10}	1.74×10^{9}	1.93×10^{9}	2.40×10^{9}
K_8 ($M^{-1}h^{-1}$)	2.34×10^{9}	7.42×10^{10}	1.53×10^{10}	1.45×10^{9}	1.37×10^{9}
K_9 ($M^{-1}h^{-1}$)	9.45×10^{9}	6.46×10^{10}	1.93×10^{10}	6.36×10^{5}	6.33×10^{7}
K_{10} ($M^{-1}h^{-1}$)	4.96×10^{4}	8.13	4.05×10^{-1}	2.41×10^{-3}	3.96
K_{11} ($M^{-1}h^{-1}$)	1.19×10^{-4}	4.01×10^{4}	2.02	3.66×10^{3}	1.48×10^{2}
K_{12} ($M^{-1}h^{-1}$)	3.63×10^{4}	2.08×10^{5}	1.49×10^{1}	1.29×10^{-3}	7.16×10^{-1}
K_{13} ($M\cdot h$)	4.14×10^{-5}	4.26×10^{-5}	1.28×10^{-6}	1.93×10^{-5}	2.06×10^{-5}
K_{14} ($M\cdot h$)	1.05×10^{-7}	5.41×10^{-7}	2.93×10^{-4}	2.23×10^{-2}	2.19×10^{-2}
K_{15} ($M\cdot h$)	7.16×10^{-1}	7.98×10^{-7}	1.81×10^{-4}	1.99×10^{-7}	2.96×10^{-4}
K_{16} ($M\cdot h$)	4.83×10^{-8}	2.53×10^{-7}	1.09×10^{-5}	2.90×10^{-6}	3.58×10^{-4}
K_{17} ($M\cdot h$)	3.42×10^{-2}	8.85×10^{6}	1.36×10^{6}	4.26×10^{5}	2.97×10^{5}
K_{18} ($M\cdot h$)	4.17×10^{6}	2.15	8.44×10^{5}	7.17×10^{2}	2.86×10^{3}
K_{19} ($M\cdot h$)	1.35×10^{-2}	4.36×10^{-1}	1.76×10^{5}	9.90×10^{5}	1.32×10^{6}
K_{20}	3.83×10^{6}	1.54×10^{7}	1.70×10^{6}	5.34×10^{5}	5.71×10^{5}

Table III-8. (*continued)*

Kinetic constants	C14:0	C16:0	C18:0	C18:1	C18:2
k_{22} (h^{-1})	1.02×10^{-5}	3.98×10^{-2}	1.61×10^{-2}	2.75×10^{-2}	2.73×10^{-2}
k_{23} (h^{-1})	5.00×10^{-2}	4.98×10^{-2}	2.66×10^{-2}	4.82×10^{-2}	4.76×10^{-2}
k_{24} (h^{-1})	5.00×10^{-2}	4.81×10^{-2}	2.29×10^{-2}	4.97×10^{-2}	4.91×10^{-2}
k_{25} (h^{-1})	1.06×10^{-5}	4.21×10^{-2}	1.10×10^{-2}	3.34×10^{-2}	3.31×10^{-2}
k_{26} (h^{-1})	5.00×10^{-2}	4.89×10^{-2}	2.20×10^{-2}	5.00×10^{-2}	4.96×10^{-2}
k_{27} (h^{-1})	1.06×10^{-5}	4.17×10^{-2}	2.19×10^{-2}	3.10×10^{-2}	3.08×10^{-2}
k_{28} (h^{-1})	4.19×10^{-2}	2.67×10^{-2}	2.13×10^{-2}	1.86×10^{-2}	1.82×10^{-2}
k_{29} (h^{-1})	4.19×10^{-2}	2.67×10^{-2}	2.14×10^{-2}	1.87×10^{-2}	1.88×10^{-2}

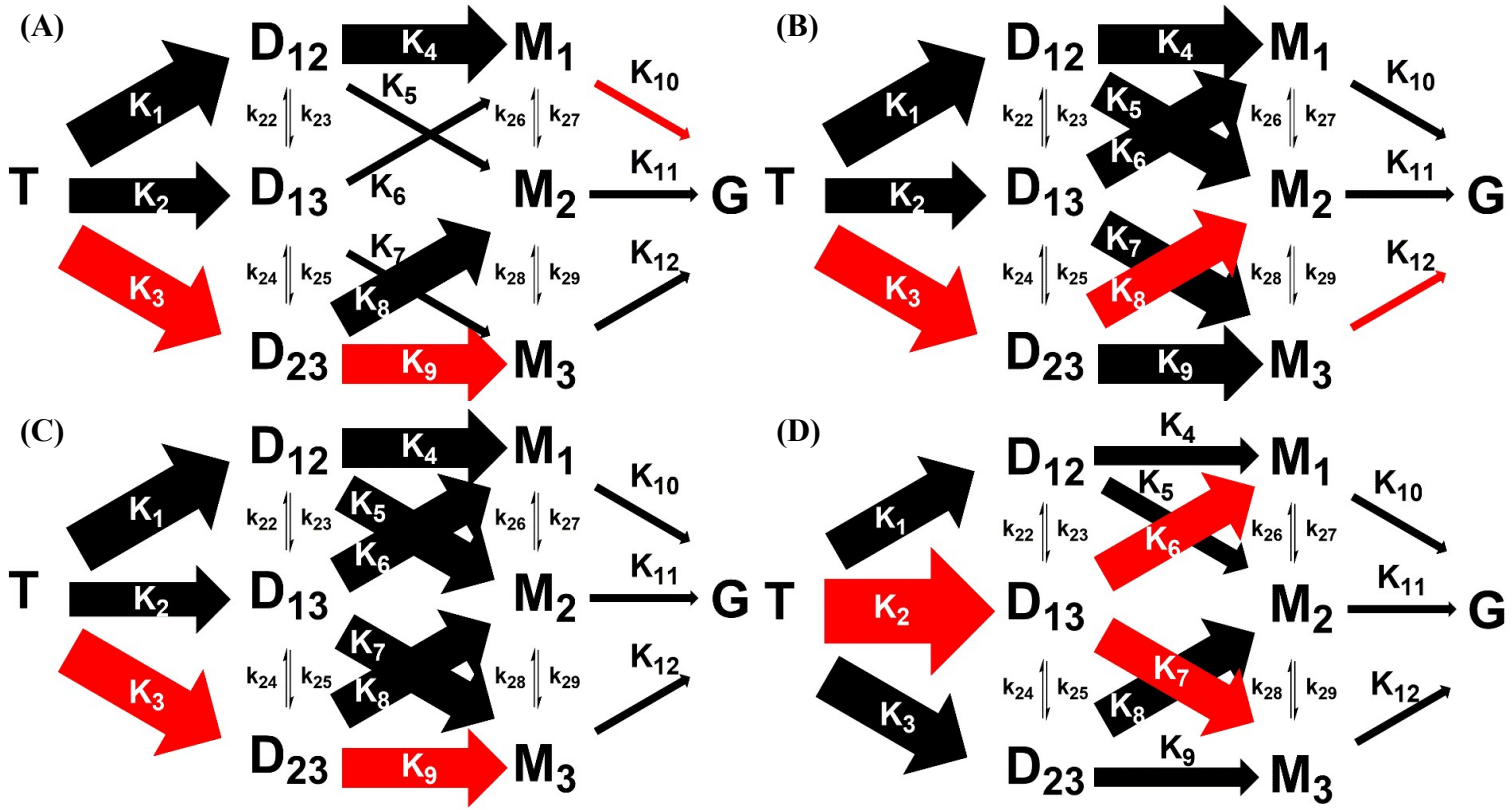

Figure III-21. Summary of triacylglycerol (TAG) hydrolysis catalyzed by lipase A from *Candida antarctica* considering integral stereoselectivity according to fatty acyl chain moiety: (A) myristic, (B) palmitic, (C) stearic and (D) linoleic acid.

III-4. Conclusions

In this chapter, simple analytical methods for the separation and quantification of FA, MAGs, DAGs, and TAG with various acyl moieties were established based on HPLC-ELSD equipped with CSP columns. The methods showed short analysis times and sufficient resolutions for TMG, TPG, TSG, TLG, and seven hydrolysates for each of the TAGs, demonstrating the fitness for a rapid and accurate evaluation of integral stereoselectivity of lipase. Using the kinetic model developed in chapter II, the integral stereoselectivity was determined for four model lipases on TMG, TPG, TSG, and TLG. As a result, in the case of PPL, CVL, and PFL, the integral stereoselectivity remained among the TAGs as indicated by the order of K_1 to K_3 while the maximum changes in fold difference of the first and second highest one was 5-fold. However, CALA reversed the order of integral stereoselectivity for TAG and DAG depending on the saturation status of the acyl moiety. Since CALA holds an industrial importance in lipid modification, these results indicated that the integral stereoselectivity of the lipases should be determined for TAGs with each different acyl chains. Collectively, the concept of integral stereoselectivity and the analytical method for its determination on TAGs with

various acyl chains provide a standard for the evaluation of lipase for stereoselective production of structured lipids including enantiomeric DAGs and MAGs, which would expedite the application of lipases in the food industry. In further works to the integral stereoselectivity in hydrolysis process, the selectivity of the lipase for interesterification process, which is used to carry a synthesis of structured lipid in industrial scale, would be established and investigated.

III-5. References

Booth, T. D., Wahnon, D., & Wainer, I. W. (1997). Is chiral recognition a three-point process? *Chirality*, 9(2), 96-98.

Borgdorf, R., & Warwel, S. (1999). Substrate selectivity of various lipases in the esterification of *cis*- and *trans*-9-octadecenoic acid. *Applied Microbiology and Biotechnology, 51*(4), 480-485.

Brundiek, H., Padhi, S. K., Kourist, R., Evitt, A., & Bornscheuer, U. T. (2012). Altering the scissile fatty acid binding site of *Candida antarctica* lipase A by protein engineering for the selective hydrolysis of medium chain fatty acids. *European Journal of Lipid Science and Technology, 114*(10), 1148-1153.

Carrière, F., Withers-Martinez, C., van Tilbeurgh, H., Roussel, A., Cambillau, C., & Verger, R. (1998). Structural basis for the substrate selectivity of pancreatic lipases and some related proteins. *Biochimica et Biophysica Acta (BBA) - Reviews on Biomembranes, 1376*(3), 417-432.

Dalgliesh, C. E. (1952). The optical resolution of aromatic amino-acids on paper chromatograms. *Journal of the Chemical Society*, 132, 3940-3942.

Ericsson, D. J., Kasrayan, A., Johansson, P., Bergfors, T., Sandström, A. G., Bäckvall, J.-E., & Mowbray, S. L. (2008). X-ray structure of *Candida antarctica* lipase A shows a novel lid structure and a likely mode of interfacial activation. *Journal of Molecular Biology, 376*(1), 109-119.

Fotia, V., Potortì, A. G., La Torre, G. L., Di Bella, G., & Saitta, M. (2021). Separation of racemic mixtures of *sn*-1(3)-monoacylglycerols by enantioselective-HPLC/ELSD. *Journal of the American Oil Chemists' Society, 98*(11), 1035-1043.

Holmberg, E., Szmulik, P., Norin, T., & Hult, K. (1989). Hydrolysis and Esterification with Lipase from *Candida Cylindracea*. Influence of the Reaction Conditions and Acid Moiety on the Enantiomeric Excess. *Biocatalysis, 2*(3), 217-223.

Pan, S.-H., Kawamoto, T., Fukui, T., Sonomoto, K., & Tanaka, A. (1990). Stereoselective esterification of halogen-containing carboxylic acids by lipase in organic solvent: effects of alcohol chain length. *Applied Microbiology and Biotechnology, 34*(1), 47-51.

Pleiss, J., Fischer, M., & Schmid, R. D. (1998). Anatomy of lipase binding sites: the scissile fatty acid binding site. *Chemistry and Physics of Lipids, 93*(1), 67-80.

Podlaha, O., & Töregård, B. (1982). A system for identification of

triglycerides in reversed phase HPLC chromatograms based on equivalent carbon numbers. *Journal of High Resolution Chromatography, 5*(10), 553-558.

Vaysse, L., Ly, A., Moulin, G., & Dubreucq, E. (2002). Chain-length selectivity of various lipases during hydrolysis, esterification and alcoholysis in biphasic aqueous medium. *Enzyme and Microbial Technology, 31*(5), 648-655.

Wainer, I. W. (1987). Proposal for the classification of high-performance liquid chromatographic chiral stationary phases: how to choose the right column. *Trends in Analytical Chemistry*, 6(5), 125-134

Xu, X. (2000). Production of specific-structured triacylglycerols by lipase-catalyzed reactions: a review. *European Journal of Lipid Science and Technology, 102*(4), 287-303.

국문 초록

라이페이스는 독특한 촉매 활성을 가진 효소로 식품가공 등 다양한 산업분야에 응용되고 있으며, 트리아실글리세롤(TAG)에서 거울상 이성질체 관계의 위치(*sn*-1 및 *sn*-3)를 구별하는 능력을 나타내는 라이페이스의 입체 선택성은 산업 분야의 적용에 중요한 특성으로 주목받고 있다. 입체선택성은 다이아실글리세롤(DAG)의 거울상 초과량의 측정을 통해 결정되어 왔으나, 이는 연속적인 반응 단계로 이루어진 TAG 가수분해의 특징과 비효소적 아실 전이반응을 고려하지 않아 진정한 입체선택성을 나타내기에는 불충분하였다. 이에 본 연구에서는 '통합적 입체선택성' 개념을 제안하고, 새롭게 정립된 분석기법을 이용하여 이를 조사하였다. 이 접근법을 통해 TAG 가수분해의 각 단계에서 생성된 모든 아실글리세롤에 대한 라이페이스의 입체 선택성을 성공적으로 분석하고 결정했다.

먼저, 트리올레오일글리세롤(TOG)과 그 가수분해물인 올레산, 모노올레오일글리세롤(MOG) 이성질체 3종 및 디올레오일글리세롤(DOG) 이성질체 3종의 직접적·동시적 분리를 위해 HPLC-ELSD 방법을 구축하였다. 아밀로오스 트리스-(3,5-

디메틸페닐카바메이트) 유도체로 구성된 단일한 키랄 고정상(CSP) 컬럼을 사용하여 MOG(1-*sn*-MOG 및 3-*sn*-MOG) 및 DOG(1,2-*sn*-DOG 및 2,3-*sn*-DOG) 거울상 이성질체를 포함한 모든 물질을 20분의 분석시간에 1.5 이상의 분해능으로 분리하였으며, 이는 이전에 확립된 직렬 컬럼을 이용한 방법보다 진보한 것이었다. 돼지 췌장(PPL), *Chromobacterium viscosum*(CVL), *Pseudomonas fluorescens* 유래 라이페이스(PFL) 및 *Candida antarctica* 유래 라이페이스 A(CALA)를 이용한 역미셀계에서의 TOG 가수분해 반응 곡선을 분석하여 확립된 방법을 검증했다. 결과적으로 4가지 모델 라이페이스 모두 이전에 보고된 것과 동일한 DOG 생성 패턴을 보여 라이페이스 촉매 TOG 가수분해 분석을 위해 새로 확립된 방법의 효율성, 정확성 및 적합성을 입증했다.

다음으로, 통합적 입체 선택성을 정량적으로 입증하기 위해 동역학 모델을 구축하고 검증했다. 동역학 모델은 라이페이스 촉매 작용의 Ping-Pong Bi-Bi 메커니즘, 지방산에 의한 경쟁적 억제 및 비효소적 아실 전이를 기반으로 구성되었다. 비선형 회귀를 이용하여 초기 기질 농도의 변화에 따른 TOG 가수분해 반응곡선을 맞추는 데 사용되었다. TAG, DAG 및

모노아실글리세롤(MAG) 이성질체의 모든 위치에서 가수분해 속도를 나타내는 12개의 동역학 파라미터 (K_1-K_{12})를 4개의 모델 라이페이스를 대상으로 결정하였다. 그 결과, PPL, CVL 및 PFL에 의한 TOG 가수분해의 주요 반응 경로는 TOG에서 1,2-*sn*-DOG 또는 2,3-*sn*-DOG을 거쳐 2-*sn*-MOG로 이어지지만, CALA에 대해서는 TOG에서 1,3-*sn*-DOG를 거쳐 1-*sn*-MOG로 이어지는 것으로 나타나는 차이를 보였다.

셋째로, 라이페이스가 촉매하는 TAG 가수분해에서 통합적 입체선택성에 대한 지방산 사슬 종류의 영향을 조사했다. 이를 위해 다양한 길이와 포화도를 갖는 지방산 사슬(C14:0, C16:0, C18:0 또는 C18:2)로 구성된 TAG, DAG 및 MAG의 모든 이성질체의 동시 분리 및 정량을 위한 HPLC-ELSD 방법을 확립했다. C16:0 지방산의 아실글리세롤은 TOG 분석에 사용된 동일한 단일 CSP 컬럼에 수정된 이동상 조건을 사용하여 분리되었다. C14:0, C18:0 및 C18:2 지방산의 아실글리세롤은 셀룰로오스 트리스-(3-클로로-4-메틸페닐카바메이트)로 구성된 CSP 컬럼을 사용하여 분리되었다. 모든 DAG 및 MAG 거울상 이성질체에 대한 분해능 계수는 1,2-*sn*-DAG 및 1,3-*sn*-

DAG(C18:0 지방산)의 경우 약 1.31을 유지한 것을 제외하고 35분의 분석 시간에 1.60 이상으로 나타났다. 이것은 다양한 지방산 사슬의 아실글리세롤을 동시에 직접 분리하는 방법을 입증한 첫 번째 연구이다.

마지막으로, 앞서 언급한 지방산으로로 구성된 TAG, DAG 및 MAG에 대한 4가지 모델 라이페이스의 통합적 입체선택성을 결정하기 위해 라이페이스에 의한 TAG 가수분해의 동역학 모델링을 수행했다. 동역학 파라미터는 TAG의 지방산 유형 변화에 따라 PPL과 CVL이 선택성에서 유의미한 차이를 나타내지 않았으며, 주요 반응 경로가 유지되었다. TOG의 *sn*-2 위치를 절단할 수 있는 것으로 나타난 PFL은 C16:0 지방산으로 구성된 TAG에 대해 예외적으로 낮은 *sn*-2 선택성을 보였다. 가장 큰 차이를 보인 CALA는 지방산의 포화 여부에 따라 대조적인 선택성을 보였다. 불포화 지방산의 경우 TAG의 *sn*-2 위치 및 DAG중 1,3-*sn*-DAG에 대한 선택성이 가장 높은 반면, 포화 지방산의 경우 TAG의 *sn*-3 위치 및 DAG 중 1,2(2,3)-*sn*-DAG에 대한 선택성이 가장 높은 것으로 관찰되었다. 이러한 입체선택성의 반전은 DAG 및 MAG 이성질체 생산에 영향을

미치는 통합적 입체선택성의 기질에 따른 평가가 필요함을 시사한다.

결론적으로 TAG와 그 가수분해물의 동시 분해능을 기반으로 한 효소적 역학 모델링에 의해 결정된 통합적 입체선택성은 라이페이스의 입체화학적 특성을 설명하는 유용한 지표로서, 궁극적으로 입체특이적 재구성지질의 생산을 위한 라이페이스의 선택, 스크리닝 및 개발 과정에 기여할 수 있을 것이다.

주제어: 라이페이스, 입체선택성, 광학 이성질체, 동역학 모델

학번: 2018-29815